ปฏิกิริยาไฮโดรจิเนชันแบบเลือกเกิดของอะเซทิลีนบนตัวเร่งปฏิกิริยาแพลเลเดียม
บนไทเทเนียมไดออกไซด์ที่เตรียมด้วยวิธีการพอกพูนโดยไม่ใช้ไฟฟ้า

นางสาวสุมนรัตน์ ริยาพันธ์

วิทยานิพนธ์นี้เป็นส่วนหนึ่งของการศึกษาตามหลักสูตรปริญญาวิศวกรรมศาสตรดุษฎีบัณฑิต
สาขาวิชาวิศวกรรมเคมี ภาควิชาวิศวกรรมเคมี
คณะวิศวกรรมศาสตร์ จุฬาลงกรณ์มหาวิทยาลัย
ปีการศึกษา 2557

SELECTIVE HYDROGENATION OF ACETYLENE ON Pd/TiO_2 CATALYSTS PREPARED BY ELECTROLESS DEPOSITION METHOD

Miss Sumonrat Riyapan

A Dissertation Submitted in Partial Fulfillment of the Requirements
for the Degree of Doctor of Engineering Program in Chemical Engineering
Department of Chemical Engineering
Faculty of Engineering
Chulalongkorn University
Academic Year 2014

Thesis Title	SELECTIVE HYDROGENATION OF ACETYLENE ON Pd/TiO_2 CATALYSTS PREPARED BY ELECTROLESS DEPOSITION METHOD
By	Miss Sumonrat Riyapan
Field of Study	Chemical Engineering
Thesis Advisor	Associate Professor Joongjai Panpranot, Ph.D.
Thesis Co-Advisor	Assistant Professor Yuttanant Boonyongmaneerat, Ph.D.

Accepted by the Faculty of Engineering, Chulalongkorn University in Partial Fulfillment of the Requirements for the Doctoral Degree

.....Dean of the Faculty of Engineering
(Professor Bundhit Eua-arporn, Ph.D.)

THESIS COMMITTEE

.....Chairman
(Associate Professor Anongnat Somwangthanaroj, Ph.D.)

.....Thesis Advisor
(Associate Professor Joongjai Panpranot, Ph.D.)

.....Thesis Co-Advisor
(Assistant Professor Yuttanant Boonyongmaneerat, Ph.D.)

.....Examiner
(Associate Professor Bunjerd Jongsomjit, Ph.D.)

.....Examiner
(Assistant Professor Suphot Phatanasri, D.Eng.)

.....External Examiner
(Assistant Professor Okorn Mekasuwandumrong, D.Eng.)

สุมนรัตน์ ริยาพันธ์ : ปฏิกิริยาไฮโดรจิเนชันแบบเลือกเกิดของอะเซทิลีนบนตัวเร่งปฏิกิริยาแพลเลเดียมบนไทเทเนียมไดออกไซด์ที่เตรียมด้วยวิธีการพอกพูนโดยไม่ใช้ไฟฟ้า (SELECTIVE HYDROGENATION OF ACETYLENE ON Pd/TiO_2 CATALYSTS PREPARED BY ELECTROLESS DEPOSITION METHOD) อ.ที่ปรึกษาวิทยานิพนธ์หลัก: รศ. ดร.จูงใจ ปั้นประณต, อ.ที่ปรึกษาวิทยานิพนธ์ร่วม: ผศ. ดร.ยุทธนันท์ บุญยงมณีรัตน์, 136 หน้า.

In the present work, support Pd catalysts are commonly used in industry to remove trace amount of acetylene from ethylene feed in the production of polyethylene. Anatase nanocrystalline TiO_2 samples were synthesized by a sol-gel method and subjected to thermal treatment under N_2, H_2, O_2, and air atmospheres at 350°C employed as supports for preparation of 1%Pd/TiO_2 catalysts. The catalysts were characterized by X-ray diffraction (XRD), BET surface areas, electron spin resonance (ESR), and X-ray photoelectron spectroscopy (XPS). The surface Ti^{3+} defects significantly increased when treated under H_2 and N_2, comparing to air and O_2 with no changes in the crystallite size, specific surface area, and pore structure. Two different preparation methods including electroless deposition (ED) and incipient wetness impregnation (I) were used to prepare 1%Pd/TiO_2 catalysts. The 1%Pd catalyst supported on the TiO_2 calcined under H_2 prepared by ED exhibited the best catalytic performances in the selective hydrogenation of acetylene corresponding to their high Pd dispersion on the TiO_2 support. In addition, Ag-Pd/TiO_2 having incremental surface coverages of Ag prepared by ED. An increased selectivity of ethylene and higher turnover frequencies for acetylene conversion were observed at high Ag coverages. The adsorption of acetylene on Pd sites as strongly adsorbed ethylidyne on large Pd ensembles led to ethane formation whereas adsorbed **π**-bonded species on small Pd ensembles favored the formation of ethylene. Kinetics study of Ag-Pd/TiO_2 catalysts reveals that the apparent activation energy for the selective hydrogenation of acetylene Ag decreased from 12.08 ± 0.1 kcal/mol to 7.74±0.2 kcal/mol with increasing Ag coverage.

ภาควิชา วิศวกรรมเคมี ลายมือชื่อนิสิต .....

สาขาวิชา วิศวกรรมเคมี ลายมือชื่อ อ.ที่ปรึกษาหลัก .....

ปีการศึกษา 2557 ลายมือชื่อ อ.ที่ปรึกษาร่วม .....

5271834321 : MAJOR CHEMICAL ENGINEERING

KEYWORDS: SURFACE TI3+ / ACETYLENE HYDROGENATION / PD/TIO2 CATALYST / ELECTROLESS DEPOSITION

SUMONRAT RIYAPAN: SELECTIVE HYDROGENATION OF ACETYLENE ON Pd/TiO_2 CATALYSTS PREPARED BY ELECTROLESS DEPOSITION METHOD. ADVISOR: ASSOC. PROF. JOONGJAI PANPRANOT, Ph.D., CO-ADVISOR: ASST. PROF. YUTTANANT BOONYONGMANEERAT, Ph.D., 136 pp.

ตัวเร่งปฏิกิริยาแพลเลเดียมบนตัวรองรับใช้ทั่วไปในอุตสาหกรรมในการกำจัดอะเซทิลีนปริมาณเล็กน้อยออกจากสายป้อนเอทิลีนในกระบวนการผลิตพอลิเอทิลีน วิทยานิพนธ์นี้ศึกษาลักษณะพื้นผิวของไทเทเนียมไดออกไซด์ที่มีขนาดอนุภาคในระดับนาโนเมตร ที่เตรียมด้วยวิธีโซลเจลและแคลไซน์ในบรรยากาศที่แตกต่างกันคือไนโตรเจน ไฮโดรเจน ออกซิเจน และอากาศ ที่อุณหภูมิ 350 องศาเซลเซียสและนำไปเป็นตัวรองรับในการเตรียมตัวเร่งปฏิกิริยา 1%โดยน้ำหนัก Pd/TiO_2 วิเคราะห์คุณลักษณะของตัวเร่งปฏิกิริยาด้วยเทคนิคต่างๆได้แก่การเลี้ยวเบนของรังสีเอกซ์ การหาพื้นที่ผิวด้วยเทคนิคบีอีที อิเล็กตรอนสปินเรโซแนนซ์ เอ็กซเรย์โฟโต้อิเล็กตรอนสเปคโตรสโกปี พบว่าไทเทเนียมไดออกไซด์มีความบกพร่องบนพื้นผิว (Ti^{3+}) สูงเมื่อแคลไซน์ในบรรยากาศของไฮโดรเจนและไนโตรเจน โดยไม่มีความแตกต่างของขนาดผลึก พื้นผิวของไทเทเนียมไดออกไซด์และโครงสร้างของรูพรุน จากนั้นเตรียมตัวเร่งปฏิกิยาแพลเลเดียมบนตัวรองรับไทเทเนียมไดออกไซด์ด้วยวิธีที่แตกต่างกัน 2 วิธี ได้แก่ วิธีพอกพูนโดยไม่ใช้ไฟฟ้าและวิธีการเคลือบฝัง ตัวเร่งปฏิกิริยาแพลเลเดียมบนตัวรองรับไทเทเนียมไดออกไซด์ที่แคลไซน์ในบรรยากาศของไฮโดรเจนและเตรียมด้วยวิธีพอกพูนโดยไม่ใช้ไฟฟ้าแสดงประสิทธิภาพสูงสุด สำหรับปฏิกิริยาไฮโดรจิเนชันของอะเซทิลีน สอดคล้องกับการกระจายตัวของแพลเลเดียมบนพื้นผิวของตัวรองรับสูง นอกจากนี้ได้ทำการศึกษาตัวเร่งปฏิกิริยา $Ag-Pd/TiO_2$ ที่มีปริมาณซิลเวอร์ปกคลุมบนพื้นผิวโลหะแพลเลเดียมต่างๆโดยการเตรียมแบบพอกพูนโดยไม่ใช้ไฟฟ้า พบว่าการดูดซับอะเซทิลีนบนผิวแพลเลเดียมที่มีการปกคลุมของซิลเวอร์น้อยชอบที่จะดูดซับเอทิลลิดีนมากกว่าจึงนำไปสู่การเกิดอีเทน ส่วนแพลเลเดียมที่มีการปกคลุมของซิลเวอร์มากจะดูดซับแบบไพบอนด์ซึ่งนำไปสู่การเลือกเกิดของเอทิลีน การจากศึกษาจลศาสตร์ของตัวเร่งปฏิกิริยาแพลเลเดียม-ซิลเวอร์บนตัวรองรับไทเทเนียมไดออกไซด์พบว่าพลังงานกระตุ้นสำหรับปฏิกริยานี้จะลดลงจาก 12.08 ± 0.1 kcal/mol เป็น 7.74±0.2 kcal/mol เมื่อมีปริมาณซิลเวอร์เพิ่มมากขึ้น

Department:	Chemical Engineering	Student's Signature	.....
Field of Study:	Chemical Engineering	Advisor's Signature	.....
Academic Year:	2014	Co-Advisor's Signature	.....

ACKNOWLEDGEMENTS

I am deeply grateful to my thesis advisor, Asst. Prof. Joongjai Panpanot for her invaluable help and constant encouragement throughout the course of this research. I am most grateful for her teaching and advice. I would not have achieved this far and this thesis would not have been completed without all the support that I have always received from her. Furthermore, I also sincerely thank my Co-advisor Assistant Professor Dr. Yuttanant Boonyongmaneerat for suggestions and all his help.

I would also like to thanks my committee member, Associate Professor Dr. Anongnat Somwangthanaroj, Associate Professor Dr.Bunjerd Jongsomjit, Assistant Professor Dr. Suphot Phatanasri, and Assistant Professor Dr. Okorn Makasuwandamrong, for letting my defense be an enjoyable moment, and for your brilliant comments and suggestions.

In addition, I would like to extend my sincerest thanks to Professor John R. Monnier of Chemical Engineering College of Engineering and Computing, University of South Carolina for suggestions and all his help

I also would like to thank the financial supports from the Royal Golden Jubilee Ph.D. scholarship from Thailand Research Fund, and Chulalongkorn University.

Finally, I most gratefully acknowledge my parent and my friends for all their support throughout the period of this research.

Sumonrat Riyapan

CONTENTS

Page

Page

Page

Page

Page

Page

List of Tables

List of Figures

CHAPTER I
INTRODUCTION

1.1 Introduction

Ethylene is a crucial reactant for many industrial reactions. The selective hydrogenation of acetylene in ethylene is an important process in ethylene polymerization [1]. Typically, ethylene is produced by thermal cracking of higher hydrocarbons. The process also generates acetylene that can poison to catalysts used for polymerization. The concentration of acetylene has to be lower than 5 ppm to prevent catalyst poisoning [2]. Pd catalysts are commonly used in industry to reduce acetylene concentration in ethylene feed stream [3]. Palladium has the ability to selectively hydrogenate alkynes to alkenes in the presence of a large excess of alkene [4]. However, the hydrogenation of ethylene to ethane on monometallic Pd catalysts is expedited with high concentration of acetylene, leading to hydrocarbon deposits that decrease the catalyst lifetime [5] . The objective of the current work is to develop new catalysts by combining Pd-based catalysts and TiO_2 support to achieve high selectivity in the selective hydrogenation of acetylene in a stream containing ethylene. The high selectivity of ethylene in the hydrogenation of acetylene over Pd catalysts is generally proposed to originate from two main factors[6].One is a thermodynamic factor. The heat of adsorption of acetylene is much greater than ethylene, so acetylene preferentially covers on the Pd surface. The other is a mechanistic factor, which means that ethylene desorbs from the palladium surface and is replaced by acetylene before it has a chance to further react to form ethane [7]. Palladium has been used in the selective hydrogenation of acetylene in industry than other metals because it exhibits both high selectivity and high activity. However, Pd is not the only metal that has high ethylene selectivity for acetylene hydrogenation. Other metals, such as nickel, copper, platinum, and iridium [8], also have good ethylene selectivity for acetylene hydrogenation [8-10]. The catalyst performances for high ethylene selectivity could be further improved by adding promoters or using different supports. In previous studies, highly efficient Pd

catalysts for selective hydrogenation have been developed using glow discharge plasma Pd/α-AlO_3,Pd/MgO [11]. Moon has reported Pd on nano-size TiO_2, and Pd/SiO_2 with different metal oxide promoters (TiO_2, CeO_2) and found that TiO_2 gave better effects than CeO_2. The TiO_2 interacted strongly with Pd after a reduction at 500°C [12]. The strong metal-support interaction (SMSI) effect to the adsorption strength of ethylene is weakened. The properties of TiO_2 depend on several factors such as the crystallite size, the crystalline phase, and particle morphology. Sol-gel method is an easy route to obtain high purity nano-sized TiO_2 at mild reaction conditions. In the present work, sol-gel TiO2 was selected as the support for preparation of Pd/TiO_2 catalysts in the selective acetylene hydrogenation.

Supported Pd catalysts are typically prepared using impregnation method which is a common and simple method for preparation of catalysts [13]. Other preparation methods include colloidal synthesis method, sol-gel, chemical vapor deposition (CVD), and electroless plating [14]. Electroless deposition is one of the preparative methodologies, chemical process reduces metal ions in an aqueous solution and deposits metal on a substrate. Electroless deposition provides to catalytically deposite in controlled manner without the use of electrical energy. The process is similar to electroplating except that no outside current is needed. The electroless deposition process and controlled pretreatment sequence are produce good adhesion of the metal to the substrate. Advantages of the electroless deposition process is very cheap, easy control, and applicable on complex shapes. Electroless deposition has been employed for preparation of supported metal catalysts such as Pd/TiO_2 nanofibrous membranes [15, 16], Pd/Al_2O_3 [17], and Pd-IB/SiO_2 [18]. Electroless deposition was employed for preparation of Pd/TiO_2 catalysts in this study and their properties were compared to those prepared by the conventional impregnation method.

In addition to Pd/TiO_2, bimetallic Pd-based catalysts were also prepared using electroless deposition method. The most widely used in industrial procedures for preparation of bimetallic catalysts are impregnation of different metal and coimpregnation. The complex mixture of monometallic and bimetallic particles

results in poor control of the catalyst performance and difficult to correlate the relationship between catalyst performance, catalyst composition and characterization [19].

Recently, it has been reported that electroless deposition method can result in the selective deposition of the secondary metal onto a mono-metallic site that has been activated by a reducing agent with no formation of isolated crystallites of the secondary metal on the catalyst support [20]. Bimetallic electroless deposition has been employed for preparation of supported metal catalysts such as Pt–Pd/C [21], Pd-Ag/SiO_2, Pd-Au/SiO_2, Pd-Cu/SiO_2 [22-24].

Calcination is another important method to modify the catalytic properties. The metallic vacancy and oxygen vacancy are the common point defects and are affected by the preparation process. Wu et al. reported that oxygen vacancy can be created in the TiO_2 lattice structure when calcination was done under inert atmosphere, such as Ar, H_2-N_2, H_2, and N_2 [25]. In a previous work that investigated the effect of calcination atmosphere on Cu/Al_2O_3 catalyst for carbon monoxide oxidation, they found that high temperature calcination in oxidizing atmosphere led to a redispersed copper surface and loss of activity, while in reducing atmosphere produced sintering of copper surface and increase of activity. Influence of gas atmosphere used in the calcination of MgO (flowing oxygen, air, helium, nitrogen) has been investigated. It was found that calcined in oxygen or air gave MgO of lower basicity than those obtained by calcination in the stream of helium or nitrogen [26]. It is widely accepted that the increase in surface basicity was caused by promoters that enhances the activity and the selectivity of MgO-based catalysts [27]. K. Suriye et al. reported that titania calcined under nitrogen and oxygen atmosphere at various composition altered the surface defect (Ti^{3+}) concentration. The amount of surface defects increase with the increasing amount of oxygen in the calcination [28]. Thus, it is interesting to investigate the effect of calcination atmosphere on the properties of TiO_2 supported Pd catalysts in the selective acetylene hydrogenation.

1.2 Objectives

The objectives of this research are

1. To investigate the effect of gas atmospheres used in the calcination of a sol-gel TiO_2 on the properties of Pd/TiO_2 prepared by electroless deposition and impregnation in the selective acetylene hydrogenation.

2. To investigate the effect of calcination temperature of TiO_2 under Hydrogen atmosphere via a sol–gel-derived TiO_2 supported Pd catalysts that were prepared by impregnation method in the selective acetylene hydrogenation.

3. To investigate the characteristics and catalytic properties of TiO_2 supported bimetallic Pd-Ag catalysts prepared by electroless deposition method in the selective acetylene hydrogenation.

1.3 Research Scope

1. Preparation of titanium dioxide using sol-gel method and calcined under oxygen, air, nitrogen, hydrogen atmosphere.

2. Preparation of titanium dioxide support Pd (1wt% Pd) using the incipient wetness impregnation method and electroless deposition method.

3. Preparation of titanium dioxide supported Pd and Ag using the electroless deposition method.

4. Characterization of the catalyst samples using X-ray diffraction (XRD), BET surface areas, electron spin resonance (ESR), X-ray photoelectron spectroscopy (XPS), and pulse CO chemisorption methods and H_2 temperature programmed reduction (H_2TPR).

5. Reaction study of the catalyst samples in selective acetylene hydrogenation at 40-100°C using a fixed-bed quartz reactor.

.

CHAPTER II

BACKGROUND AND LITERATURE REVIEWS

2.1 Synthesis and applications of sol-gel TiO_2

2.1.1 Basic properties of TiO_2

Titanium dioxide is a naturally occurring oxide of the titanium. The chemical formula TiO_2 is referred to titanium (IV) oxide or titania. Titanium dioxide occurs naturally as three mineral compounds known as anatase, rutile and brookite. Brookite is a polymorph with two other minerals and all have the same chemistry. The structures of anatase, rutile and brookite have different structures [29]. Titanium dioxide is extracted from titanium tetrachloride by reduction with carbon.

Anatase trends to more stable at low temperature, while rutile tends to be more stable at high temperatures and bookite is usually found only in minerals has a structure belonging to the orthorhombic crystal system (Henrich 1985). Crystal structures of TiO_2 are shown in **Figure 2.1** and bulk properties of TiO_2 are shown in **Table 2.1**

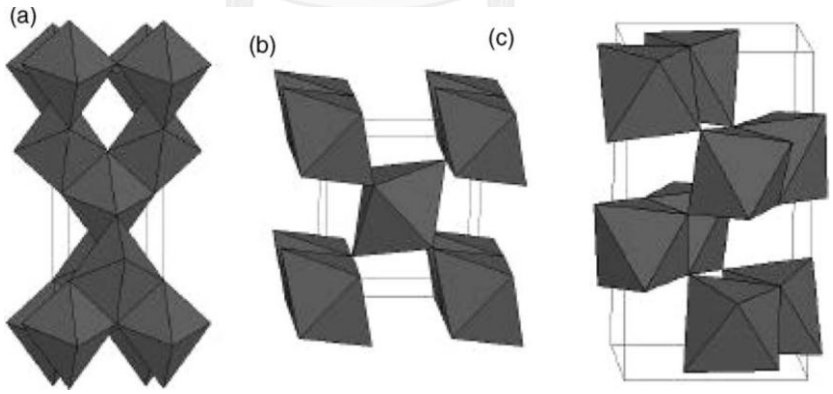

Figure 2.1 Crystal structures of anatase (a), rutile (b), and brookite (c). [30]

Table 2.1 Bulk properties of TiO_2 [31]

Properties	Anatase	Brookite	Rutile
Crystal structure	Tetragonal	Orthorhombic	Tetragonal
Optical	Uniaxial, negative	Biaxial, positive	Uniaxial, negative
Density, kg/m^3	3830	4170	4240
Harness,Mohs scale	$5^1/_2$-6	$5^1/_2$-6	7-$7^1/_2$
Unit cell	$D_4a^{19}.4TiO_2$	$D_2h^{15}.8TiO_2$	$D_4h^{12}.3TiO_2$
Dimension, nm			
a	0.3758	0.9166	0.4584
b	-	0.5436	-
c	0.9514	0.5135	2.953
Refractive index	2.52	-	2.52
Permittivity	31	-	114
Melting point	Changes to rutile at high temperature	-	1858 ^oC

Titanium dioxide is used in heterogeneous catalysis as a gas sensor, photocatalyst and white pigment use for optical coating in ceramics and in electric devices. Improvement of catalytic properties is one main driving force for surface modification on TiO_2. Because most heterogeneous catalysts consist of small metal clusters on the oxide support, so metals on TiO_2 were investigated in many studies [31].

2.1.2 Sol-gel TiO_2

Sol-gel synthesis is often used to prepare materials with a variety of shapes, such as porous structures, thin fibers, dense powders and thin films. The method is based on the phase transformation of a sol obtained from metallic alkoxides or organometallic precursors. This sol is containing particles in suspension, is polymerized to form a wet gel. The sol is going to be densified through a thermal annealing and finally dry gel. This method used for production of inorganic oxide materials at low temperature. The sol-gel process may be used to yield for amorphous form or multi-component oxides as crystalline**.** This process occurs in liquid solution of organimetallic precursors by hydrolysis and condensation reaction of metalorganic precursors, lead to the formation of sol. [32]

$$\text{M-O-R} + H_2O \longrightarrow \text{M-OH} + \text{R-OH} \quad \text{(Hydrolysis)} \qquad (2.1)$$

$$\text{M-O-H} + \text{HO-M} \longrightarrow \text{M-O-M} + H_2O \quad \text{(Water condensation)} \qquad (2.2)$$

$$\text{M-O-R} + \text{HO-M} \longrightarrow \text{M-O-M} + \text{R-OH} \quad \text{(Alcohol condensation)} \qquad (2.3)$$

A typical example of a sol-gel method is the addition of metal alkoxide to water and then the alkoxides are hydrolyzed giving the oxide as a colloidal product.

The sol is made of solid nanoparticles, suspended in a liquid phase. The particles condense into gel and was dried at low temperature produces porous solid matrices or xerogels. Finally, the gel is heated to decompose alkoxides or carbonates to give oxides and allows the cryatallization to occur.

In addition, the advantages are that the metal oxides are prepared easily at room temperature and the possibility to obtain high purity materials with the composition is perfectly controlled.

Various techniques have been reported for the preparation of nano-TiO_2 including solvothermal method [33-36], precipitation method [37], sol-gel method [32], chemical vapor deposition [38] and thermal decomposition of alkoxide [39]. The sol-gel method is an easy method but the precipitated powders obtained are amorphous in nature and further heat treatment is required for crystallization.

Solvothermal method is a direct (one-step) synthesis of pure anatase nano-TiO_2. This method can be control the particle morphology, crystalline phase of support, and surface chemistry by regulating precursor composition, reaction temperature, pressure, solvent property, and aging time.

Table 2.2 The advantages and disadvantages of sol-gel and solvothermal synthesis of TiO_2

Properties	Sol-gel	Solvothermal
Reaction at mild condition	√	X
Purity, homogeneity	√	X
Require thermal treatment	√	X
Repeatable	X	√

The properties of sol-gel TiO_2 depend on several factors. Factors affecting the sol-gel process include the reactivity of metal alkoxides, pH of the reaction medium, water:alkoxide ratio, reaction temperature, and nature of solvent and additive. By varying these processing parameters, materials with different microstructure and surface chemistry can be obtained. Typically, sol-gel-derived precipitates are amorphous in nature, requiring further heat treatment to induce crystallization. The calcination process frequently gives rise to particle agglomeration and grain growth and may induce phase transformation. Hydrothermal treatment represents an alternative to calcination for promoting crystallization under milder temperatures. Hydrothermal processing is adopted to produce nanocrystalline oxides with ultrafine particle size. In the hydrothermal treatment, grain size, particle morphology, crystalline phase, and surface chemistry can be controlled via processing variables such as sol composition and pH, reaction temperature and pressure, aging time, and nature of solvent and additive. The recent studies on the synthesis of TiO_2 by sol-gel method are summarized in **Table 2.3**.

Table 2.3 Summary of the recent research on the synthesis of sol-gel TiO_2

Reference	Parameter studied	Conclusions	Crystallite size and phase
Zaharescu et al. (1997)	-molar ratio ROH:$Ti(OR)_4$, H_2O:$Ti(OR)_4$, and HNO_3:$Ti(OR)_4$	-Increasing the water amount leads to decreasing of the specific surface area and of the pore volume; increasing the solvent quantity, both properties increase, too.	-surface area is high, generally over 130 m^2/g -the pore volume is high, generally over 0.19 cm^3/g
Y. Ying et al. (1999)	-water:alkoxide ratio -calcination temperature	-The crystallite size increase with increasing calcination temperature. -Water:alkoxide ratio increase crystallite size decrease	-crystallite sizes of 6-7 nm and 9-10 nm water:alkoxide ratio of 50 at 80 and 180 ^{o}C, respectively. surface area: not determined
Jiaguo Yu et al. (2000)	-various amounts of polyethylene glycol (PEG)	- Porous thin films is found to increase with increasing amount of PEG	- the single anatase phase is precipitated at 500^{o}C surface area: not determined

Reference	Parameter studied	Conclusions	Crystallite size and phase
Harizanov et al. (2000)	-Titanium dioxide and mixed oxide system TiO_2–MnO	-The presence of MnO in titania xerogel is effective in decreasing the anatase–rutile transformation temperature.	-Calcination temperature range 250-550^{o}C was TiO_2 anatase. crystallite size :23 nm above 800^{o}C shows TiO_2 - - rutile crystallite size : 14.8 nm - rutile $MnTiO_3$ 8 nm and $MnTi_2O_4$ 6.4 nm. surface area: not determined
Hahn et al. (2001)	-Various calcination temperatures	-The phase transformation has been dependent upon the concentration of catalyst HCl. -crystallite size was increased with increasing calcination temperature.	- Calcination temperature at 400–900^{o}C were anatase. -rutile phase occurred at 1000^{o}C crystallite size 9.6 to 38.2 nm with increasing temperature from 400 to 1000^{o}C surface area: not determined
Chen et al. (2002)	- Varied pH - Various calcinations temperature	- The crystallite size increase with increasing calcination temperature.	-calcined 400^{o}C (anatase) crystallite size:10 nm surface area : 106.9m^2/g

Reference	Parameter studied	Conclusions	Crystallite size and phase
Chen et al. (2002)	- Varied pH - Various calcinations temperature	-The crystallite size increase with increasing calcination temperature -pH=2 has a regular paticle size distribution.	-calcined 400°C (anatase) crystallite size:10 nm surface area : 106.9m^2/g - calcined 600°C(rutile)
C. P. Sibu et al. (2002)	-Titanium oxide with and without addition of lanthanum oxide	- Surface area decreased with the temperature was increased.	- The presence of 1 wt % of lanthanum oxide causes an increase in specific surface area of titania to as high as 160 m^2/g, which decreases to 52 m^2/g, upon calcining at 700°C - titania possessed only 1 m^2/g after calcining at 700°C.
C. Su et al. (2004)	-Titanium (IV) n-butoxide in iso-propyl alcohol various calcinations temperature	-The crystal size increased with the temperature was increased. - Surface area decreased with the temperature was increased.	- calcined 400°C (anatase) to 700°C (rutile) Surface area : 122 to 11.5 m^2/ g Crystallite size: 4 to 35 nm

Reference	Parameter studied	Conclusions	Crystallite size and phase
Mahshid et al. (2006)	Titanium-isopropoxide - varied pH - various calcinations temperature	-The crystal size increased with the temperature was increased -The powder obtained from a solution of pH = 2 consists of very fine anatase crystallites	-TiO_2 calcined 100^{o}C (anatase) to 800°C (rutile) crystallite size:7.6-53.4 nm surface area: not determined
Wetchakun et al. (2007)	- Effect of the calcination temperature on phase transformation of titanium dioxide nanoparticle	-The transformation of anatase to rutile increased with a boost of calcination temperature to about 700–800^{o}C -crystal size increased with the temperature was increased	-Anatase calcined at 400°C for 3 h possessed high specific surface area of 121 m^2/g -Cystallite sizes of anatase phase increased from 15 nm at 400^{o}C to 60 nm at 700^{o}C

2.2 The Pd catalysts supported on sol-gel TiO_2

Sol-gel TiO_2 have been employed as Pd catalyst supports and studied in various reactions including selective hydrogenation. **Table 2.4** summarizes recent research on the Pd catalysts supported on sol-gel derived TiO_2

Table 2.4 Summary of the recent research on the Pd catalysts supported on sol-gel TiO_2

Reference	Reactions studied	Characterization	Conclusions
Xu et al. (2005)	-Pd/TiO_2 liquid phase hydrogenation of maleic anhydride (MA) -Reaction conditions: MA = 40 mmol, catalyst = 0.5g H_2 = 3 MPa, stirrer = 700 rpm, duration = 2 h.	BET, TEM, XRD XPS and TPR	-The high conversion of maelic anhydride and high yield towards butyric acid were attributed to the strong adsorption of MA species via the C = 0 bond in di-**σ** mode on the inter-facial Pd-TiO_2 site which was induced by the high temperature reduction step.
Panpranot et al. (2006)	- Pd/TiO_2 selective hydrogenation of acetylene -Reaction conditions: temperature, 40 ^{o}C. Feed gas composed of 1.46% C_2H_2, 1.71%H_2, 15.47% C_2H_6 and balanced C_2H_4 and a GHSV of 5400 h^{-1}	BET, TEM, XRD and ESR	-Acetylene conversions were found to be merely dependent on Pd dispersion, ethylene selectivity appeared to be strongly affected by the presence of Ti^{3+} in the TiO_2 samples.

Reference	Reactions studied	Characterization	Conclusions
Martínez et al. (2006)	-The oxidative destruction of dichloromethane (DCM) in the presence of water vapor. -Reaction conditions: total flow of 20 mL/min of a gas stream containing 1945 ppm CH_2Cl_2 and space velocity was 0.005 g min/mL	XRF,BET, XRD TEM, and EDX	-Catalysts prepared by impregnation exhibited higher activity than those prepared by cogellation and Pd was more effective than Ni for burning-off coke deposited over support surface.
Xu et al. (2006)	-Liquid phase hydrogenation of maleic anhydride -Reaction conditions: MA=40 mmol, catalyst=SG, 0.5 g, H_2=3 MPa, Stirrer=700 rpm, duration=2 h.	BET, TEM, XRD, XPS and TPR	-The catalyst exhibited excellent activity and high yield to butyric acid.

Reference	Reactions studied	Characterization	Conclusions
Gu. et al. (2006)	-Bimetallic Au-Pd/ TiO_2-Al_2O_3 catalysts for thiopene hydrodesulfurization	BET, TEM, XRD, and XPS	-Au-Pd/TiO_2-Al_2O_3 catalysts had smaller Au_xPd_y crystal size, larger active specific surface area, better active component dispersion, more AuxPdy alloy content and more acid sites. Apparent activation energy of HDS catalyzed by Au-Pd/TiO_2-Al_2O_3 was low.
Impalà et al. (2008)	-Enantioselective hydrogenation of the C=C double bond in (E)-2-methyl-2-butenoic acid -Reaction conditions: T = 298 K, H_2 = 4 MPa; solvent (n-hexane) = 75 mL; tiglic acid/solvent = 1:30 v/v, tiglic acid/CD = 50:1 mol/mol; Pd/CD = 1:3 mol/mol, reaction time = 120 min	BET, XRD, XPS NH_3–TPD, and H_2-chemisorption	-The influence of preparation conditions on support texture and metal dispersion was evidenced and tentatively correlated with activity and enantioselectivity.

Reference	Reactions studied	Characterization	Conclusions
Guofu et al. (2010)	-The diesel hydrodearoma-tization (HDA) and hydrodesulfurization (HDS) -Reaction conditions: 603 K, 5 MPa, and 1.0 h^{-1} (LHSV).	UV-vis, BET, XRD, and DRS spectra	-The enhanced HDA activity and sulfur tolerance of Pt-Pd/ATS were likely attributed to the incorporations of Ti and Si into Al_2O_3, which optimized the interaction between the catalyst support and active metals.
Ino et al. (2011)	-Hydrogenation of naphthalene in the presence of CO	UV-vis	-Using pure hydrogen as the reactant, Pd/TiO_2-Al_2O_3 catalysts containing 50-80 wt% of TiO_2 had high activity. Using hydrogen containing 2% CO, Pd/TiO_2- Al_2O_3 catalyst containing 80 wt% of TiO_2 had the highest activity.

The Pd catalysts supported on sol-gel TiO_2 have been studied in various reactions such as hydrogenation of maleic anhydride, acetylene, maleic anhydride, naphthalene , (E)-2-methyl-2-butenoic acid , diesel hydrodearomatization (HDA) and hydrodesulfurization (HDS), and oxidative destruction of dichloromethane (DCM). The influences of preparation conditions on the support texture and metal dispersion

have been investigated and were found to affect the conversion and selectivity of the reactions.

2.3 Selective acetylene hydrogenation over Pd based catalysts

2.3.1 General information of selective acetylene hydrogenation

Previous studies [40-42] showed that acetylene hydrogenation produces ethylene, which is then hydrogenated to ethane. The initial steps of the acetylene hydrogenation mechanism include dissociative adsorption of hydrogen on the catalyst surface. The adsorption of acetylene and ethylene are also co-adsorbed on the catalyst surface before reaction. The rate-determining step is addition of the first hydrogen atom to acetylene or ethylene. [43]. Generally, it involves two main factors that make the Pd a highly selective catalyst for the hydrogenation of acetylene [44]. One is a thermodynamic factor. The heat of adsorption of acetylene covers on the surface of Pd much greater than that of ethylene. The other is a mechanistic factor, which means that the ethylene desorbs from the Pd surface and is replaced by acetylene before it has a chance to further form to ethane. Generally, there are two primary reactions processding during acetylene hydrogenation:

$$C_2H_2 + H_2 \xrightarrow{k1} C_2H_4 \qquad H= -42{,}000 \text{ kg-cal/kg-mol} \qquad (2.4)$$

$$C_2H_4 + H_2 \xrightarrow{k2} C_2H_6 \qquad H= -32{,}900 \text{ kg-cal/kg-mol} \qquad (2.5)$$

The reaction (2.4) is the desired reaction to produce the ethylene product whereas the second reaction (2.5) is an undesired side reaction due to loss of ethylene production. The reaction (2.6) occurring during normal operation, affects the catalyst performance, i.e. Green oil is formed by side reactions of acetylene in the feed stream with itself to form a longer chain molecule.

$$C_2H_2 + (n)\, C_2H_2 \xrightarrow{k3} C_xH_x \text{ (polymer/green oil)} \qquad (2.6)$$

The influence parameter of acetylene hydrogenation is reaction temperature, which has a direct relationship with the kinetic of the reaction. The rate of polymerization increases with increasing temperature led to the formation of green

oil can affect catalyst activity by occupying active sites. The selective hydrogenation of acetylene to ethylene is critical to maintain the differential the activation energies of reaction between (eq.2.4) and (eq.2.5). Once energy is supplied to the reaction over a given catalyst by increase the reaction temperature. At higher temperature reduces selectivity of ethylene due to ethylene convert to ethane, thereby increasing ethylene loss. The ratio between hydrogen and acetylene (H_2:C_2H_2) affect to the ethylene selectivity. Theoretically, the H_2:C_2H_2 ratio would be 1:1, which mean that no hydrogen remain for further hydrogenated after acetylene hydrogenation.

To design a novel catalyst with improved performance in acetylene hydrogenation, it is necessary to consider the reaction mechanism for acetylene hydrogenation, which consists of several reaction paths, as shown in **Figure 2.2** [42]. Path I is the partial hydrogenation of acetylene to ethylene (Path II) or further hydrogenated ethylene to ethane (Path III). So, the high ethylene selectivity should be promoted Path II and suppressed Path III. Suppression of ethane formation in stream by add CO to the reaction stream, which adsorbs more strongly on catalyst surface than ethylene (Path II) [45]. The other is to maintain a low concentration of H_2/acetylene ratio in the feed stream such that the catalyst surface is due to a decrease in the surface coverage of hydrogen and thus the full hydrogenation of ethylene (Path III) is retarded [46]. Path IV is the direct full hydrogenation of acetylene to ethane due to the high acetylene coverage on the catalyst surface and low partial pressures of hydrogen [47]. Path V is lowers the ethylene selectivity due to the dimerization of the C_2 species, which allow the formation of green oil [48]. The reaction pathway of acetylene hydrogenation indicates that the improvement of ethylene selectivity Path I and Path II should be promoted while the other paths should be suppressed.

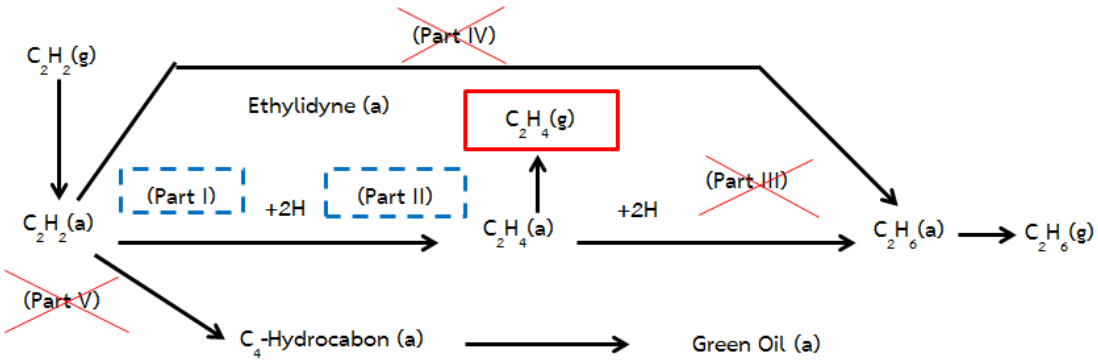

Figure 2.2 Reaction paths of acetylene hydrogenation [42]

For acethylene adsorbed species have been reported, these are shown in **Figure 2.3**. The various modes of acetylene can adsorbon the metal sites of a catalyst. Acetylenee can mainly adsorb on a catalyst surface as a di-**σ**-bonded species, as a di-**π**-bound associated species or as ethylidyne. The formation of ethylidyne involves the hydrogen on the catalyst surface further reacts with acetylene adsorbs to form more ethylidyne. Ethylidyne can form to ethane via a series of adsorbed components by the following sequential hydrogenation process: ethylidyne » ethylidene » ethyl » ethane.

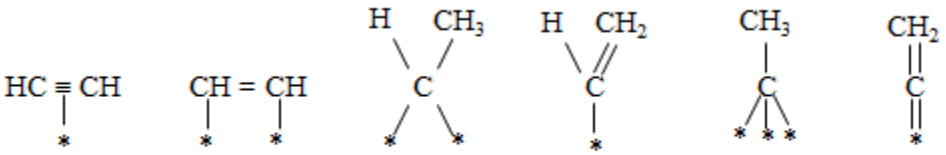

π-complex di-**σ**-bonded ethylidene vinyl ethylidyne vinylidene

Figure 2.3 Adsorption forms of acetylene on Pd.

2.3.2 Effect of support modification on the properties of Pd catalysts in the selective hydrogenation of acetylene.

The effect of Pd dispersion obtained on different supports on their catalytic properties in the selective hydrogenation of acetylene has been reported. In these previous studies, they suggest that high metal dispersion yields a structure sensitivity reaction and Pd particle size effect on the acetylene hydrogenation. Additions of promoter decreased the formation of ethane, C_4 alkenes and green oil and improve of ethylene selectivity in acetylene hydrogenation. In addition, the promoted catalysts also showed lower rates of catalyst deactivation.

Table 2.5 Summary of the recent research on the Pd catalysts in selective hydrogenation of acetylene.

Reference	Parameter studied and Characterization	Conclusions
Shin et al. (1998)	Pd catalysts modified with Si deposited on them by silane decomposition Catalysts : Pd/Al_2O_3, $Si\text{-}Pd/Al_2O_3$ Characterization : acetylene-TPD, IR, XPS, and CO chemisorption	When used in acetylene hydrogenation, the Si-modified catalysts show higher selectivity for ethylene and produce less amount of green oil than the unmodified Pd catalysts.
Moon et al. (2002)	Performance of TiO_2-modified Pd catalysts Catalysts : $Pd–Ti/SiO_2$, Pd/SiO_2 ,Pd/TiO_2 Characterization : ethylene TPD, XPS, and CO chemisorption	$Pd–Ti/SiO_2$/reduce 500 ^{o}C, showed a higher selectivity for ethylene production than either the Pd/TiO_2 or Pd/SiO_2 catalyst.

Reference	Parameter studied and Characterization	Conclusions
Moon et al. (2002)	Supported Pd catalyst modified with Si Catalysts : Pd/SiO_2 , $Pd-Si/SiO_2$ Characterization : XPS, CO chemisorptions and ethylene TPD	The adsorption strength of ethylene on Pd becomes weak and the amount of adsorbed hydrogen decreases when the Pd catalyst is modified with Si.
Moon et al. (2003)	The deactivation behavior of Si-modified Pd catalysts in acetylene hydrogenation Catalysts :Pd/SiO_2 , $Pd-Ti/SiO_2$ Characterization :TGA ,and IR	The improvement in the deactivation behavior of the Si-modified catalyst is believed to arise from the geometric modification of the Pd surface with small clusters of the Si species.
Moon et al. (2004)	Performance of TiO_2-modified Pd catalysts Catalysts : Pd/SiO_2 , $Pd-Ti/SiO_2$ Characterization : CO-IR, XPS XRD, FT-IR, and CO-chemisorption	The added TiO_2 also retarded the sintering of Pd particles during catalyst regeneration, presumably due to the anchoring effect of TiO_2, and suppressed green oil formation, even after the regeneration step.

Reference	Parameter studied and Characterization	Conclusions
Moon et al. (2004)	Effect of potassium (K) addition on the performance of a TiO_2-modified Pd catalyst in the hydrogenation of acetylene. Catalysts : K-Pd-Ti/SiO_2 Characterization : XPS, XRD, FT-IR, and CO-chemisorption	Potassium (K) was added to Pd-Ti/SiO_2, the resulting catalyst showed an improved selectivity for ethylene production over a wide range of conversions, when the catalyst was reduced at 300 °C.
Panpranot et al. (2005)	The supports for Pd and Pd–Ag catalysts for hydrogenation of acetylene. Catalysts :Pd/TiO_2, Pd-Ag / TiO_2 Characterization : XPS, XRD, ESR, SEM, and CO-chemisorption	Pd supported on titania synthesized in 1,4-butanediol (lower defective sites) exhibited higher activity and selectivity for selective acetylene hydrogenation than the ones supported on titania synthesized in toluene (higher defective sites).
Kang et al. (2006)	The performance of TiO_2-modified Pd catalysts Catalysts :Pd/TiO_2, Pd/SiO_2, Pd–Ti/SiO_2 Characterization : EDS, ethylene-TPD, and XPS	The Pd/TiO_2 and Pd/SiO_2 catalyst showed a lower selectivity for ethylene production than Pd–Ti/SiO_2/500°C.

Reference	Parameter studied and Characterization	Conclusions
Panpranot et al. (2006)	Pd/TiO_2 catalysts have been prepared using TiO_2 supports consisting of various rutile/anatase crystalline phase compositions. Catalysts: Pd/TiO_2 Characterization : H_2-TPR, XRD, CO-chemisorption, XPS, and ESR	Pd/TiO_2-R44 suggests an optimum anatase/rutile composition of the TiO_2 used to obtain high selectivity of ethylene in selective acetylene hydrogenation.
Moon et al. (2006)	Pd catalysts promoted by La_2O_3 and Nb_2O_5 for selective hydrogenation of acetylene. Catalysts: Pd-La / SiO_2 , Pd-Nb / SiO_2 Characterization : H_2-TPR, ethylene-TPD, H_2 chemisorption	The Nb_2O_5 - added catalysts showed the highest activity and longest catalyst lifetime due to the additional activity of Nb oxides for hydrogenation. Consequently, the former catalysts would be advantageous for use at high temperatures and the latter at low temperatures.
Komhom et al. (2008)	The catalytic performances of Pd catalysts supported on γ-Al_2O_3, α-Al_2O_3, and mixed phases Al_2O_3 in the hydrogenation of acetylene. Catalysts: Pd/ γ-Al_2O_3, Pd/α-Al_2O_3 Characterization : EDS, acetylene-TPD, and XPS	64% α-Al_2O_3 was the best (optimum) composition to prepare Pd/Al_2O_3 catalysts with high acetylene conversion and high ethylene selectivity.

Reference	Parameter studied and Characterization	Conclusions
Wongwara non et al. (2008)	The catalytic performance of Pd catalysts supported on nanocrystalline α-Al_2O_3 and Ni-modified α-Al_2O_3 Catalysts: Pd/α-Al_2O_3, Pd/Ni-modified α-Al_2O_3 Characterization : H_2-TPR, XRD, CO-chemisorption, XPS, ESR, SEM and BET	Ethylene selectivities were improved in the order: Pd/Ni-modified α-Al_2O_3–sol–gel > Pd/Ni-modified α-Al_2O_3-solvothermal ≈ Pd/α-Al_2O_3–sol–gel > Pd/α-Al_2O_3-solvothermal ≈ Pd/ α-Al_2O_3-commercial.
Moon et al. (2011)	Cu-promoted Pd/Al_2O_3catalysts were prepared by selectively depositing Cu onto the Pd surface using a surface redox (SR) method. Catalysts: Pd-Cu/Al_2O_3 Characterization : H_2-TPR, XRD, and XPS	The Cu-promoted catalysts prepared by SR showed higher ethylene selectivity and activity than Ag-promoted catalysts, particularly with small amounts of added promoter.
Moon et al. (2012)	The effects of Ni addition on the performance of Pd-Ag/Al_2O_3 catalysts in the selective hydrogenation of acetylene. Catalysts: Ni-Pd-Ag/Al_2O_3 Characterization : CO-IR, ethylene-TPD, and H_2-TPR	Ni-added Pd-Ag catalysts showed higher conversions than Pd-Ag catalyst. Added Ni also modified the geometric nature of the Pd surface by blocking large ensembles of Pd into isolated ones, which eventually improved ethylene selectivity.

Reference	Parameter studied and Characterization	Conclusions
Moon et al. (2013)	The performance of Ag-promoted Pd/Al_2O_3 catalysts, which were prepared by the selective deposition of Ag onto Pd using a surface redox (SR) method. Catalysts: $Pd\text{-}Ag/Al_2O_3$ Characterization : IR, XPS, and acetylene-TPD	The catalyst prepared by SR showed a higher ethylene selectivity than the one prepared by impregnation, because SR allowed both the preferential deposition of Ag on the low coordination sites of Pd and a greater electronic modification of Pd by Ag.

2.4 Electroless deposition method

2.4.1 Theory

The electroless deposition method is a catalytic process to chemically reduce a metallic salt into a catalytically active site in an aqueous solution. The overall reaction (2.7) for electroless deposition is a combination of anodic (2.8) and cathodic (2.9) electrochemical partial reactions [49-51]. However, the anodic and cathodic reactions are determined by the nature of metal source, reducing agent, supported metal substrates and any other additive. In these equations, the R is the reducing agent, z is the valence and M is the electroless deposited metal.

$$M^{z+} + R^{n-} \longrightarrow M^{0} + R^{z-n} \quad (2.7)$$

$$R^{n-} \longrightarrow R^{n+z} + ze- \quad (2.8)$$

$$M^{z+} + ze- \longrightarrow M^{0} \quad (2.9)$$

The overall reaction for the electroless deposition (reaction 2.7) is thermodynamically favorable, but is kinetically limited by the reaction at the anode (reaction 2.8) and is controlled by activation of the reducing agent. Since the deposited metal (M) is often catalytically active for the reducing agent reaction at the anode, further reduction can occur, resulting possibly in multiple layers around the core increasing the thickness of the shell if the reaction conditions allow.

Up to this time, the following metals are known to be electrolessly deposited for various applications: Ni, Pd, Cu, Ag, Cd, In, Sn, Pb, Sb, Co, Ru, Rh, Pt, Au and Bi [52]. A diagram of the process is presented in **Figure 2.3** Second a metal core (B^{n+}) is deposited on the catalytic metal site. The reducing agent (RA) is catalytically activated at the surface of the metal core to produce electrons. The electrons flow through the metal core and reduced the metal (A) at the surface of the metal core.

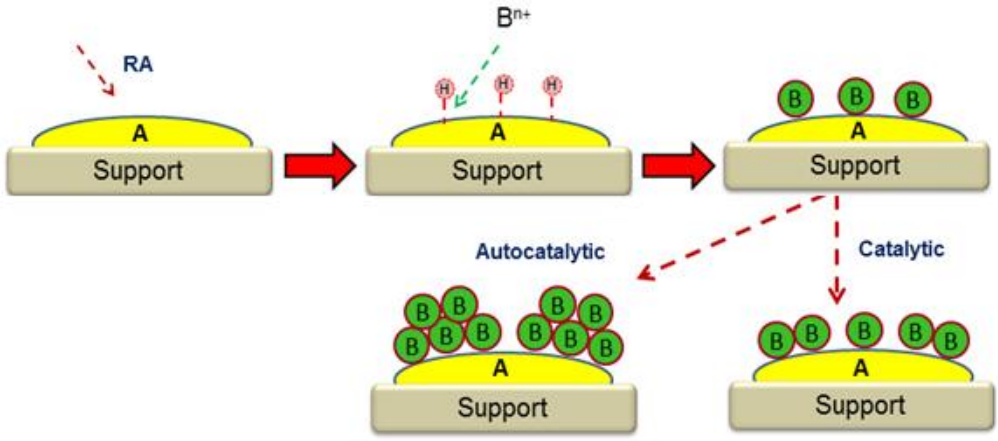

Figure 2.4 Schematic diagram of bimetallic electroless deposition.

This process is known as autocatalysis depending on the nature of the activated metal site and the reducing agent. Typical reducing agents for electroless deposition include formaldehyde, borohydrides and hydrazine [53]. Selecting a

reducing agent will depend on the metal source of the process. The standard redox potential of the reducing agent must be more electronegative than that of metal being reduced. The reduction takes place in a bath. The bath is generally composed of a metal source, a reducing agent, a complexing agent, and a stabilizing agent to enhance metal deposition on the surface of catalyst [49].

The stabilizing agents have similar functions as complexing agents are used to increase the useful life time of the baths. The thermal instability occurs when metal particles precipitate from the electroless deposition solution and can be cause by dust particles or other contaminants [24]. For the catalytic electroless deposition, the selection of stabilizing agent depends on choice of metal source. It decreases the metal reduction rate, balance between these components to obtain a stable bath and avoid formation of small insoluble precipitates. If these conditions are not attained, the metal can reduce and precipitate rather than deposited into the catalytic sites.

The disadvantage is that only some metals can be electrolessly deposited and requires a bath with the right agent to achieve the deposition of metals into support. Also, it requires several ashing procedures to remove the impurities. The several advantages of electrolessly deposited method over traditional bimetallic methods. One is further deposition into another metal and the particle control. The dispersion of the catalyst is high with small particle sizes and is suitable for large-scale.

2.4.1.1 Electroless Deposition Bath Parameters

These parameters describe the solution (often called the electroless deposition bath) in which deposition takes place. The bath is usually aqueous and is generally composed of a metal ion source, a reducing agent, a complexing agent, a stabilizing agent, and possibly an accelerant [54]. In order for catalytic electroless deposition to be achieved, a delicate balance must exist between these components such that a stable bath is attained. Otherwise, rather than depositing the metal at

active catalytic sites, the metal will simply be thermally reduced and will precipitate from solution [55].

2.4.1.2 Metal Ion Sources

Industrially-feasible metal ion sources are typically inexpensive, water-soluble metal salts [51]. Furthermore, due to environmental concerns, certain hazardous salts, such as those containing cyanide, are generally avoided [54]. In cases where the purity of the coating is essential, hydroxide-based metal salts have been used, since they do not contain heteroatom anions that might be incorporated into the deposited metal coating [56]. Some commonly used metal ions include $CoSO_4$, $AgNO_3$, $CuSO_4$, $Na_3Au\ (SO_3)_2$, $PdCl_2$, H_2PtCl_6 and $Na_2Pt\ (OH)_6$, among many others [57].

2.4.1.3 Reducing Agents

The reducing agent, as discussed previously, donates electrons to the metal that is being reduced. Typical reducing agents for electroless deposition include hypophosphite, alkali borohydrides, formaldehyde, dialkylamine borane, and hydrazine [58]. There are several factors that influence which reducing agent is chosen. In order for the process to be catalytic, the standard redox potential of the reducing agent must be more electronegative than that of the metal that is being reduced. For example, sodium hypophosphite is a practical reducing agent for nickel since its redox potential is -0.5 V while that of nickel is only -0.25 V [59].

Finally, some reducing agents are “clean” and some are not. In other words, when certain reducing agents such as formaldehyde and hydrazine are used, the resulting metal deposit is pure. When hydrazine is used it results in 97-99% pure deposits with the balance being oxygen and nitrogen. However, when DMAB is used, up to 4% boron can be incorporated into the metal coating; likewise, when hypophosphite is used for acidic nickel deposition, 6-12% phosphorous may be incorporated. The incorporation of these materials may affect the resulting metal coating properties. However, these levels of impurities are incorporated for electroless deposition of thick films. For lower levels of electroless deposition, such as those used in this research program, the levels of incorporated impurities should

be negligible. The primary reducing agents used herein are dimethylamine borane, hydrazine, and formaldehyde. These specific reducing agents are briefly discussed below[51].

2.4.2 Synthesis of Pd-based catalysts by electroless deposition method

The properties of Pd-based catalysts by electroless deposition method depend on several factors deposition rate, different for the hydrazine and hypophosphite-based electroless baths, deposition time, optimization of the kinetic parameters of electroless deposition, concentrations of the bis-cyano metal salt and reducing agent, solution pH, and temperature.

Table 2.6 Summary of the recent research on the Pd-based catalysts prepared by electroless deposition method.

Reference	Metal and Characterizations	Studied	Conclusions
Cheng et al. (1998)	Pd-Ag/porous Vycor glass tubes Characterization : XRD, SEM, and XPS	The proper conditions for simultaneous, co-deposition of palladium and silver from a mixed plating bath were identified.	In addition, the formation of a single-phase alloy results in substantial enhancement in the hydrogen permeation rate.
Cheng et al. (2000)	Pd/porous Vycor glass tubes Pd/porous stainless steel Characterization : XPS, and SEM	Two palladium electroless plating solutions, hydrazine-based and hypophos-phite-based plating baths	The hypophosphite-based plating bath has a slower plating rate, but provides better plating efficiency than a hydrazine-based plating bath.

Reference	Metal and Characterizations	Studied	Conclusions
Chen et al. (2004)	Pd-Ag/Al_2O_3 Characterization : SEM, and XRD	Effects of plating time, Ag composition and total concentration of metal ions on surface morphologies, composition and microstructure of the resulting layers.	Surface morphology of the deposited Pd-Ag layer is strongly affected by the Ag content of the plating bath. The differences of deposition rates and growth modes are observed between Pd and Ag grains, the PdAg layer exhibits the dendritic structure.
Schaal et al. (2007)	Cu-Pd/SiO_2 Characterization : FT-IR, and CO-chemisorption	Cu–Pd/SiO_2 bimetallic catalysts for the hydrogenation of 3,4-epoxy-1-butene	The bimetallic Cu–Pd sites that are formed exhibit unusually high activity for EpB conversion and selectivity towards unsaturated alcohols and aldehydes.

Reference	Metal and Characterizations	Studied	Conclusions
Kiliςarslan et al. (2008)	Pd/Al_2O_3 Pd/Glass Characterization : EDS, and SEM	Effects of pore structure of the support on the plating morphology, thickness, and composition in an electroless plating procedure.	The number of pores corresponding to the mesoporous region increased after the second plating step. After the fourth plating step, the number of pores in this region decreased while pores in the macroporous region remained basically the same in the structure.
Foletto et al. (2008)	Pd-Ag/Porous Vycor glass tube Characterization : XPS, and SEM	Pd-Ag alloy membranes for hydrogen separation	On temperatures above 623 K, silver content is an important parameter that influences hydrogen permeation through the membranes. Other important parameters are pressure, temperature and probably surface morphology.

Reference	Metal and Characterizations	Studied	Conclusions
Monnier et al. (2010)	Au-Pd Ag-Pd and Cu-Pd/SiO_2 Characterization : XPS, FTIR, and UV–visible spectra	Effective methodology for preparing bimetallic catalysts with systematic variation in composition.	Deposition of Cu and Ag are selective towards Pd(1 1 1) sites, while Au deposits non-discriminately on all Pd sites. Finally, XPS measurements for each family of bimetallic catalysts suggest a net electron transfer from the Pd to the deposited metal.
Monnier et. Al. (2014)	Au-Pd/SiO_2 Ag-Pd/SiO_2 Characterization : AAS, and H_2 chemisorption	Effect of Ag- and Au–Pd/SiO_2 bimetallic catalysts having incremental surface coverages of Ag and Au on the Pd surface. The catalysts were prepared by electroless deposition for acetylene hydrogenation	The catalyst performance results suggest that at high coverages of Ag or Au on Pd, that result in small ensembles of Pd sites, acetylene is adsorbed as a **π**-bonded species that favors hydrogenation to ethylene.

CHAPTER III
MATERIALS AND METHODS

This chapter describes the experimental procedure used in this research which can be divided into three sections. The preparations of catalysts are shown in section 3.1. Properties of the catalysts characterized by various techniques are discussed in section 3.2. Finally, the reaction study in acetylene selective hydrogenation is given in section 3.3.

3.1 Preparation of catalysts

3.1.1 Preparation of titanium dioxide using the sol-gel method

The three components used in the preparation of the TiO_2 sol-gel were titanium isopropoxide (Aldrich Chemical Ltd), 70% nitric acid (Asia Pacific Specialty Chemical Limited) and distilled water. First, 70% nitric acid 7.33 ml was added to 1000 ml of distilled water. The mixture was continually stirred using a magnetic stirrer addition .While the mixture was stirred, 83.5 ml of titanium isopropoxide was added slowly. The mixture was stirred continually for about 3 days at room temperature until clear sol was obtained. After that, the sol was dialyzed in a cellulose membrane with a molecular weight cutoff of 3500 (Spectrum Companies, Gardena, CA). Before using the cellulose membrane, the dialysis tubing was wash in an aqueous solution of 2% sodium hydrogen carbonate and 0.001M Ethylenediaminetetraacetic acid (EDTA) prepare by dissolving 0.372 grams of EDTA (Asia Pacific Specialty Chemical Limited) and sodium hydrogen carbonate 43 grams in 1 liter of distilled water. Dialysis tubing was cut to a length of 32 cm and was submerged in the wash solution. After that the membrane was heated to 80°C and held there for 30 minutes while simultaneously being stirred. Then the solution was cooled to room temperature. The membrane was again wash with distilled water and again immersed in one liter of distilled water while being stirred continuously. Then the solution was heat to 80°C. The membrane was rinsed one more time and was stored in distilled water at 4°C until needed. The clear sol was placed in dialysis

tubing. A ratio of 100 ml of sol per 700 ml of distilled water the sol was submerged in distilled water. The water was changed daily for 3-4 days until the pH of water reached 3.5. The solvent was removing and was dried at 110°C overnight. Finally, the resulting material was calcined at 350°C in flowing hydrogen, oxygen, nitrogen and air atmosphere for 2 hour and the heating rate was at 10°C/min.

Table 3.1 Chemical composition use for TiO_2 prepared by Sol- gel

Chemicals	Formula	Quantity per 1000 ml bath
Titanium isopropoxide (Aldrich)	$Ti[OCH(CH_3)_2]_4$	83.5 ml
Nitric acid (APSC) 70%	HNO_3	7.33 ml

3.1.2 Preparation of Pd/TiO_2 using the electroless deposition method

Titanium dioxide was coated with palladium. Before electroless deposition, activation was performed on the TiO_2 support. The support was sensitized and activation with $SnCl_2$ and $PdCl_2$ acidic solution, firstly TiO_2 was activated by mixing 14% HCl for 15 min and rinsed with deionized water 2 times. Then support was activated in $SnCl_2$ (Fluka) and $PdCl_2$ (Aldrich) acidic solution for 20 min, the suspension was centrifuged and washed with deionized water. The TiO_2 support was dried at 110°C overnight. After activated, the support was transferred to Pd electroless deposition bath. The electroless deposition bath were prepared using $PdCl_2$ precursor adding in 9.2 ml of HCl (Carlo Erba) and the solution diluted to 100 ml DI water. Ammonium chloride (Carlo Erba) is added to stabilize the bath for extended use. Hypophosphite (Carlo Erba) was added last. The optimized electroless bath contained $PdCl_2$ and $NaH_2PO_2.H_2O$ in a 1:10 molar ratio. During Electroless deposition at room temperature, the bath was continuously stirred and the pH was maintained 10 for 1h. After stirring for 1 h, the suspension was centrifuged and washed with deionized water. The catalyst was then dried at 110°C overnight and calcined in air at 450°C for 1 h.

Table 3.2 Chemical composition of the electroless deposition bath

Chemicals	Formula	Electroless bath
Sensitization		
Palladium (II) chloride (Aldrich)	$PdCl_2$	0.015 g
Tin (II) chloride (Aldrich)	$SnCl_2$	5 g
Hydrochloric acid (ACS)	HCl (37%)	9.2 ml
Electroless deposition		
Palladium (II) chloride (Aldrich)	$PdCl_2$	0.0168 g
Hydrochloric acid (ACS)	HCl (37%)	0.4 ml
Ammonia hydroxide (Aldrich)	NH_4OH (28% NH_3)	16 ml
Ammonium chloride (Carlo Erba)	NH_4Cl	2.7 g
Sodium hypophosphite	$NaH_2PO_2.H_2O$	0.1006 g

3.1.3 Preparation of Pd/TiO_2 using impregnation method

1wt% Pd over TiO_2 supports were prepared by the sequential impregnation technique detailed as follows:

(1) Titanium dioxide supports were impregnation with an aqueous solution of palladium chloride by the incipient impregnation wetness technique.

(2) The impregnated support was left to stand for 6 hours to assure adequate distribution of metal complex. The support was subsequently dried at 110°C in air overnight.

(3) The dried impregnation support was calcined under nitrogen with heating rate was at 10°C/min until the temperature reached 450°C. Then flowing air was

switched into the reactor to replace nitrogen and the temperature was help at 450^{o}C for 3 hour.

(4) The calcined sample was finally cooled down and stored in a glass bottom for later use.

3.1.4 Preparation of Pd/TiO_2 using strong electrostatic adsorption method

The Pd/TiO_2 catalyst was prepared by strong electrostatic adsorption (SEA). The Titanium dioxide support was obtained from Sigma Aldrich. The surface area of the titanium dioxide was measured by the BET method to be 50 m^2/g and the optimized PZC value of TiO_2 (Sigma Aldrich, 99.7%) is 5.7. Palladium tetraammine (PdTA, $[(NH_3)_4Pd]^{+2}$, 99.9%) from Aldrich was used for metal precursor on TiO_2. Uptake–pH surveys were conducted 50 mL of 200 ppm metal solutions and pH values of all these solutions were adjusted using NaOH between pH 9 to 12.5. Metal concentrations were measured by ICP (Perkin Elmer Optima 2000) before and after contact with TiO_2 to determine the metal uptake. The mass of the TiO_2 (0.4g) was adjusted so that Surface loading = 10^3 m^2/L in 25 ml (5 ml for measured initial concentration of metal, ICP) of aqueous solution of PdTA. The slurries were placed on a rotary shaker for 1 h, after which the final pHs of these slurries were measured again. Furthermore, 5 ml of the contacted slurries was withdrawn and filtered. The remaining concentration of Pd in the solution was determined by inductively coupled plasma (ICP). Pd uptakes from pH 9 to 12.5 were determined from the difference in Pd concentration between the precontacted and postcontacted solutions. The maximum Pd uptake at a initail pH around 11.8. The Larger batch of Pd/TiO_2 catalyst was prepared at this pH and was subsequently filtered and measured metal loading by ICP. The solution is trapped by the vacuum filter and the liquid is drawn through the funnel into the flask below and dried for 24 h at room temperature. Then the Pd/TiO_2 catalyst was reduced with H_2 for 1 h at 200^{o}C for 2 h.

Table 3.3 Chemical composition use for prepared Pd/TiO_2 by strong electrostatic adsorption (SEA)

Chemicals	Formula
Titanium dioxide 99.7% (Aldrich)	TiO_2, 99.7%
Palladium tetraammine (Aldrich)	$[(NH_3)_4Pd]^{+2}$, 99.9%
Sodium hydroxide (Aldrich)	NaOH

3.1.5 Preparation of Ag-Pd/TiO_2 using electroless deposition method

The 0.97wt% Pd/TiO_2 catalyst was used for prepared Ag on Pd/TiO_2 by electroless deposition method (ED). The Pd dispersion of 21% corresponded to calculated Pd particles of 5 nm diameter. The dispersion of Pd was determined by hydrogen titration of oxygen pre-covered Pd sites using a Micromeritics AutoChem 2920 Automated Analyzer. The Ag–Pd/TiO_2 bimetallic catalysts were synthesized using cyanide metal precursors. The molar ratio of Metal salt/reducing agent was 1:10. Potassium silver cyanide ($KAg(CN)_2$, 99% purity, Technic, Inc.) and hydrazine (N_2H_4, 35 wt% aqueous solution, Sigma-Aldrich) were used as the metal sources and the reducing agent. Initial concentrations of the metal salts were selected based on theoretical coverage of Ag on Pd, assuming monolayer deposition and 1:1 surface stoichiometry of Ag deposited on Pd. Using this methodology, a series of Ag–Pd/TiO_2 catalysts with varying Ag coveraged on Pd. The volume of the electroless bath was 100 mL for 1g of the Pd/TiO_2 catalyst. The pH of bath solution at ~ 10 ± 0.5 (NaOH, pellets, J.T. Baker) and a pH probe was immersed in the ED bath throughout the deposition sequence. During electroless deposition at room temperature, the bath was continuously stirred. Liquid samples were periodically taken from the bath, immediately preceding sample filtration to remove catalyst particles at different time intervals. Nitric acid 5 vol% (HNO_3, 68–70%, BDH) was added to the withdrawn sample aliquot in order to ensure complete solubilization of the Ag^+ species. The solutions were analyzed by atomic absorption spectroscopy (AAS, PerkinElmer AA

analyst 400) to determine the Ag^{+} concentration remaining in the bath and used to determine the Ag loadings on the catalysts. After 1 h of deposition time, the slurry was then filtered and washed thoroughly with deionized water to remove all soluble ligands and salts. The sample were dried under vacuum at room temperature and stored at ambient conditions.

Table 3.4 Chemical composition use for prepared Ag-Pd/TiO_2 using electroless deposition method

Chemicals	Formula
Potassium silver cyanide	$KAg(CN)_2$, 99% purity
Hydrazine (Aldrich)	N_2H_4, 35 wt%
Sodium hydroxide (Pellets, J.T. Baker)	NaOH
Nitric acid (BDH)	HNO_3, 68–70%

3.2 Catalyst Characterization

3.2.1 X-Ray Diffraction (XRD)

The X-ray diffraction (XRD) pattern of the TiO_2 supports and Pd/ TiO_2 catalysts were determine the crystalline phases and average crystallite size using Scherrer's equation. X-ray diffraction (XRD) was obtained with SIEMENS XRD D5000, with CuK_{α} radiation. Scans were performed over the range 20-80 degrees.

3.2.2 BET Surface Area

Surface area (BET) was a physical adsorption of nitrogen gas on the surface of catalyst to find the total surface area, nitrogen as the adsorbate using a Micromeritic ASAP 2000 automated system degassing at 200°C for 1 hour prior to N_2 physisorption of Chemical Laboratory of Department of Engineering, Chulalongkorn University.

3.2.3 Scanning electron microscope (SEM)

SEM was used to determine the sample morphology and element distribution were obtained using a JEOL JSM-35F scanning electron microscope. SEM was operated using the back scattering electron mode at 20 kV. at the Chemical Laboratory of Department of Engineering, Chulalongkorn University.

3.2.4 Transmission Electron Microscopy (TEM)

The palladium oxide particle size and distribution of palladium on titanium dioxide were observed using JEOL-JEM 200 CX transmission electron microscope operated at 100kV.

3.2.5 Electron Spin Resonance (ESR)

The surface Ti^{3+} on surface TiO_2 supports were measured by Electron spin resonance spectroscopy (ESR) was conducted at power 1mW and amplitude 2.5x100 without illumination using a JEOL, JES-RE2X electron spin resonance spectrometer at Chulalongkorn University. It was performed to monitor the surface Ti^{3+} on the surface of the titanium dioxide.

3.2.6 X-ray Photoelectron Spectroscopy (XPS)

The XPS analysis was performed using an AMICUS photoelectron spectrum spectrometer equipped with an MgK_{α} X-ray as primary excitation and KRATOS VISION2 software. XPS elemental spectra were acquired with 0.1 eV energy step at a pass energy of 75 kV. The C 1s line was taken as an internal standard at 285.0 eV.

3.2.7 Temperature programmed reduction (TPR)

Temperature programmed reduction used to determine the reducibility and reduction temperature of palladium catalysts. Approximately, 0.1 g of catalyst sample was used in the operation and temperature ramping from 30°C to 500°C at 10°C/min. The carrier gas was 10% H_2 in Ar. The amount of hydrogen during the reduction was measure by thermal conductivity detector (TCD).

3.2.8 CO-Pulse Experiment

Metal active sites were measured using CO chemisorption technique. The amounts of CO chemisorbed on the catalysts were measured using Micromeritics ChemiSorb 2750 (pulse chemisorptions system). 0.1g of the catalyst sample was packed in a quartz tube, incorporated in a temperature-controlled oven and connected to a thermal conductivity detector (TCD). Helium gas was introduced into the reactor at the flow rate of 30 ml/min for 10 min in order to remove remaining air. Prior to chemisorptions, the sample was reduced in a H_2 flow rate of 50 ml/min with heated at an increasing from room temperature to 40°C and held at this temperature for 2 hour after that cooled down to ambient temperature in a He flow . The catalyst was then ready to measure metal active sites. Purity carbon monoxide gas was injected to adsorb on the metal surface of catalyst. Carbon monoxide was repeatedly injected until the sample did not any longer adsorbed carbon monoxide.

3.2.9 Inductively coupled plasma–atomic emission spectrometry (ICP)

The actual Pd content of the catalysts after adsorption was measured by inductively coupled plasma–atomic emission spectrometry (ICP-AES), using an Iris advantage Thermo Jarrel Ash device.

3.2.10 Atomic absorption spectroscopy (AAS)

The elemental concentrations of Ag in the electroless solutions were determined by Atomic absorption (AA) spectroscopy (Perkin-Elmer Model 3300 or Perkin-Elmer Analyst Model 400) using standard protocol methods. The bulk, metallic compositions of the bimetallic catalysts were digested in aqua regia (3:1 of HCl to HNO_3 by volume) at 120°C for 4 h prior to AA analysis. The linear calibration curves were determined using asset of standards with known concentration of each specific element. For the case of Ag metal analysis, the standard sand samples were diluted using 5% (v/v) HNO_3 solution for better sensitivity and accuracy at the Chemical Laboratory of Department of Engineering, University of South Carolina.

3.2.11 Scanning Transmission Electron Microscopy (STEM)

The particle size determination for the catalysts were made with an aberration-corrected JEOL 2100F scanning transmission electron microscopy (STEM) using Z-contrast imaging at the Chemical Laboratory of Department of Engineering, University of South Carolina.

3.2.12 Hydrogen–Oxygen Titration

Chemisorption using hydrogen pulse titration of oxygen-precovered Pd was performed using a Micromeritics Autochem II 2920 automated chemisorption analyzer to determine the concentration of surface Pd sites following ED of the bimetallic Ag–Pd/TiO_2. Briefly, approximately 0.1g sample was reduced in flowing 20% H_2/balance argon at 200°C for 2h and then purged with pure argon for 1 h. After cooling to 40°C inflowing Ar, the sample was exposed to 10%O_2/balance Ar for 30 min to saturate the Pd surface with adsorbed atomic oxygen to form Pd-O surface species. Following exposure to100% Ar for 30 min to remove residual O_2 and weakly adsorbed oxygen on the support, the sample was ready for pulse flow H_2 titration. Finally, 10% H_2/balance Ar was dosed until all surface Pd-O species reacted with hydrogen to form H_2O and replace the adsorbed oxygen atom with atomic hydrogen. Hydrogen consumption was quantitatively was quantitatively determined by means of a calibrated, high sensitivity thermal conductivity detector (TCD) below the sample cell. The Ag is inactive for hydrogen–oxygen titration, the concentration of Pd surface sites that were covered by Ag can be determined by subtracting the Pd surface site concentration of the bimetallic catalysts from the total number of surface Pd sites for the monometallic Pd/TiO_2 catalyst.

3.3 Reaction study in acetylene hydrogenation

The catalytic performance for the selective acetylene hydrogenation was investigated using a GHSV of 28,819.36 h^{-1}. Feed gas composed of 1.5%C_2H_2, 1.7%H_2, and balance C_2H_4. All of gases were supplied by Thai Industrial Gas Limited (TIG). Feed stream and composition of product were measure using Shimadzu FID GC 8A, carbosieve column S-II equipped with FID for separating CH_4, C_2H_4 and C_2H_6.

Concentration of H_2 was analyzed by GC 8A molecular sieve 5A. The operating condition for each instrument are shown in table

Catalyst 0.15 g was pack in a quartz tubular down flow reactor. Reactor was placed into the furnace and argon was introduced into the reactor in order to remove remaining air. The catalyst was reduced with 100 ml/min hydrogen by heating from room temperature to 150°C and held at that temperature for 2 hour. Then argon was switched in to replace hydrogen for cooled down to the reaction temperature 40°C. The reactant gases was introduce at temperature from 40°C to 100 °C and 1 atm, sampling was undertaken when the steady state of the system was reached, which was approximately within 1 hour. Feed and product were analyzed by a two gas chromatographs with TCD detector (SHIMADZU TCD GC-8A) and FID detector (SHIMADZU TCD GC-9A).

Table 3.5 Operating conditions of gas chromatograph for selective hydrogenation of acetylene

Gas Chromatograph	**SHIMADZU TCD**	**SHIMADZU TCD**
Detector	TCD	FID
Packed column	Molecular sieve 5A	Carbosieve column S-II
Carrier gas	Ultra high purity Ar	Ultra high purity N_2
Carrier gas flow rate (ml/min)	40-60	40-60
Injector temperature (°C)	80	180
Detector temperature (°C)	80	180
Initial column temperature (°C)	50	100
Programmed rate (°C/min)	-	10
Final column temperature (°C)	50	160
Current (mA)	70	-
Analyzed gas	H_2	CH_4, C_2H_2 , C_2H_4,C_2H_6

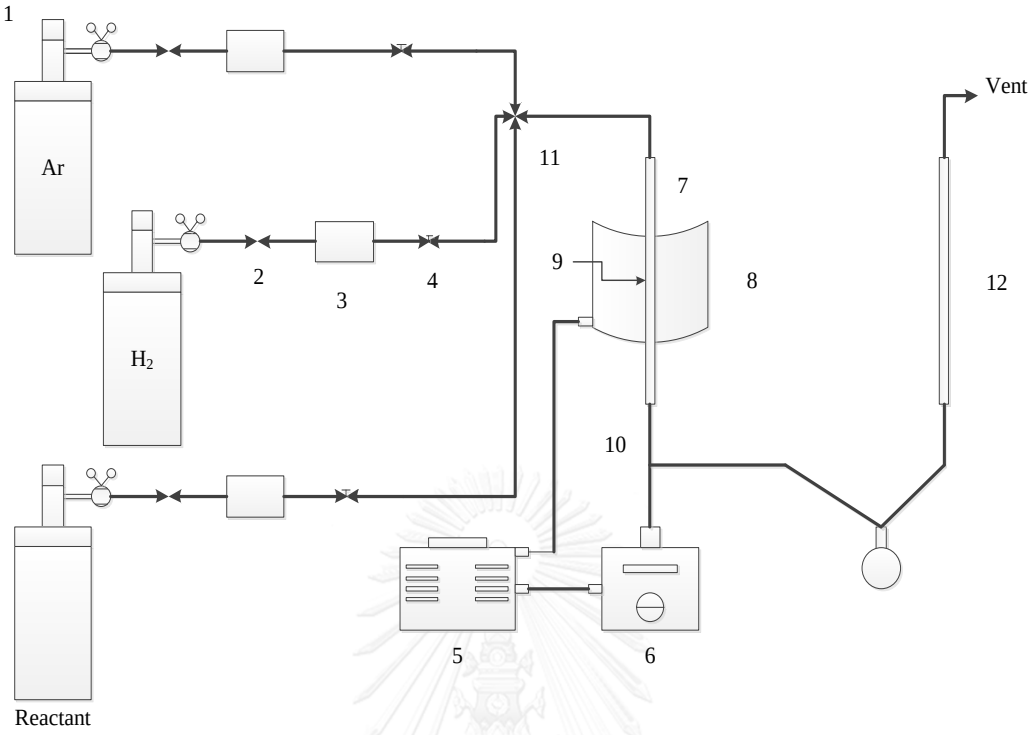

Figure 3.1 A schematic of acetylene hydrogenation system

1. pressure regulator
2. on-off value
3. gas filter
4. needle value
5. variable voltage transformer
6. temperature controller
7. reactor
8. furnace
9. catalyst bed
10. thermocouple
11. 4-way joint
12. Bubble flow meter

3.4 Reaction study in acetylene hydrogenation (PART III).

Selective acetylene hydrogenation was performed in a tubular reactor (316stainless steel). Catalysts were evaluated in a single pass, 0.19 in ID and packed bed. The reactor was encased in a 1.0 in OD, jacketed shell with liquid inlet and exit ports at the bottom and top of the shell, respectively, which was connected to an ethylene glycol/H_2O recirculation bath to maintain isothermal behavior at 65^{o}C for this highly exothermic reaction. The reactor was typically loaded with 5 mg of catalyst diluted by 30 mg of the TiO_2 support. Prior to the start of each experimental run, the catalyst was reduced with in flowing 20% H_2/balance He by heating from room temperature to 200^{o}C for 2 h. Then the reactor was purged with He and cooled down to the reaction temperature 65^{o}C. All gas flows were maintained by mass flow controllers; the reaction feed stream for catalyst screening consisted of 1% C_2H_2, 20% C_2H_4, 5% H_2, balance He at a total flow rate of 50 SCCM.

The kinetic measurements for acetylene hydrogenation were studied using a flow rate was 200 SCCM and the reaction temperature was 50^{o}C. For determination reaction orders of C_2H_2, partial pressures were varied between 0.005 and 0.012 atm with constant pressure of H_2 at 0.05 atm. The calculation of H_2 dependencies, partial pressures ranged between 0.02 and 0.10 atm and pressure C_2H_2 was constant at 0.01 atm. The activation energies conversion conditions for Pd/TiO_2 and Ag-Pd/TiO_2 were determined between 40 and 70^{o}C using the standard feed composition of 1% C_2H_2, 20% C_2H_4, 5% H_2, balance He.

CHAPTER IV

RESEARCH METHODOLOGY AND RESEARCH PLAN

4.1 The research methodology

The research methodology comprises of the following tasks

Part I is the investigation of the effect of gas atmospheres used in the calcination of TiO_2, which is prepared via a sol-gel method on the properties of Pd/TiO_2 in the selective acetylene hydrogenation.

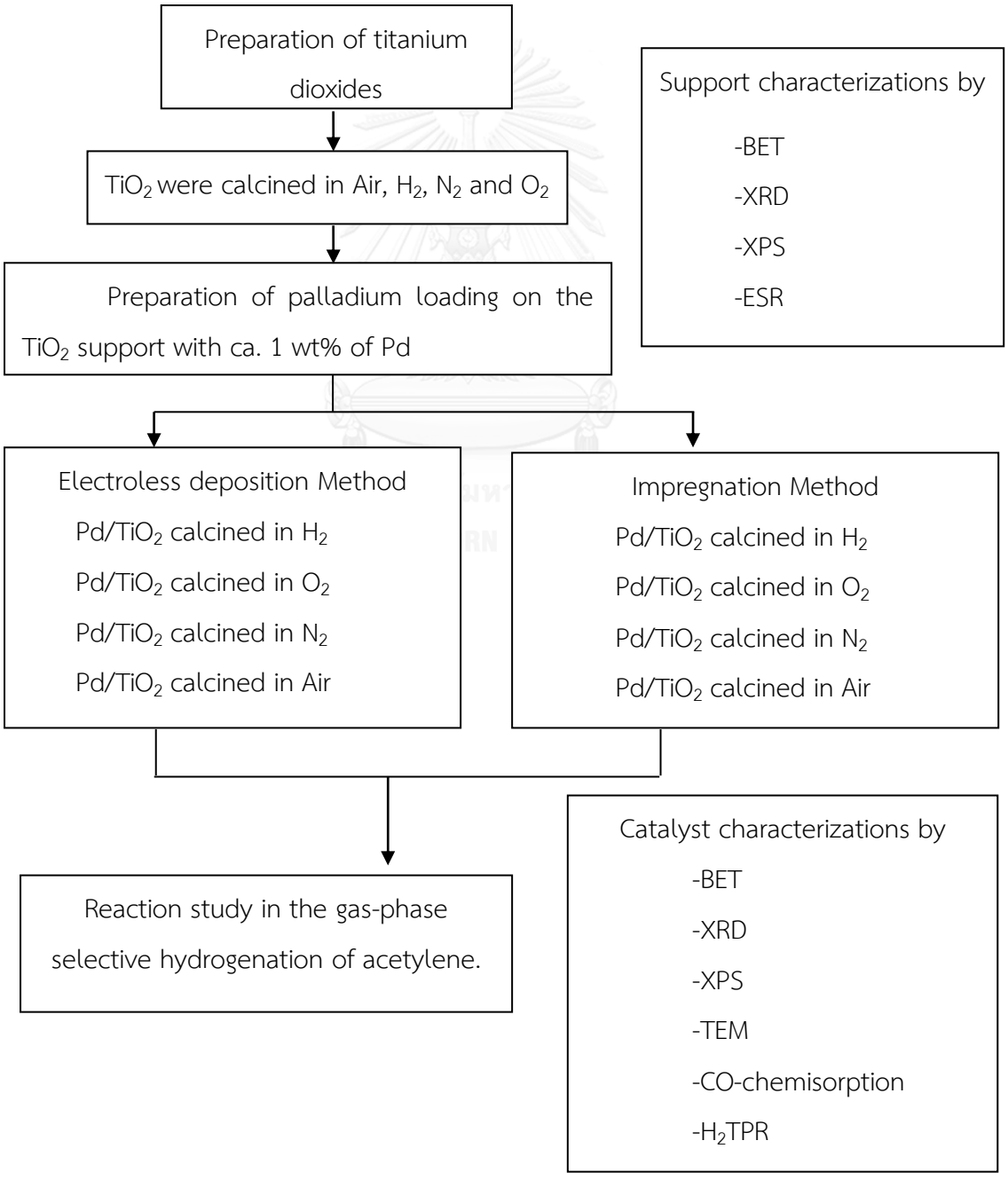

Part II is the investigation effect of calcination temperature under hydrogen atmosphere of TiO_2 nanocrystalline prepared by sol–gel-derived supported Pd catalysts for the selective hydrogenation of acetylene.

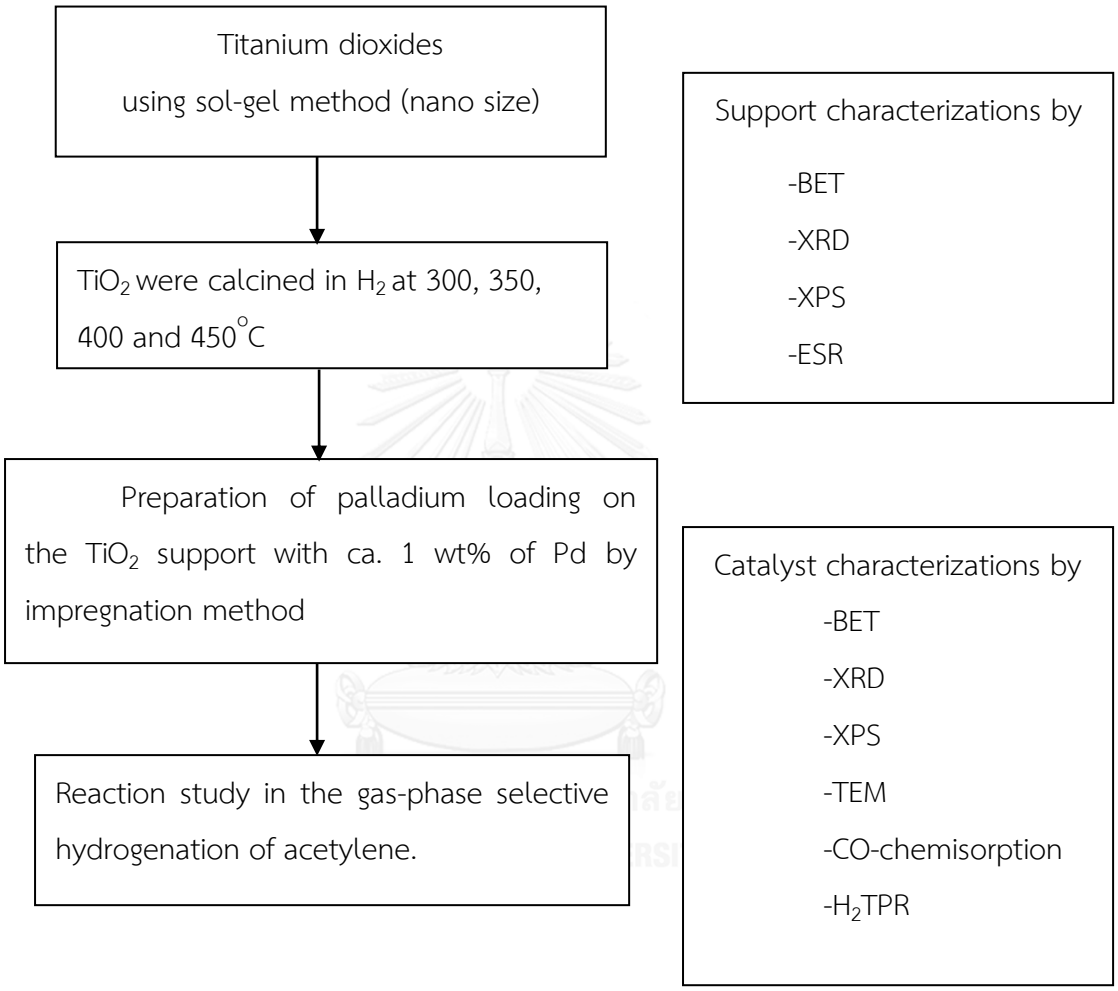

Part III is the investigation of the characteristics and catalytic properties of TiO_2 supported bimetallic Pd-Ag catalysts prepared by electroless deposition method in the selective acetylene hydrogenation.

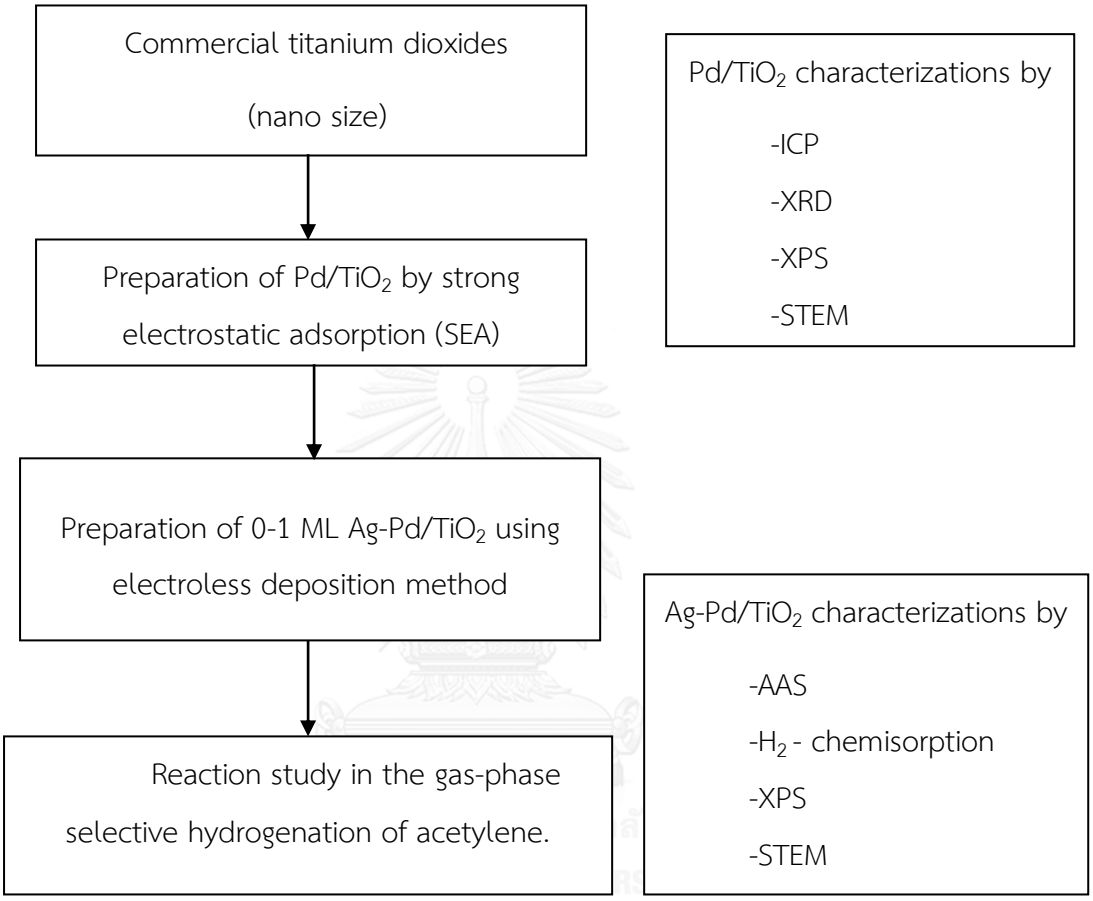

CHAPTER V
RESULTS AND DISCUSSION

These chapters are divided into three parts. In the first part the effect of gas atmospheres used in the calcination of sol-gel TiO_2 on the properties of Pd/TiO_2 in the selective acetylene hydrogenation was investigated. The titanium dioxide particles were investigated by XRD, BET surface areas, ESR and XPS. The characteristics and catalytic properties of Pd (1wt% Pd) prepared by the incipient wetness impregnation method (I) and electroless deposition method (ED) in the selective acetylene hydrogenation were analyzed by XRD, N_2-physisorption, XPS, TEM, H_2 temperature programmed reduction (H_2TPR), infrared spectroscopy of adsorbed CO (CO-IR) and CO-pulses chemisorption. In the second part, the effect of calcination temperature of the TiO_2 under hydrogen atmosphere on the TiO_2 supported Pd catalysts prepared by impregnation method was investigated in the selective acetylene hydrogenation. The characterization of the catalyst samples include XRD, BET surface areas, ESR, XPS, pulse CO chemisorption and H_2TPR. In the third part, the characteristics and catalytic properties of TiO_2 supported bimetallic Pd-Ag catalysts prepared by electroless deposition method in the selective acetylene hydrogenation was reported. The Pd/TiO_2 was prepared by electrostatic adsorption method and then the Ag coverage on the surface of Pd was achieved by electroless deposition method. The catalytic properties were investigated by XRD, ICP, Atomic absorption spectroscopy (AAS), Scanning Transmission Electron Microscopy (STEM), and hydrogen–oxygen titration.

PART I

Effect of gas atmospheres used in the calcination of sol-gel TiO_2 on the properties of Pd/TiO_2 in the selective acetylene hydrogenation.

5.1. Properties of TiO_2 calcined under hydrogen and air atmosphere.

The anatase nanocrystalline TiO_2 samples were synthesized by a sol-gel method and subjected to thermal treatment under air and H_2 atmospheres at 350°C. The properties of TiO_2 supports after calcined were investigated by X-ray powder diffraction, N_2 physisorption, electron spin resonance (ESR) and X-ray photoelectron spectroscopy (XPS).

5.1.1 X-ray diffraction (XRD)

The sol-gel method was used for preparation of TiO_2 nanoparticles. TiO_2 supports were calcined under H_2, and air at 350°C. The properties of the samples were obtained from the N_2 physisorption and XRD data. The measurements were carried out at the diffraction the angles (2**Θ**) between 20° and 80°. Broadening of the diffraction peaks were used to estimate crystallite diameter from Scherrer Equation **(APPENDIX B)**. The XRD patterns of TiO_2 calcined in H_2 and air atmospheres are shown in **Figure 5.1**. All samples exhibited anatase phase peaks at 25°, 37°, 48°, 55°, 56°, 62°, 71°, and 75° 2**Θ** and the peak at 30.81° corresponded to brookite phase TiO_2. A mixture of anatase/brookite polymorphs was often found on nano-TiO_2 powder prepared by a sol–gel method at a sintering temperature of 350°C [60]. The average crystallite sizes of TiO_2 supports calcined under different atmosphere calculated from the full width at half maximum of peak at 2**Θ** =25° using Scherrer equation. The crystal sizes of the anatase TiO_2 calcined under H_2 and air at 350°C were around 4-4.2 nm. The XRD patterns of the catalysts calcined under different calcination atmosphere were very similar, which suggests that the catalysts still maintained the well-ordered nanostructure XRD patterns of the calcined TiO_2 samples.

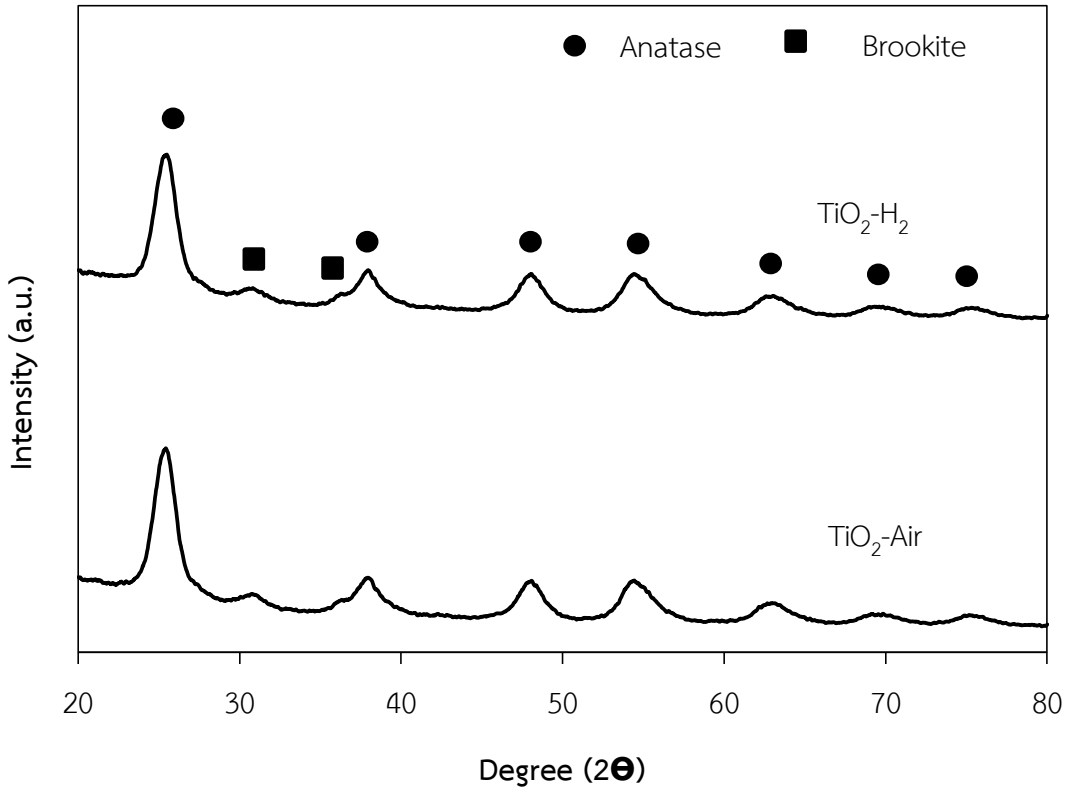

Figure 5.1 The XRD patterns of TiO_2 calcined under H_2 and Air atmosphere.

5.1.2 N_2-physisorption

The BET surface area, pore diameter and pore volume of the TiO_2 calcined under H_2 and air atmospheres at 350°C were 187 and 198 m^2/g with pore volume 0.3 cm^3/g and average pore diameter 4.7 nm. The N_2 adsorption isotherms of TiO_2 calcined under H_2 and air atmospheres are shown in **Figure 5.2.** All of the TiO_2 supports exhibited type-IV isotherm with hysteresis loop, describing the characteristic of mesoporous materials with pore diameters between 2 and 50 nm. The shape of hysteresis loop of all the catalysts was type H1, which corresponded to narrow distribution of relatively uniform pores. The calcination atmosphere did not have any influence on the structural properties of the sol–gel derived TiO_2.

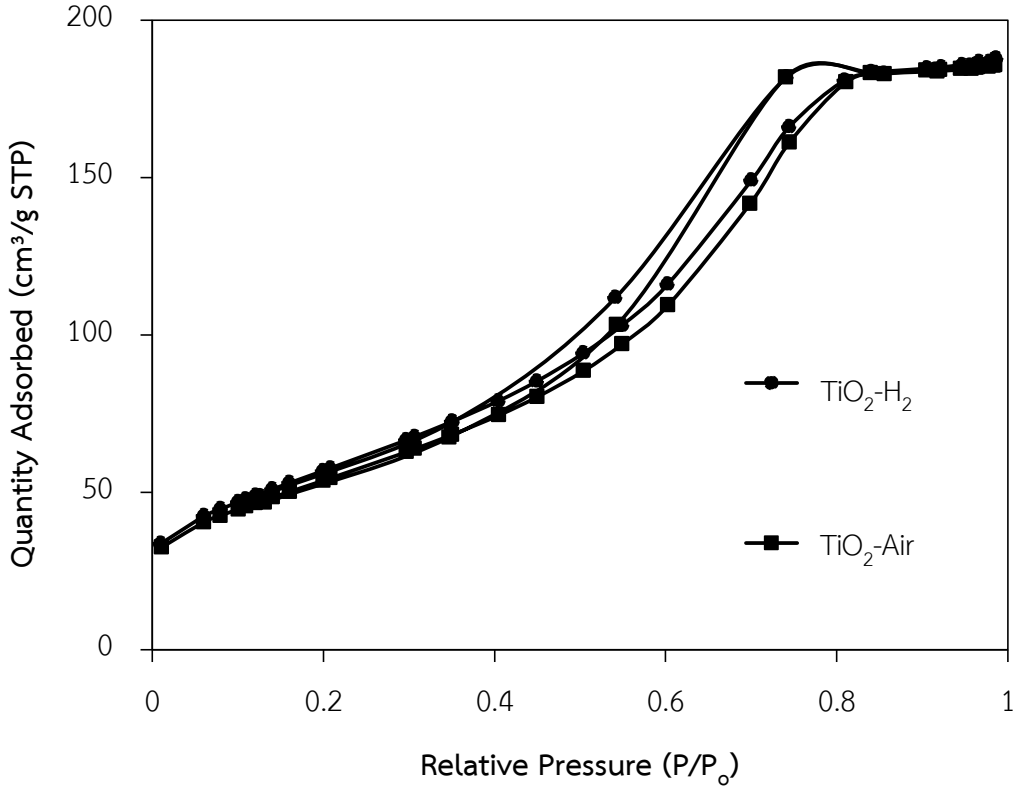

Figure 5.2 N_2 adsorption isotherm of TiO_2 calcined under H_2 and air atmospheres.

Table 5.1 Physicochemical properties of TiO_2

Catalysts	Crystallite size[a] of TiO_2 (nm)	BET surface area (m^2/g)	Pore volume[b] (cm^3/g)	Avg. pore[b] diameter (nm)
TiO_2-H_2	4.0	198	0.30	4.8
TiO_2-Air	4.2	187	0.29	4.7

[a] Based on the XRD results.

[b] Based on BJH method

5.1.3 Electron Spin Resonance (ESR)

The number of defective sites of TiO_2 was determined using electron spin resonance spectroscopy technique. This technique is used for studying chemical species that have one or more unpaired electrons. The ESR spectra of the TiO_2 samples are shown in **Figure 5.3**. The signals of g values less than 2 were assigned to Ti^{3+} (3d1) [61]. Nakaoka and Nosaka [62] reported that six signals of ESR measurement occurring on the surface of titania: (i) $Ti^{4+}O^{-}Ti^{4+}OH^{-}$, (ii) surface Ti^{3+}, (iii) adsorbed oxygen (O^{2-}), (iv) $Ti^{4+}O^{2-}Ti^{4+}O^{2-}$, (v) inner Ti^{3+}, and (vi) adsorbed water. In this study, it is seen that the TiO_2 calcined under H_2 and Air atmosphere exhibited only one signal at g value of 1.975 which can be attributed to Ti^{3+} at the surface. The Ti^{3+} species are produced by trapping of electrons at defective sites in TiO_2 and the accumulated electrons may reflect the number of defective sites [63]. The intensity of the Ti^{3+} signal was increased with TiO_2 was calcined under H_2 atmosphere. The intensity of ESR signal of the TiO_2-H_2 was found to be stronger than the TiO_2-Air and indicating a larger amount of Ti^{3+} defects on theTiO_2 surface. The formation of Ti^{3+} occurred during calcination due to the removal of hydroxyl group. The defect Ti^{3+} on the surface of TiO_2 can be generated by reduction of Ti^{4+} to Ti^{3+} is usually accompanies by oxygen loss from the surface of TiO_2. Ti^{3+} surface defect plays a significant role in enhances the dispersion and stability of the supported metal via the strong interaction between defect sited on the support and metal [63].

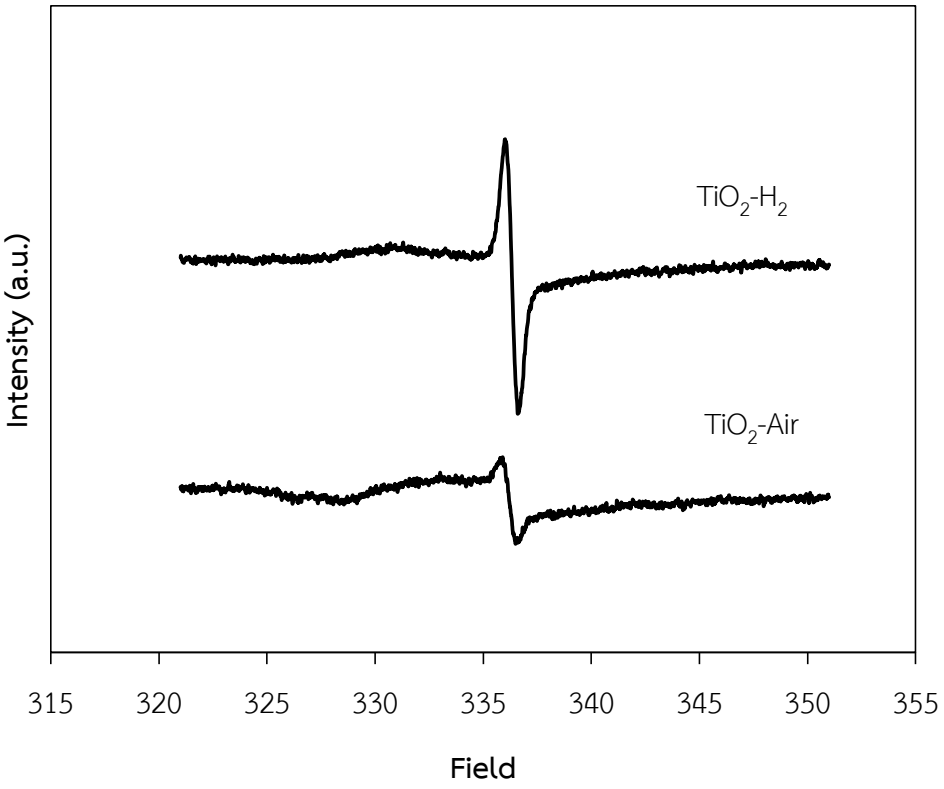

Figure 5.3 The ESR results of TiO_2 calcined under H_2 and Air atmospheres at 350°C.

5.1.4 X-ray photoelectron spectroscopy (XPS)

The survey XPS spectra show the external surface element concentrations which may influence on the catalytic activity. The XPS spectra for anatase TiO_2 samples was recorded with photon energy of 1256 eV (MgK_{α}), the kinetic energies of the emitted electrons being in the range of 0-1000 eV. The binding energy and atomic concentration of Ti 2p and O 1s and the relative concentration of Ti and O on TiO_2 are summarized in **Table 5.2**. The ratios of Ti/O were found in the range of 0.20-0.21. The binding energies of the Ti $2p_{3/2}$ are 458.8 to 459.0 eV and and Ti $2p_{1/2}$ peaks 464.5 to 464.8 eV, indicating of only Ti^{4+} in the TiO_2 [64]. The binding energy of the O1s peak is 530.0 to 530.5 eV.

Table 5.2 The atomic concentration of Ti and O on TiO_2 surface from XPS results.

Catalysts	Ti 2p		O 1s		Atomic concentration		Ti/O
	B.E. (eV)	FWHM	B.E. (eV)	FWHM	Ti	O	
TiO_2-H_2	458.8	1.450	530.2	1.702	13.06	50.26	0.21
TiO_2-Air	458.9	1.511	530.3	1.632	11.72	47.36	0.20

5.2. Properties of 1%Pd/TiO_2 prepared by electroless deposition and incipient wetness impregnation method.

In this section, the sol-gel derived TiO_2, which was calcined under H_2 and air was employed as the supports for preparation of 1%Pd/TiO_2 catalysts and studied in the selective hydrogenation of acetylene at 40-100°C. Deposition of Pd on the TiO_2 supports was prepared by electroless deposition and incipient wetness impregnation. The catalyst properties of the Pd/TiO_2 according to the characterization results from X-ray diffraction (XRD), N_2 physisorption, X-ray photoelectron spectroscopy (XPS), transmission electron microscopy (TEM), H_2 temperature programmed reduction (H_2TPR), infrared spectroscopy of adsorbed CO (CO-IR), and pulse CO chemisorption.

5.2.1 X-ray diffraction (XRD)

The X-ray diffraction petterns of 1%Pd/TiO_2 catalysts prepared by electroless deposition method (ED) and incipient wetness impregnation (I) method are shown in **Figure 5.4**. All Pd/TiO_2 catalysts exhibited TiO_2 anatase phase peaks at 25°, 37°, 48°, 55°, 56°, 62°, 71°, and 75° 2**θ** and brookite phase at 30.81°. There were no changes in the crystalline phase of theTiO_2 after palladium loading for all the catalyst samples. The PdO peak were observed at 2**θ** = 33.8° were appear in the catalysts prepared by electroless deposition method after calcinations step because PdO occurred during in the calcination step in air and no peak of Pd^0 at 2**θ** = 40.2° and 46.7°. The average

crystallite size of TiO_2 after Pd loading around 4-5 nm calculated from Scherrer Equation.

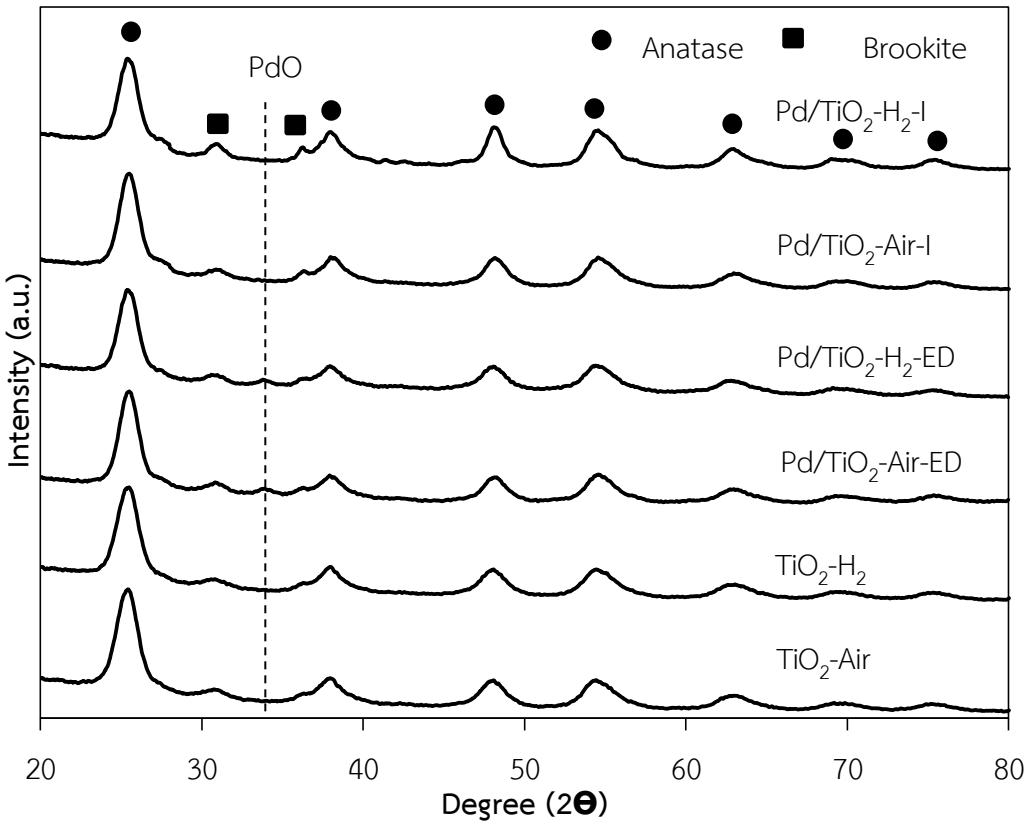

Figure 5.4 The XRD patterns of 1%Pd/TiO_2 prepared by electroless deposition and incipient wetness impregnation.

5.2.2 N_2-physisorption

The surface area, pore volume, and average pore diameter of the 1%Pd/TiO_2 catalysts are shown in **Table 5.3**. There were no significant changes of the average crystallite of anatase phase TiO_2 upon metal loading and calcination at 450°C. However, the BET surface area and pore volume of the TiO_2 supports decreased after the Pd/TiO_2 catalysts prepared by electroless deposition due to pore blockages. The Pd/PdO particles/clusters may locate deep inside the pores of the TiO_2 when prepared by electroless deposition led to lower amount of pore volume. Electroless

deposition is a simple methodology to synthesize supported Pd catalyst with uniform and nano-sized Pd particles. Pd precursor can be interacted directly with the Sn^{2+} ions, and subsequently transformed into Pd nanoparticles deposited on the support.

Table 5.3 Physicochemical properties of 1%Pd/TiO_2 catalysts.

Catalysts	Crystallite size[a] of TiO_2 (nm)	BET surface area (m^2/g)	Pore volume[a] (cm^3/g)	Avg. pore[a] diameter (nm)
1%Pd/TiO_2-H_2-ED	4.2	126	0.19	3.8
1%Pd/TiO_2-Air-ED	4.6	124	0.21	4.1
1%Pd/TiO_2-H_2-I	4.3	144	0.23	4.4
1%Pd/TiO_2-Air-I	4.5	149	0.24	4.6

[a] Based on the XRD results.

[b] Based on BJH method

5.2.3 X-ray photoelectron spectroscopy (XPS)

The surface composition and electronic state surface of Pd/TiO_2 catalysts prepared by electroless deposition and incipient wetness impregnation method were determined by X-ray photoelectron spectroscopy. The XPS spectra for all samples was recorded with photon energy of 1256 eV (MgK_{α}), the kinetic energies of the emitted electrons being in the range of 0-1000 eV. The surface compositions of the catalysts as well as the interaction between Pd and the TiO_2 supports were confirmed by XPS analysis. The binding energies of Pd $3d_{5/2}$ at around 336.6 can be assigned to PdO and Ti $2p_{3/2}$ at around 458.8 to 459.0 eV. The binding energies and atomic concentrations of Ti 2p, O1s and Pd 3d on various Pd/TiO_2 catalysts are given in **Table 5.4**. The binding energy of Ti 2p around 459 eV and O 1s around 530 eV for all catalysts can be attributed to Ti^{4+} and oxygen lattice of TiO_2. The ratio of Pd/Ti surface concentration increased in the order of 1%Pd/TiO_2-H_2-ED> 1%Pd/TiO_2-H_2-I >1%Pd/TiO_2-Air-ED >1%Pd/TiO_2-Air-I, respectively

Table 5.4 The atomic concentration of Pd and Ti on TiO_2 surface from XPS results.

Catalysts	Ti 2p		O 1s		Pd 3d		Atomic concentration			Pd/Ti
	B.E. (eV)	FWHM	B.E. (eV)	FWHM	B.E. (eV)	FWHM	Pd	Ti	O	
TiO_2-H_2	458.9	1.450	530.2	1.702	-	-	-	13.06	50.26	-
TiO_2-Air	458.9	1.511	530.3	1.632	-	-	-	11.72	47.36	-
Pd/TiO_2-H_2-ED	459.0	1.683	530.7	2.444	337.1	1.441	0.36	9.26	53.83	0.038
Pd/TiO_2-Air-ED	458.9	1.485	530.2	1.762	336.2	0.508	0.16	14.07	47.28	0.011
Pd/TiO_2-H_2-I	458.9	1.575	530.3	2.001	336.9	2.154	0.19	13.47	50.71	0.014
Pd/TiO_2-Air-I	459.0	1.640	530.4	2.006	336.4	1.150	0.14	13.64	49.53	0.010

5.2.4 Transmission electron microscopy (TEM)

The TEM images of 1%Pd/TiO_2 catalysts prepared by electroless deposition and incipient wetness impregnation method are shown in **Figure 5.5** (a) 1%Pd/TiO_2-Air-ED, (b) 1%Pd/TiO_2-H_2-ED, (c) 1%Pd/TiO_2-Air-I, and (d) 1%Pd/TiO_2-H_2-I, respectively. The catalyst particles showed spherical shape with average size around 4 to 5 nm which were consistent to those obtained from the XRD results. It is difficult to measure the size of the primary spherical particles accurately. Pd/TiO_2 prepared by electroless deposition method is quite difficult to distinguish Pd/PdO clusters from the TiO_2. However, some agglomeration of metal particles can be seen on the impregnation-made catalysts.

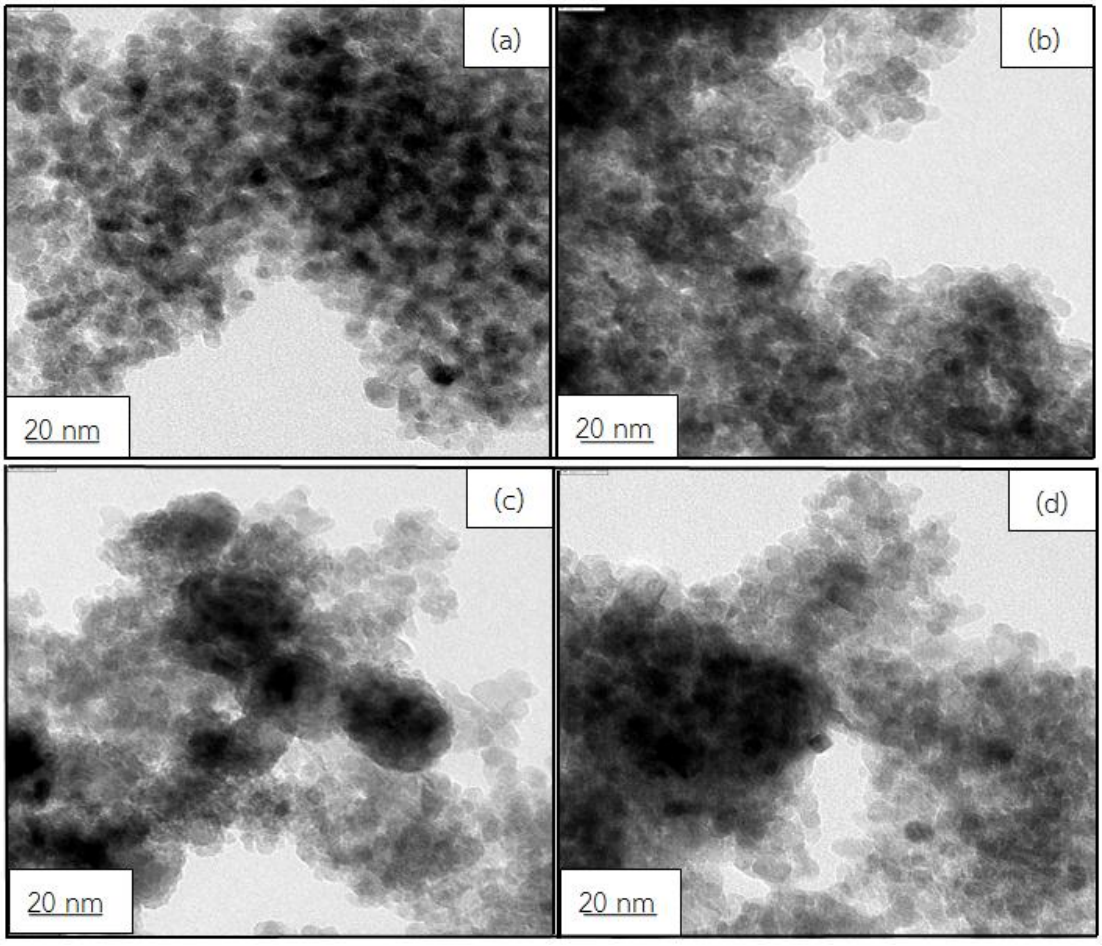

Figure 5.5 Transmission electron microscopy of 1%Pd/TiO_2 catalysts.

5.2.5 Hydrogen Temperature program reduction (H_2-TPR)

Temperature program reduction of hydrogen measurements was executed to study the reduction behaviors of palladium catalysts. The TPR profiles of Pd supported on TiO_2 are shown in **Figure 5.6**. The palladium catalysts distinctly presented two overlap peaks of reduction located at ca. 30-500°C (a) Pd/TiO_2-H_2-ED, (b) Pd/TiO_2-Air-ED, (c) Pd/TiO_2-Air-I, and (d) Pd/TiO_2-H_2-I. The negative peak at about 80°C is due to the hydrogen desorption on palladium [65]. The large peak observed between 300 and 450°C is due to the reduction of TiO_2. The presence of noble metal should enhance the reduction of TiO_2. The TPR profiles of Pd/TiO_2 peak appeared at about 300°C can be assigned to Ti^{4+} reduced to Ti^{3+} in the presence of Pd even at lower reduction temperature, which is caused by the dissociatively chemisorbed hydrogen on palladium diffusing from Pd to TiO_2 and reducing Ti^{4+} to Ti^{3+}. The peak at 450°C appeared at the TPR profiles shows that Ti^{4+} can be reduced to Ti^{3+} [66]. The TPR profiles of all catalysts exhibited similar peak position. Pd/TiO_2 catalyst which TiO_2 calcined in H_2 atmosphere facilited H_2 reduction at lower temperature.

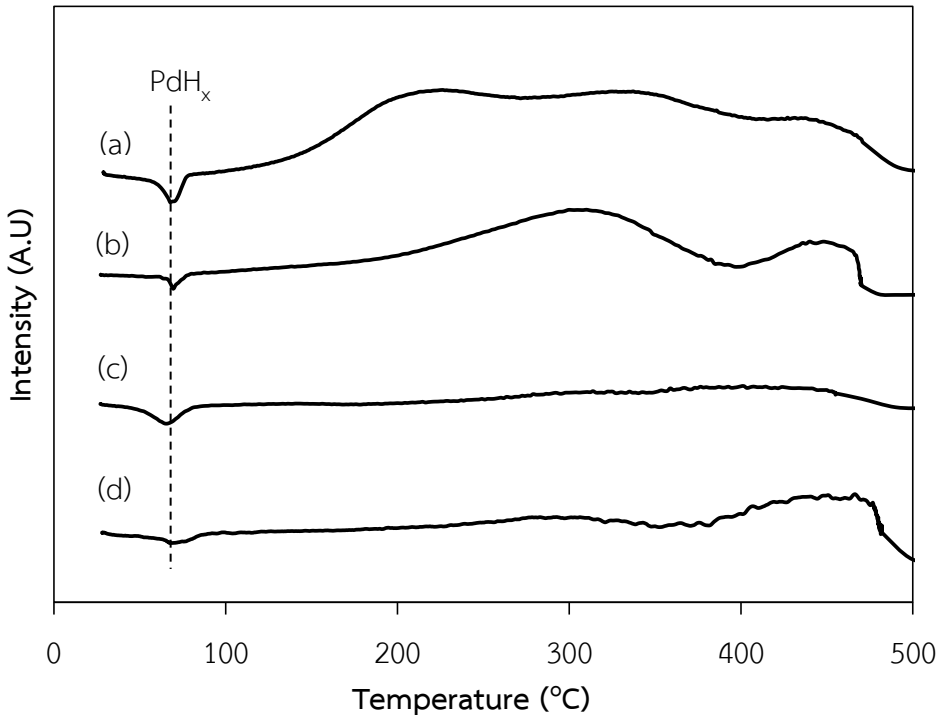

Figure 5.6 The H_2-TPR profiles of Pd catalysts

5.2.6 Infrared spectroscopy of adsorbed CO (CO-IR)

The amount of Pd active sites is usually calculated from chemisorption results based on the assumption that only CO molecule adsorbs on one Pd site (Anderson et al., 1985), however, various CO adsorbed species are actually present on metallic Pd. From the literatures [67], the IR spectra of adsorbed CO show typical four peaks corresponding to different CO adsorbed species on Pd surface including linear (2100–2050 cm^{-1}), compressed-bridged (1995–1975 cm^{-1}), isolated-bridged (1960–1925 cm^{-1}), and tri-coordinated (1890–1870 cm^{-1}) species. **Figure 5.7** shows the IR spectra of adsorbed CO on the various Pd/TiO_2 catalysts. The area ratio (A_l/A_m) of the peaks corresponding to linearly and multiply bound CO. The A_l/A_m ratios increased in the order of Pd/TiO_2–H_2-ED > Pd/TiO_2–H_2-I > Pd/TiO_2–Air-ED ≈ Pd/TiO_2–Air-I are given in **Table 5.5**. The low-coordination sites are low in electron density compared with the high-coordination sites such as the Pd (1 1 1), allow the desorption of highly active subsurface hydrogen and also the preferential adsorption of electron-rich hydrocarbons such as acetylene. The reaction between the highly active hydrogen and acetylene at high-coordination lead to the full hydrogenation of acetylene to ethane, while the reaction on the low-coordination Pd sites is lower the ethylene selectivity [68].

Table 5.5 Normalized peak area of various CO adsorbed species from the CO-IR results on 1% Pd/TiO_2 catalysts.

Catalyst	Tri-coordinated	Isolated-bridged	Compressed-bridged	Linear	A_l/A_m *
Pd/TiO_2-H_2-(ED)	0.12	0.46	0.06	0.36	0.52
Pd/TiO_2-Air-(ED)	0.19	0.6	0.15	0.06	0.06
Pd/TiO_2-H_2-(I)	0.17	0.55	0.07	0.21	0.27
Pd/TiO_2-Air-(I)	0.55	0.3	0.07	0.08	0.09

* Al: peak area of linear-bound CO and Am: peak area of multi-bound CO

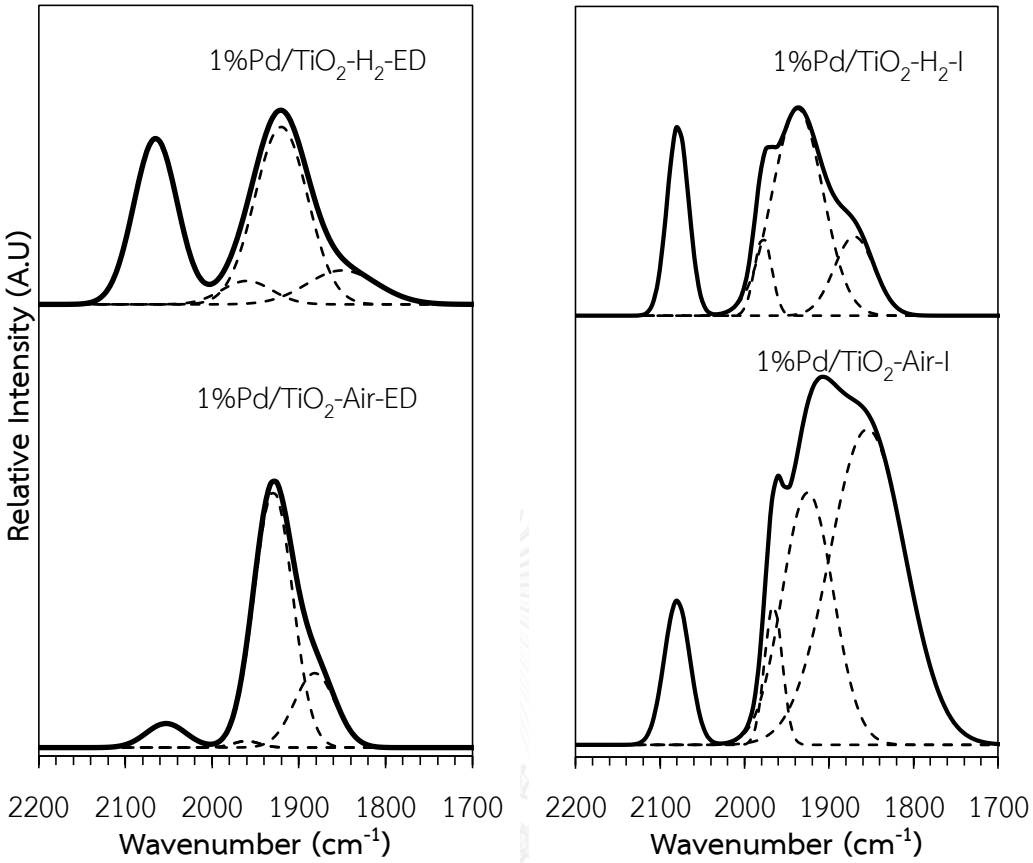

Figure 5.7 CO-IR spectra of 1%Pd/TiO_2 catalysts.

5.2.7 CO-pulses chemisorption

Metal dispersion is evaluated by measuring chemisorption of CO. The amounts of CO chemisorption on the 1 wt% Pd/TiO_2 prepared by electroless deposition method and incipient wetness impregnation method were reduced at 150^{o}C and The amount of Pd active sites is usually calculated from chemisorption results based on the assumption that only CO molecule is adsorbed on one Pd site, however, various CO species are actually adsorbed on metallic Pd. The CO chemisorption results of 1%Pd/TiO_2 catalysts are also given **Table 5.6**. The Pd catalysts supported on TiO_2-H_2 exhibited larger amounts of CO chemisorption than TiO_2-Air supported of both preparation methods due to TiO_2 support calcined under H_2 atmosphere exhibited high amount of Ti^{3+} on the surface of TiO_2 lead to the high

dispersion of metal. The Pd dispersion was increased in the order: 1%Pd/TiO_2–H_2-ED > 1%Pd/TiO_2–H_2-I > 1%Pd/TiO_2–Air-ED > 1%Pd/TiO_2–Air-I.

Table 5.6 CO chemisorption results of 1%Pd/TiO_2 catalysts.

Catalysts	CO Chemisorption (x 10^{19} molecule CO/ g.)	Pd dispersion (%)	$d_P Pd^0$ (nm)
1%Pd/TiO_2-H_2-ED	4.0	69	1.1
1%Pd/TiO_2-Air-ED	3.2	56	2.0
1%Pd/TiO_2-H_2-I	3.7	65	1.7
1%Pd/TiO_2-Air-I	2.3	39	2.8

5.3. Reaction study in selective hydrogenation of acetylene.

5.3.1. 1%Pd/TiO_2 prepared by electroless deposition and incipient wetness impregnation method with TiO_2 calcined under hydrogen and air atmosphere.

The catalytic performance of 1 wt% Pd catalysts supported on sol-gel derived TiO_2 calcined under H_2 and air were investigated in the selective hydrogenation of acetylene. Acetylene hydrogenation was performed in a pyrex tube reactor, the catalysts were reduced with hydrogen at 150°C for 2h. The reactant gas mixture composed of 1.5% C_2H_2, 1.7% H_2, and balanced C_2H_4. The C_2H_2 conversion is defined as the ratio of moles of C_2H_2 converted with moles of C_2H_2 in feed. Ethylene selectivity is defined as the percentage of acetylene hydrogenated to ethylene over totally hydrogenated acetylene (**APPENDIX F**). The ethylene being hydrogenated to ethane (ethylene loss) is the difference between all the hydrogen consumed and all the acetylene which has been totally hydrogenated. **Figure 5.8** shows the acetylene conversion as a function of reaction temperature for 1% Pd/TiO_2 catalysts with different preparation method. The conversion of acetylene for 1%Pd/TiO_2-H_2-ED and

was 100% after 100°C. The catalyst performance plots are illustrated in **Figure 5.10**. Since ethylene is produced as an intermediate in acetylene hydrogenation, which is a typical consecutive reaction, the ethylene selectivity decreases with acetylene conversion. High ethylene selectivity (~94%) can be obtained at complete acetylene conversion (100%) over 1 wt.% Pd/TiO_2-H_2-ED and 1 wt.% Pd/TiO_2-H_2-I. For the same preparation method, the 1 wt.% Pd/TiO_2-H_2 showed higher Pd dispersion than 1 wt.% Pd/TiO_2-Air and, as a consequence, they exhibited higher hydrogenation activity. Because all the prepared TiO_2 supports possessed similar average crystallite size, BET surface area, pore volume, and pore diameter, the higher Pd dispersion on the catalysts supported on H_2-treated sol-gel TiO_2 was attributed to the larger amount of surface Ti^{3+} on the TiO_2 supports. The higher defects could lead to numerous crystal boundaries, where a larger number of Pd atoms can be deposited; hence higher Pd dispersion was obtained. As can be seen from **Figure 5.9**, ethylene selectivity was higher on the Pd catalysts supported on H_2-treated TiO_2 than Pd/TiO_2-Air, regardless of the preparation method used. Ethylene selectivity over Pd-based catalysts was found to increase with increasing A_l/A_m ratio. It has been rationalized that the presence of more isolated adsorption sites could be responsible for the increased selectivity to ethylene[68]. The number of isolated adsorption sites was greatly enhanced on the H_2-treated sol-gel TiO_2 supports than the ones calcined in air. The presence of surface Ti^{3+} led to a well-defined homogeneous distribution of the active sites, probably via the covalent bonding between Pd and Ti. The growth of Pd crystallite size lowered the A_l/A_m ratio. In addition, diffusion of Ti^{3+} from the lattice of TiO_2 to surface Pd particles has shown to result in the SMSI effect so that the adsorption strength of ethylene is weakened.

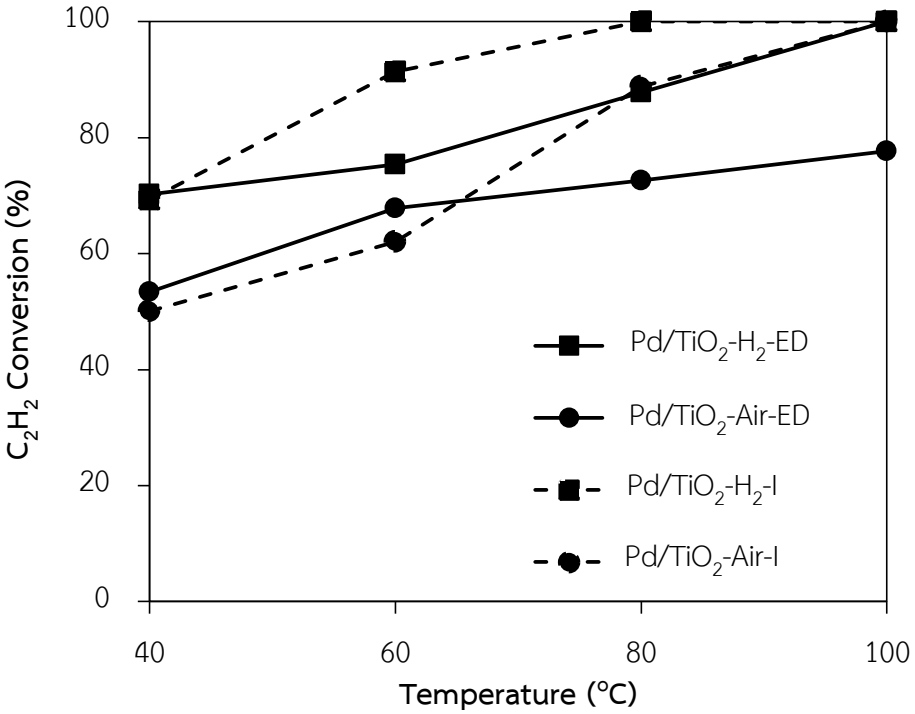

Figure 5.8 Acetylene conversion as a function of reaction temperature for 1% Pd/TiO_2 catalysts prepared by electroless deposition method

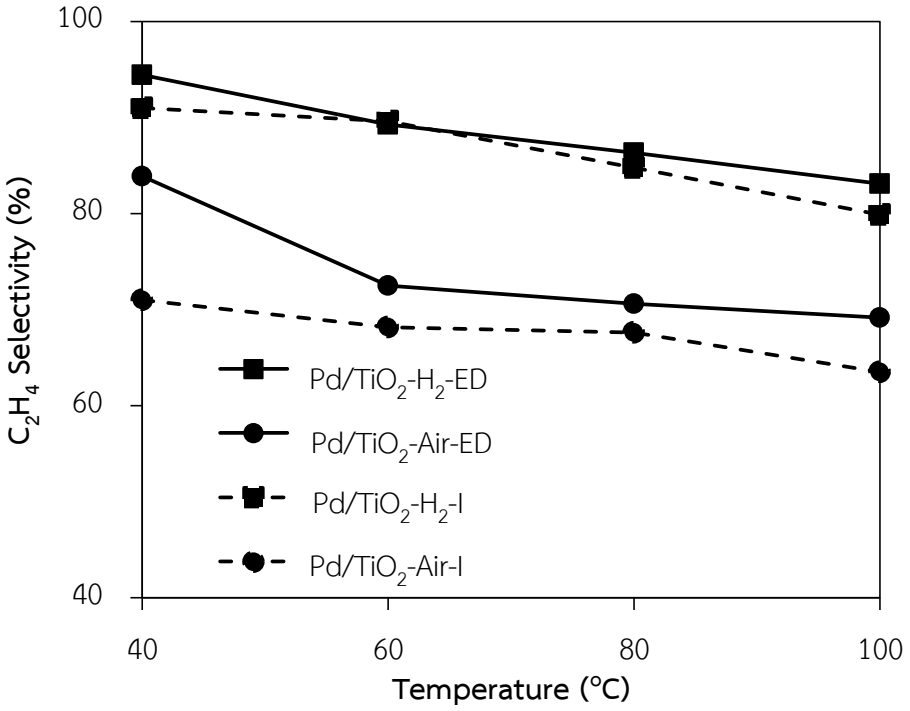

Figure 5.9 Ethylene selectivity as a function of reaction temperature for 1% Pd/TiO_2 catalysts.

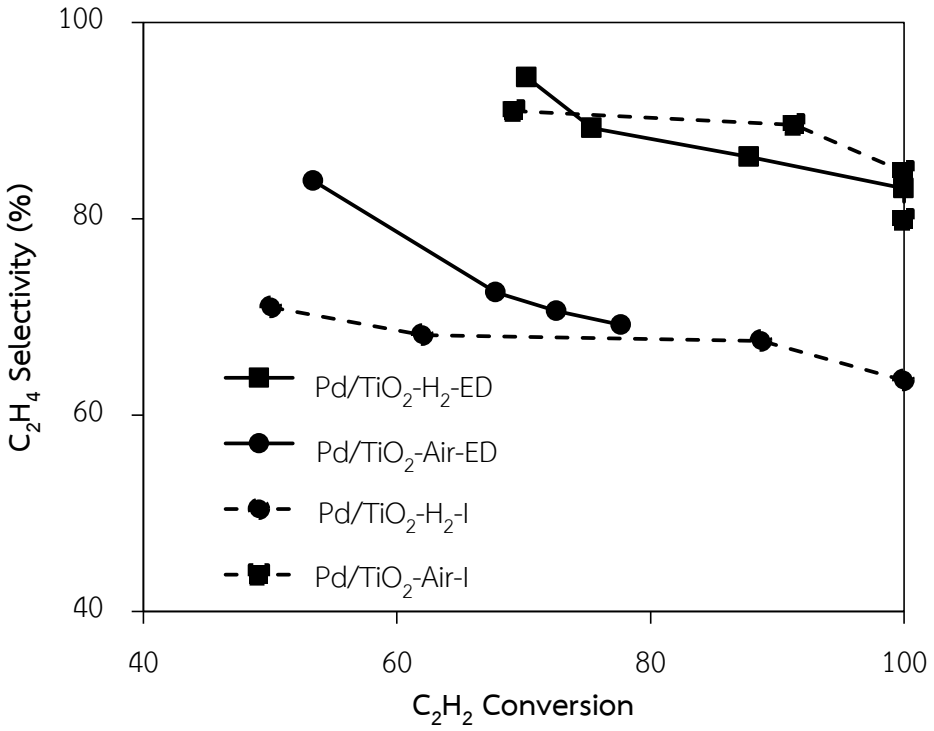

Figure 5.10 The catalytic performance of 1%Pd/TiO_2 catalyst in the selective hydrogenation of acetylene.

.

5.4. Properties of TiO_2 calcined under Nitrogen and Oxygen atmosphere.

In this section, the effect of calcination atmosphere was further investigated under N_2 and O_2 atmosphere. The anatase nanocrystalline TiO_2 samples were synthesized by a sol-gel method with a thermal treatment under N_2 and O_2 atmospheres at 350°C. The properties of TiO_2 supports after calcined were investigated by X-ray powder diffraction, N_2 physisorption, electron spin resonance (ESR) and X-ray photoelectron spectroscopy (XPS).

5.4.1 X-ray diffraction (XRD)

The sol-gel method was used for preparation of TiO_2 nanoparticles. The TiO_2 supports were prepared by sol-gel and calcined under N_2 and O_2 at 350°C. The properties of the samples were obtained from the N_2 physisorption and XRD data. The measurements were carried out at the diffraction the angles (2**θ**) between 20° and 80°. Broadening of the diffraction peaks were used to estimate crystallite diameter from Scherrer Equation. The XRD patterns of TiO_2 supports prepared by sol-gel method and calcined under O_2 and N_2 are shown in **Figure 5.11**. The XRD characteristic peaks of anatase TiO_2 were presented at 2**θ** = 25° (major), 37°, 48°, 55°, 56°, 62°, 71°, and 75° and the peak at 30.81° 2**θ** corresponded to brookite phase TiO_2. The crystal size of the anatase TiO_2 calcined at 350°C under different calcination atmospheres was similar at 4 nm.

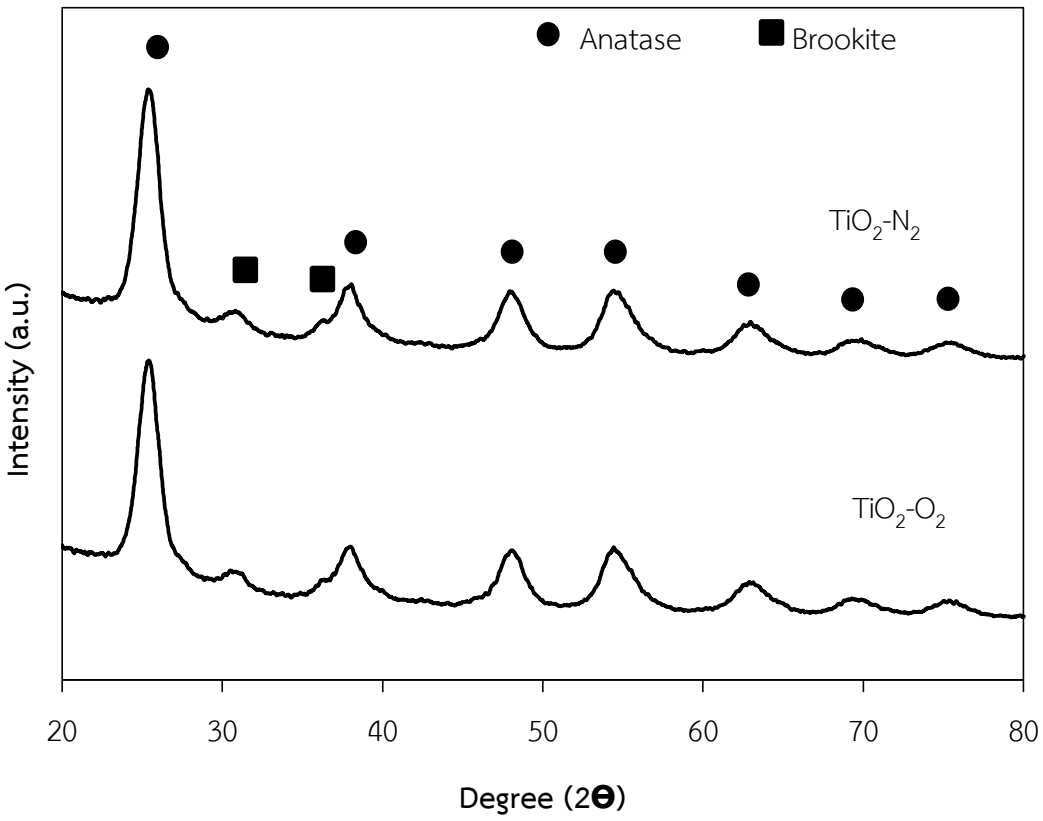

Figure 5.11 The XRD patterns of TiO_2 calcined under N_2 and O_2 atmosphere.

5.4.2 N_2-physisorption

The BET surface area, pore diameter and pore volume of the TiO_2 calcined under N_2 and O_2 and air atmospheres at 350°C were 185-210 m^2/g with pore volume 0.3 cm^3/g and average pore diameter 4.3 nm. The N_2 adsorption isotherm of TiO_2 calcined under N_2 and O_2 atmospheres are shown in **Figure 5.12.** All of the TiO_2 supports exhibited type-IV isotherm with hysteresis loop, describing the characteristic of mesoporous materials with pore diameters between 2 and 50 nm. The shape of hysteresis loop of all the catalysts was type H1, which corresponded to narrow distribution of relatively uniform pores. The calcination atmosphere did not have any influence on the structural properties of the sol–gel derived TiO_2.

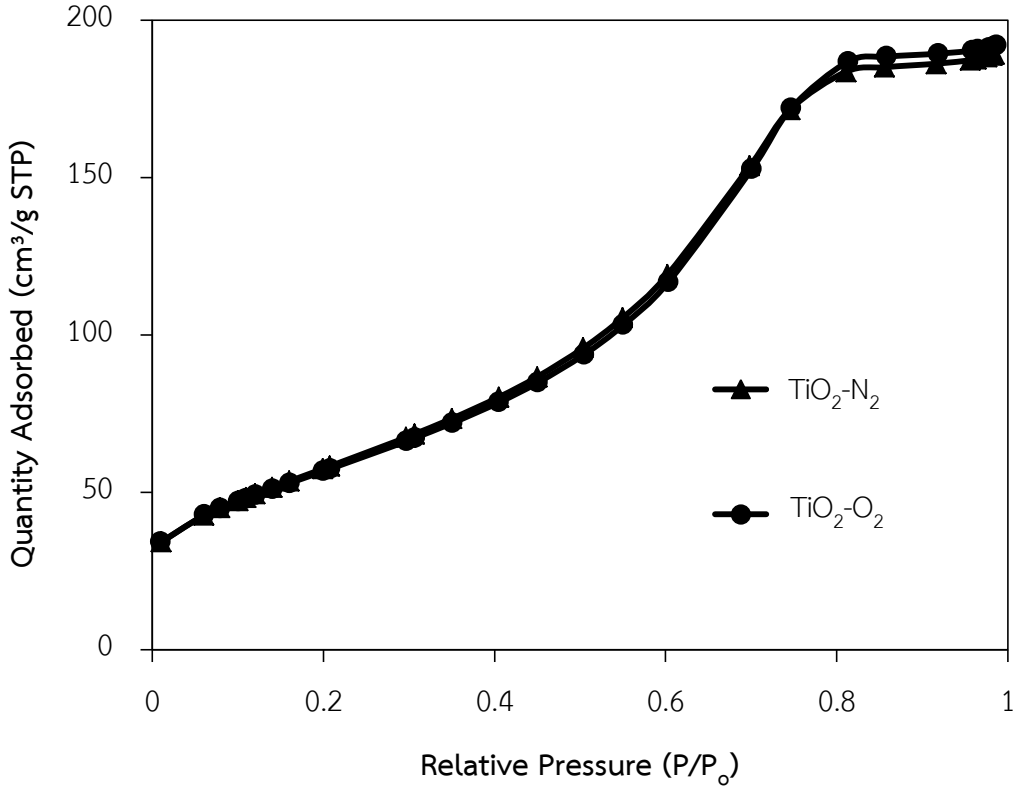

Figure 5.12 N_2 adsorption isotherm of TiO_2 calcined under N_2 and O_2 atmospheres.

Table 5.7 Physicochemical properties of TiO_2

Catalysts	Crystallite size[a] of TiO_2 (nm)	BET surface area (m^2/g)	Pore volume[b] (cm^3/g)	Avg. pore[b] diameter (nm)
TiO_2-N_2	4.2	210	0.32	4.3
TiO_2-O_2	4.1	208	0.29	4.3

[a] Based on the XRD results.

[b] Based on BJH method

5.4.3 Electron Spin Resonance (ESR)

The number of defective sites of TiO_2 was determined using electron spin resonance spectroscopy technique. The ESR results of the TiO_2 samples calcined under O_2 and N_2 atmosphere are shown in **Figure 5.13**. The formation of Ti^{3+} occurred during calcination due to the removal of hydroxyl group. The defect Ti^{3+} on the surface of TiO_2 can be generated by reduction of Ti^{4+} to Ti^{3+} is usually accompanies by oxygen loss from the surface of TiO_2. The defect of Ti^{3+} on surface plays a significant role in enhances the dispersion and stability of the supported metal via the strong interaction between defect sited on the support and metal [63].

The supports exhibited one major signal at g value of 1.975, which can be attributed to Ti^{3+} at the surface. The Ti^{3+} species are produced by trapping of electrons at defective sites in TiO_2 and the accumulated electrons may reflect the number of defective sites. The results clearly show that the TiO_2-N_2 possessed more Ti^{3+} defective sites than TiO_2-O_2. The higher metal dispersion has been correlated with the presence of Ti^{3+} on the TiO_2 supports. The intensity of ESR signal of the TiO_2-N_2 was found to be stronger than the TiO_2-O_2, indicating a larger amount of Ti^{3+} defects on theTiO_2 surface.

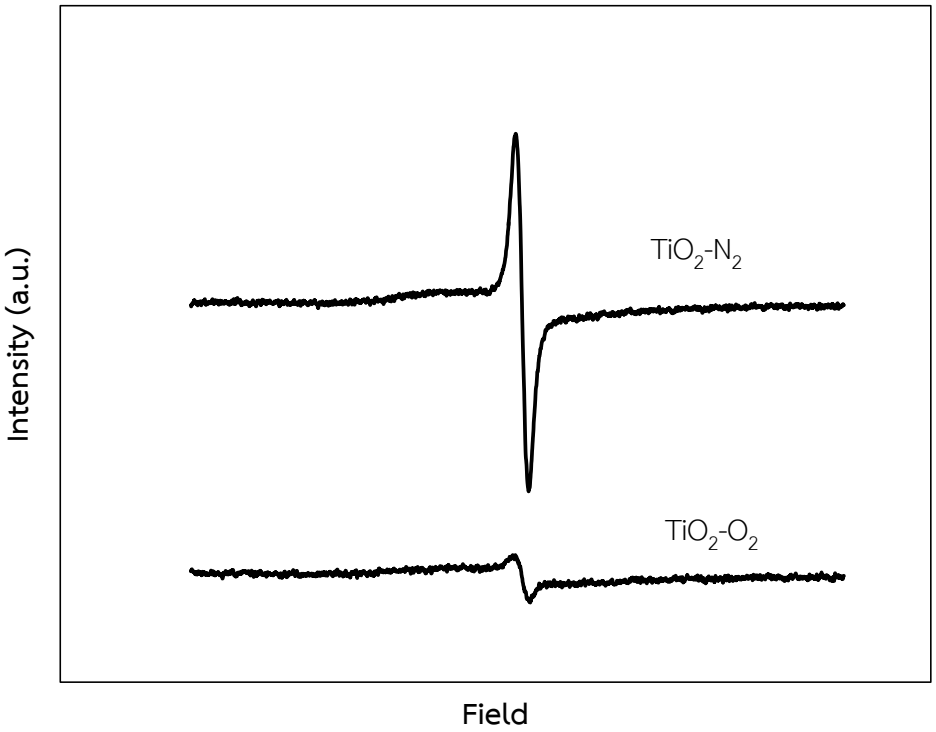

Figure 5.13 The ESR results of TiO_2 calcined under N_2 and O_2 atmospheres at 350°C.

5.4.4 X-ray photoelectron spectroscopy (XPS)

The survey XPS spectra convince the external surface element concentrations influence on the catalytic activity. The XPS spectra for anatase TiO_2 samples was recorded with photon energy of 1256 eV (MgK_α), the kinetic energies of the emitted electrons being in the range of 0-1000 eV. The binding energies of the Ti $2p_{3/2}$ are 458.8 to 459.0 eV and Ti $2p_{1/2}$ peaks 464.5 to 464.8 eV, indicating of only Ti^{4+} in the TiO_2 [64]. The binding energy of the O1s peak is 530.0 to 530.5 eV. The survey XPS spectra were obtained in order to determine the concentration of surface elements of Ti and O on TiO_2 and the results are also given in **Table 5.8**. It can be seen that for a similar TiO_2 supports (N_2 or O_2 treated), the ratios of Ti/O were found in the range of 0.20-0.25.

Table 5.8 The atomic concentration of Ti and O on TiO_2 surface from XPS results.

Catalysts	Ti 2p		O 1s		Atomic concentration		Ti/O
	B.E. (eV)	FWHM	B.E. (eV)	FWHM	Ti	O	
TiO_2-N_2	458.8	1.395	530.1	1.630	12.44	37.49	0.25
TiO_2-O_2	458.9	1.386	530.1	1.625	12.30	50.26	0.20

5.5. Properties of 1%Pd/TiO_2 prepared by electroless deposition and incipient wetness impregnation method.

In this section, the properties of 1%Pd/TiO_2 catalysts by electroless deposition and impregnation method via sol-gel derived TiO_2, which was calcined under N_2, and O_2 atmosphere for selective hydrogenation of acetylene at 40-100°C are reported. The catalyst properties of the Pd/TiO_2 catalysts according to the characterization results from X-ray diffraction (XRD), transmission electron microscopy (TEM), N_2 physisorption, X-ray photoelectron spectroscopy (XPS), infrared spectroscopy of adsorbed CO (CO-IR), H_2 temperature programmed reduction (H_2TPR) and CO pulse chemisorption.

5.5.1 X-ray diffraction (XRD)

The XRD patterns of 1%Pd/TiO_2 catalysts prepared by electroless deposition and impregnation methods are shown in **Figure 5.14**. The measurements were carried out at the diffraction the angles (2**Θ**) between 20° and 80°. Broadening of the diffraction peaks was used to estimate the average crystallite diameter from the Scherrer equation and the average crystalline size after Pd loading around 4-5 nm. The XRD characteristic peaks of anatase TiO_2 were presented at 2**Θ** = 25° (major), 37°, 48°, 55°, 56°, 62°, 71°, and 75° and the peak at 30.81° 2**Θ** corresponded to brookite phase TiO_2. After Pd loading were no changes in the crystalline phase of theTiO_2 of all the catalyst samples. No peak of Pd^0 at 2**Θ** = 40.2° and 46.7° and observed PdO

peak at 2**θ** = 33.8° were observed in all Pd/TiO_2 samples method after calcinations step because PdO occurred during in the calcination step in air.

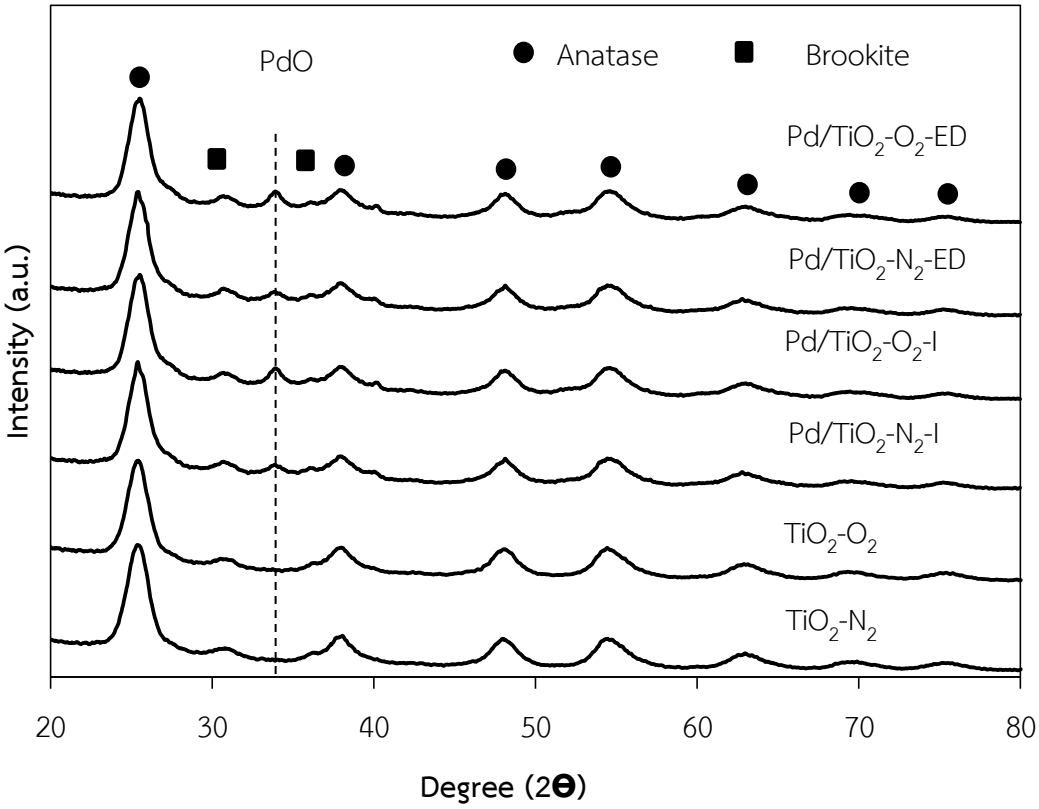

Figure 5.14 The XRD patterns of 1%Pd/TiO_2 catalysts.

5.5.2 N_2-physisorption

The average TiO_2 crystallite size, BET surface area, pore volume, and pore diameter. The BET surface area of Pd/TiO_2 with TiO_2 calcined under O_2, and N_2 atmospheres were 156-125 m^2/g with pore volume ~ 0.22 cm^3/g and average pore diameter ~3.8 nm are given **Table 5.9**. However, the BET surface area and pore volume of the Pd/TiO_2 decreased after metal loading due to pore blockages. The decrease in pore volume was seen for all the catalysts after Pd loading with no significant change in the average pore diameter. The average crystallite sizes of anatase phase TiO_2 after Pd loading and calcination at 450°C for 3 h were 4-5 nm. Compared to the ones prepared by impregnation method and preparation by

electroless deposition resulted in lower pore volume with the Pd/TiO_2 calcined in N_2 showed the least pore volume.

Table 5.9 Physicochemical properties of 1% Pd/TiO_2 catalysts.

Catalysts	Crystallite size[a] of TiO_2 (nm)	BET surface area (m^2/g)	Pore volume[a] (cm^3/g)	Avg. pore[a] diameter (nm)
1%Pd/TiO_2-N_2-ED	4.2	139	0.21	3.74
1%Pd/TiO_2-O_2-ED	4.6	125	0.17	3.90
1%Pd/TiO_2-N_2-I	4.3	156	0.24	3.81
1%Pd/TiO_2-O_2-I	4.5	154	0.24	3.91

[a] Based on the XRD results.

[b] Based on BJH method

5.5.3 X-ray photoelectron spectroscopy (XPS)

The surface composition and electronic state of Pd/TiO_2 catalysts were determined by X-ray photoelectron spectroscopy. The XPS spectra for Pd/TiO_2 samples was recorded with photon energy of 1256 eV, the kinetic energies of the emitted electrons being in the range of 0-1000 eV. The surface compositions of the catalysts as well as the interaction between Pd and the TiO_2 supports were confirmed by XPS analysis. The survey XPS spectra were obtained in order to determine the concentration of surface elements on the Pd/TiO_2 catalysts and the results are also given in **Table 5.10**. It can be seen that for a similar TiO_2 supports (N_2 or O_2 treated), the Pd/Ti ratios of the Pd/TiO_2 catalysts prepared by electroless deposition were lower than those prepared by impregnation method. In addition, regardless of the preparation method, the use of N_2-treated TiO_2 resulted in lower Pd/Ti ratio (0.02-0.05) than O_2-treated ones (0.09-0.10). The XPS results exhibited the binding energy of Ti 2p around 459.0 eV, O 1s around 530.4 eV and Pd 3d around 366.9 for all catalysts can be attributed to Ti^{4+}, oxygen lattice of TiO_2 and PdO.

Table 5.10 The atomic concentration of Pd and Ti on TiO_2 surface from XPS results.

Catalysts	Ti 2p		O 1s		Pd 3d		Atomic concentration[a]			Pd/Ti
	B.E. (eV)	FWHM	B.E. (eV)	FWHM	B.E. (eV)	FWHM	Pd	Ti	O	
Pd/TiO_2-O_2-ED	459.0	1.720	530.3	2.302	336.5	1.752	0.2	9.58	53.43	0.02
Pd/TiO_2-N_2-ED	459.0	1.558	530.5	1.883	336.5	1.752	1.09	11.32	48.28	0.09
Pd/TiO_2-O_2-I	459.0	1.829	530.3	2.595	336.9	1.742	0.39	8.59	56.70	0.05
Pd/TiO_2-N_2-I	459.0	2.032	530.4	2.516	337.1	2.193	1.33	12.11	54.04	0.10

5.5.4 Transmission electron microscopy (TEM)

The morphologies of 1%Pd/TiO_2 catalysts were investigated by the transmission electron microscopy (TEM). The particles of TiO_2 products by sol-gel synthesis showed spherical shape with average size around 4-5 nm which were consistent to those obtained from the XRD results. Pd/TiO_2 particles are aggregated into clusters, it is difficult to measure the size of the primary spherical particles accurately. Pd/TiO_2 prepared by electroless deposition method is quite difficult to distinguish metal from the TiO_2 supports. However, catalyst prepared by impregnation can be seen some agglomeration of metal particles. The morphologies of 1%Pd/TiO_2 catalysts are shown in **Figure 5.15** (a) 1%Pd/TiO_2-O_2-ED, (b) 1%Pd/TiO_2-N_2-ED, (c) 1%Pd/TiO_2-O_2-I, and (d) 1%Pd/TiO_2-N_2-I, respectively.

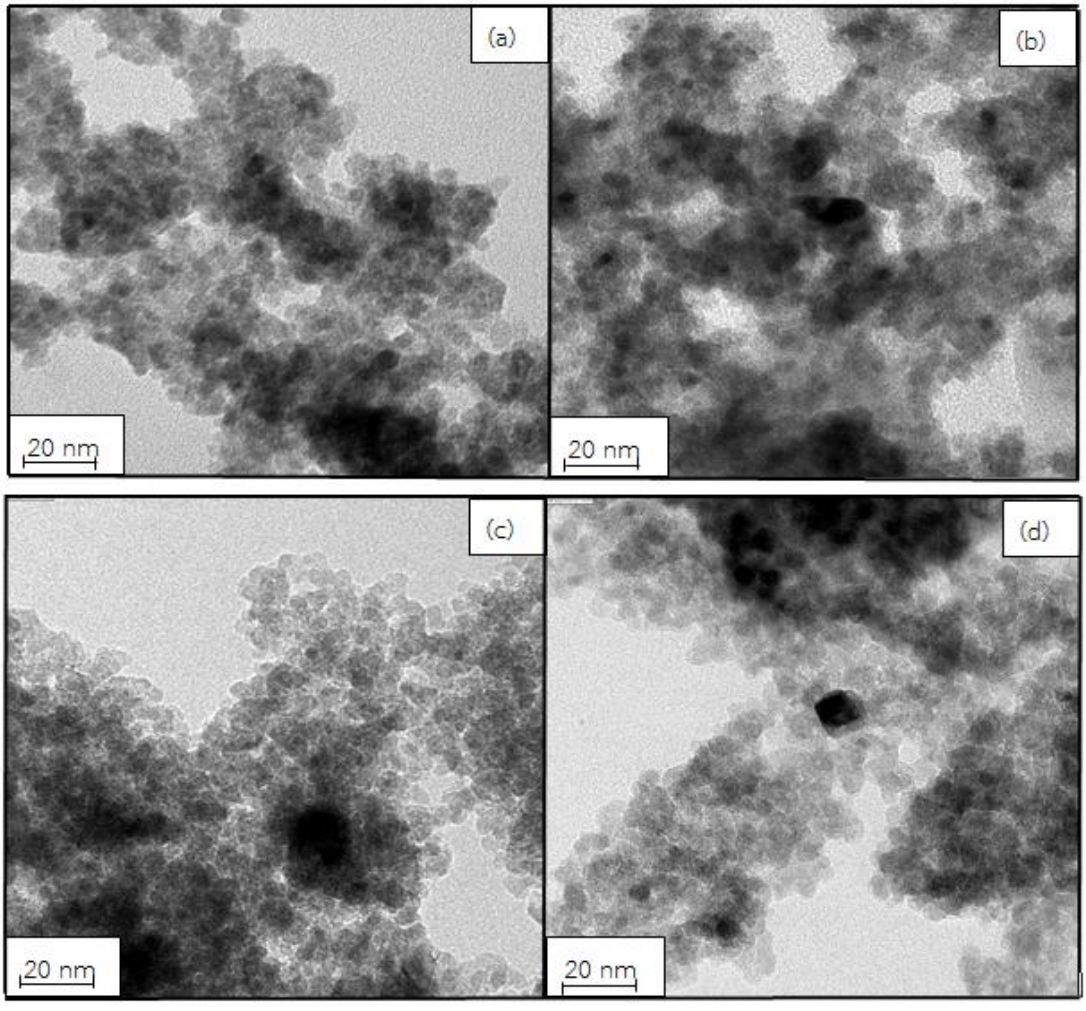

Figure 5.15 Transmission electron microscopy of Pd/TiO_2 catalysts.

5.5.5 Hydrogen Temperature program reduction (H_2-TPR)

The H_2-TPR measurements were carried out to study the reduction behaviors of palladium catalysts. The TPR profiles of Pd catalysts supported on different TiO_2 are shown in **Figure 5.16**. The palladium catalysts distinctly presented two overlap peaks of reduction located at ca. 30-500°C, the negative peak at about 80°C is due to the release of hydrogen from the decomposition of palladium hydride species. The large peak observed between 300 and 450°C is due to the reduction of TiO_2. The TPR profiles of Pd/TiO_2 peak appeared at about 300°C at the TPR profiles of four catalysts, this result suggests that Ti^{4+} can be reduced to Ti^{3+} in the presence of Pd even at lower reduction temperature, which is caused by the dissociatively chemisorbed hydrogen on palladium diffusing from Pd to TiO_2 and reducing Ti^{4+} to Ti^{3+}. The peaks at 450°C assign to Ti^{4+} reduce to Ti^{3+}. Pd/TiO_2 catalyst which TiO_2 calcined in N_2 facilitated the reduction of H_2 at lower temperature.

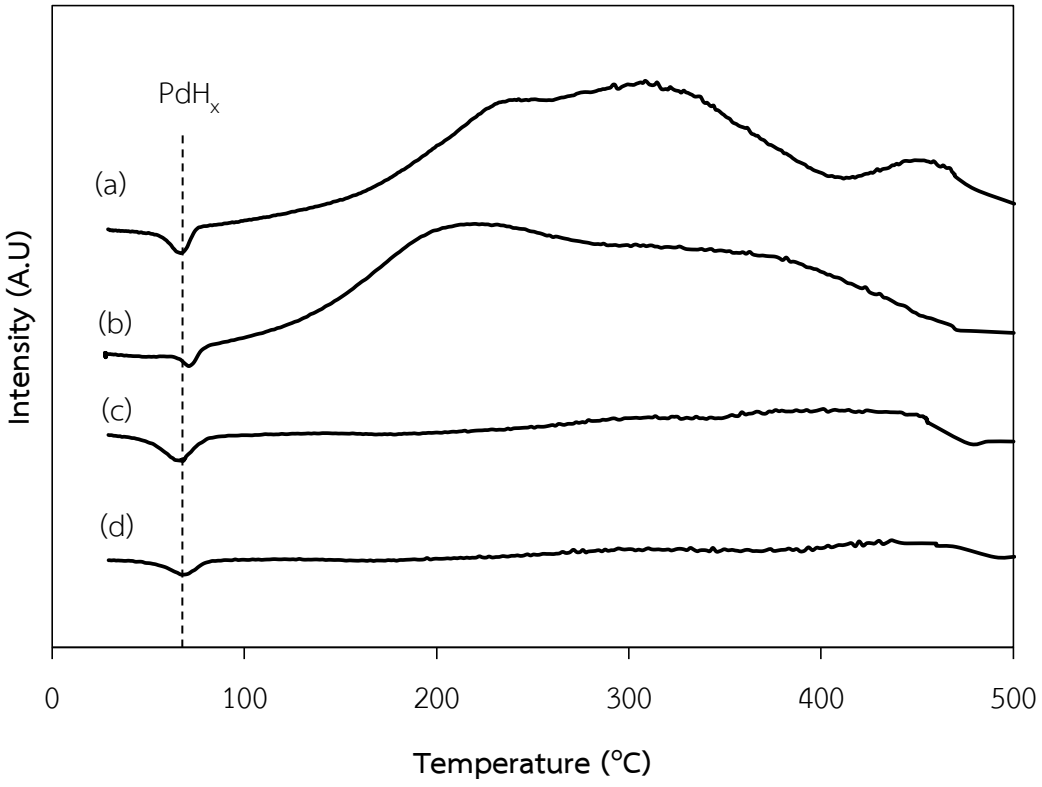

Figure 5.16 The H_2-TPR profiles of Pd catalysts (a) Pd/TiO_2–N_2-ED, (b) Pd/TiO_2–O_2-ED, (c) Pd/TiO_2–N_2-I; (d) Pd/TiO_2–O_2-I.

5.5.6 Infrared spectroscopy of adsorbed CO (CO-IR)

The amount of Pd active sites is usually calculated from chemisorption results based on the assumption that only CO molecule adsorbs on one Pd site. The IR spectra of adsorbed CO show typical four peaks corresponding to different CO adsorbed species on Pd surface including linear (2100–2050 cm^{-1}), compressed-bridged (1995–1975 cm^{-1}), isolated-bridged (1960–1925 cm^{-1}), and tri-coordinated (1890–1870 cm^{-1}) species. **Figure 5.17** shows the IR spectra of adsorbed CO on the 1%Pd/TiO_2–N_2-ED and Pd/TiO_2–O_2-ED catalysts. The A_l/A_m ratio of the peaks corresponding to linearly and multiply bound. The A_l/A_m ratios of Pd/TiO_2–N_2-ED and Pd/TiO_2–O_2-ED catalysts are given in **Table 5.11.** The higher A_l/A_m ratio can be promoted the ethylene selectivity due to The reaction between the highly active hydrogen and acetylene at high-coordination lead to the full hydrogenation of acetylene to ethane, while the reaction on the low-coordination Pd sites is lower the ethylene selectivity .

Table 5.11 Normalized peak area of various CO adsorbed species from the CO-IR results on 1% Pd/TiO_2 catalysts.

Catalyst	Tri-coordinated	Isolated-bridged	Compressed-bridged	Linear	A_l/A_m *
Pd/TiO_2-N_2-(ED)	0.11	0.48	0.25	0.16	0.19
Pd/TiO_2-O_2-(ED)	0.21	059	0.15	0.05	0.05

* A_l: peak area of linear-bound CO and A_m: peak area of multi-bound CO

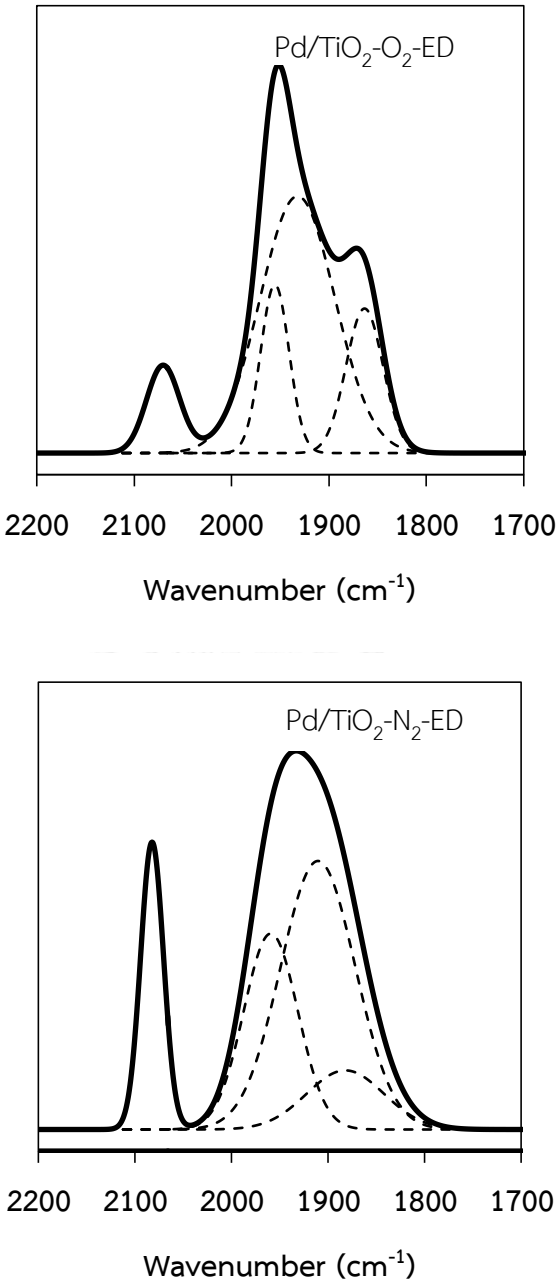

Figure 5.17 CO-IR spectra of 1%Pd/TiO_2–O_2-ED and 1%Pd/TiO_2–N_2-ED catalysts.

5.5.7 CO-pulses chemisorption

The amounts of CO chemisorption on the various Pd/TiO_2 catalysts reduced at 150°C and the percentages of palladium dispersion are given **Table 5.12**. It was found that the Pd catalysts supported on TiO_2-N_2 exhibited higher amount of CO chemisorption than those supported on TiO_2-O_2. Comparing the preparation method, the catalysts prepared electroless deposition showed higher Pd dispersion than those prepared by impregnation method. The Pd dispersion increased in the order: Pd/TiO_2-N_2(ED) > Pd/TiO_2-N_2(I) > Pd/TiO_2-O_2(ED) > Pd/TiO_2-O_2(I).

Table 5.12 CO chemisorption results of $1\%Pd/TiO_2$ catalysts prepared by impregnation method.

Catalysts	CO Chemisorption ($\times 10^{19}$ molecule CO/ g.)	Pd dispersion (%)	$d_P Pd^0$ (nm)
$1\%Pd/TiO_2$-N_2-ED	3.4	66	1.7
$1\%Pd/TiO_2$-O_2-ED	2.5	48	2.3
$1\%Pd/TiO_2$-N_2-I	3.1	58	1.9
$1\%Pd/TiO_2$-O_2-I	2.4	43	2.6

5.6. Reaction study in selective hydrogenation of acetylene.

5.6.1. 1%Pd/TiO_2 prepared by electroless deposition and incipient wetness impregnation method with TiO_2 calcined under nitrogen and oxygen atmosphere.

The catalytic performances of the Pd catalysts supported on the sol-gel derived TiO_2 calcined under N_2 and O_2 were investigated in the selective hydrogenation of acetylene to ethylene. **Figure 5.18, Figure 5.19** and **Figure 5.20** summarize the results of acetylene conversion, ethylene selectivity and catalytic performance of the Pd/TiO_2 catalysts with the reduction at 150^{o}C for 2 h. The conversion of C_2H_2 of all the samples increased with increasing reaction temperature. The conversion of Pd/TiO_2-N_2-ED was 66% at 40^{o}C and reached 100% at 100^{o}C. Typically, the selectivity for ethylene on supported Pd catalysts decreases when acetylene conversion is high However, high ethylene selectivity (~92%) can be obtained at complete acetylene conversion (100%) over the 1%Pd/TiO_2-N_2-ED. The ethylene selectivity was improved in the order: 1%Pd/TiO_2-N_2-ED>1%Pd/TiO_2-N_2-I>1%Pd/TiO_2-O_2-ED>1%Pd/TiO_2-O_2-I. The catalysts prepared by electroless deposition methods exhibited higher activity than the conventional impregnation-made catalysts. Typically, metal dispersion affected the catalytic activity and selective hydrogenation of acetylene to ethylene. The presence of Ti^{3+} significantly increased dispersion of palladium on the titania supports, as a consequence higher dispersion and hydrogenation activity were obtained over the Pd/TiO_2-N_2 catalysts. Because the prepared TiO_2 supports possessed similar average crystallite size, BET surface area and pore diameter, the higher Pd dispersion on the N_2-treated sol-gel TiO_2 was attributed to the higher amount of surface Ti^{3+} on the TiO_2 supports. The presence of Ti^{3+} site that were in contact with the palladium surface promoted the SMSI effect and ethylene desorption.

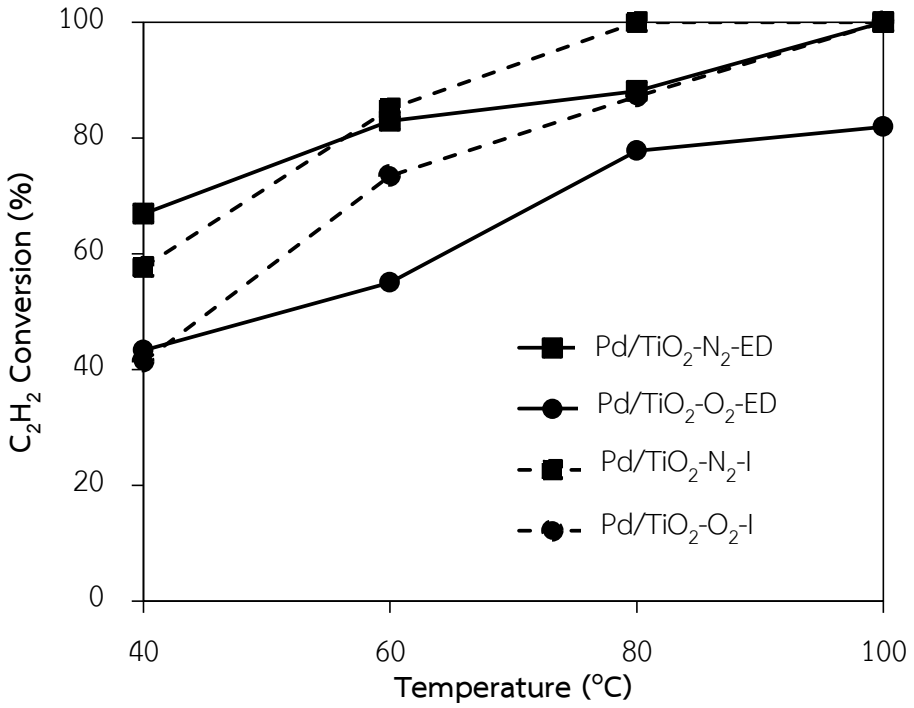

Figure 5.18 Acetylene conversion as a function of reaction temperature for 1% Pd/TiO_2 catalysts.

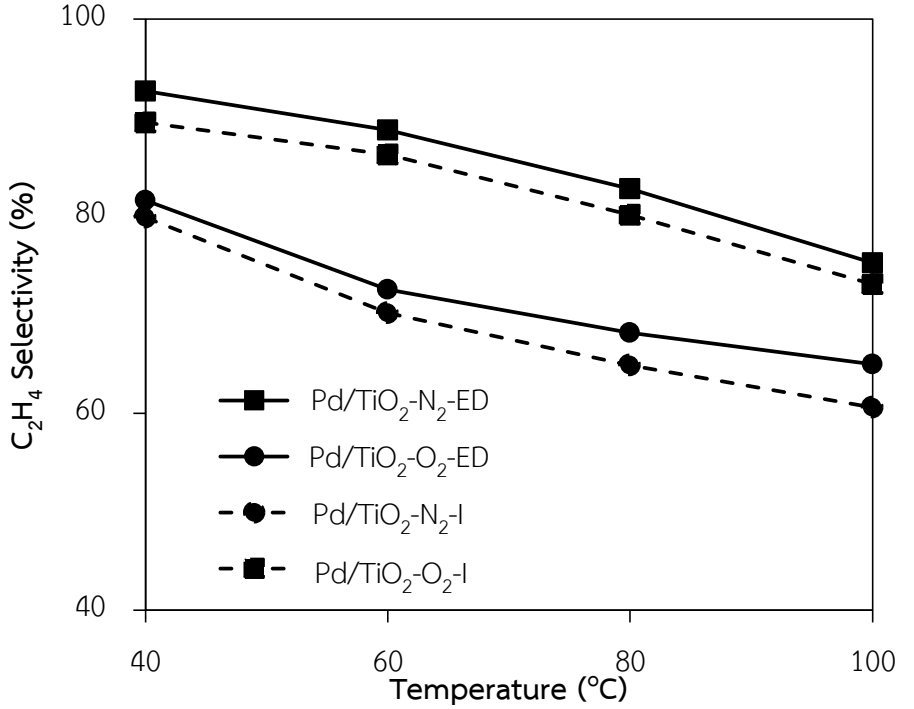

Figure 5.19 Ethylene selectivity as a function of reaction temperature for 1% Pd/TiO_2 catalysts.

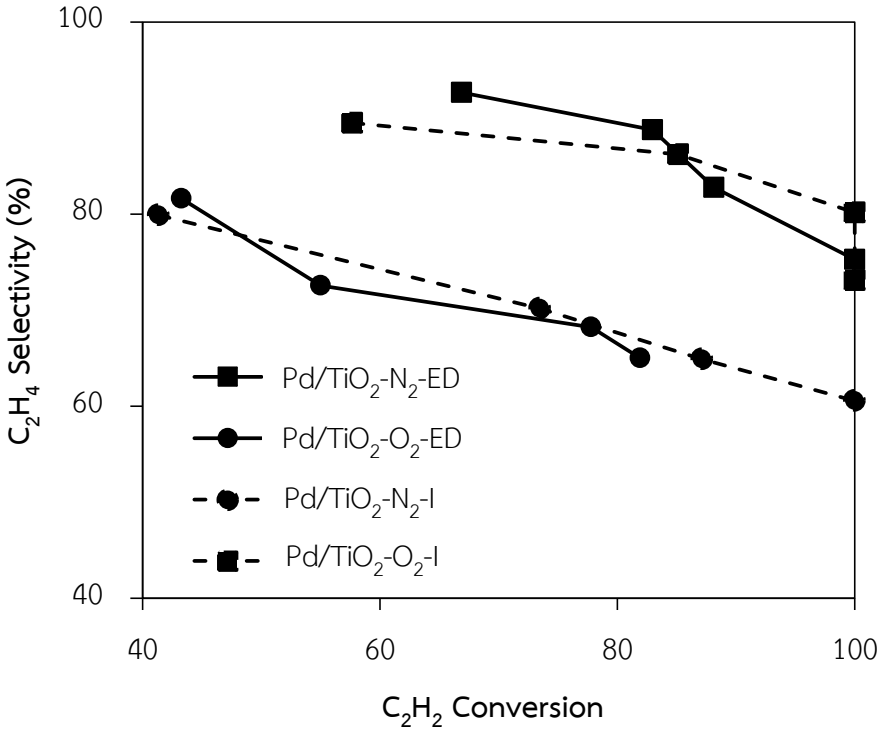

Figure 5.20 The catalytic performance of 1%Pd/TiO_2 catalyst in the selective hydrogenation of acetylene.

PART II

Effect of calcination temperature of TiO_2 under Hydrogen atmosphere via a sol–gel-derived TiO_2 supported Pd catalysts that were prepared by incipient wetness impregnation method in the selective acetylene hydrogenation

In this section, the effect of calcination temperature of TiO_2 was further investigated under H_2 atmosphere. The anatase nanocrystalline TiO_2 samples were synthesized by a sol-gel method with a thermal treatment under H_2 from 300-450°C. The properties of TiO_2 supports after calcined were investigated by X-ray powder diffraction, N_2 physisorption, electron spin resonance (ESR) and X-ray photoelectron spectroscopy (XPS).

5.7 Characteristic and properties of TiO_2 support

5.7.1 X-ray diffraction (XRD)

Calcination is a common treatment that used to improve the crystallinity of TiO_2 powders. When TiO_2 powders are calcined at higher temperatures, the transformations such as amorphous to anatase, anatase to rutile may occur. The XRD patterns of TiO_2 supports were prepared by sol-gel and calcined under H_2 atmosphere at 300-450°C are shown in **Figure 5.21**. The samples calcined at 300-350 $^{\circ}$C exhibit peaks of both anatase and brookite phase. For the anatase titania, XRD peaks at 25°, 37°, 48°, 55°, 56°, 62°, 71°, and 75° 2**θ** were evident. A peak at 30.81° 2**θ** corresponded to brookite phase TiO_2. The XRD patterns of the TiO_2 samples after heat treatment at 400-450°C appeared rutile peaks at 28° 2**θ**. The peak intensities of anatase increased, indicating the improvement of crystallization of anatase phase. With further increase in the calcination temperature from 400 to 450°C, the intensity of rutile phase increased. It is known that thermal treatment and surface defects are two important factors in TiO_2 phase transformation. The primary formed TiO_2 particles usually contain large portion of defect sites, high temperature facilitates bond breaking as well as atoms rearrangement and therefore the anatase to rutile occurs

easily. On the other hand, anatase to rutile transformation is initiated by forming the rutile nuclei along the anatase {1 1 2} twin interface, which has the structural similarity to rutile and thus the rutile structure develops directly at the expense of anatase crystallites [69]. As the temperature increases from 300 to 450°C, the intensities of the anatase peaks increase, implying an improvement in crystallinity from 3.9 to 6 nm. The crystallite size of TiO_2 can be deduced from XRD line broadening using the Scherrer's equation.

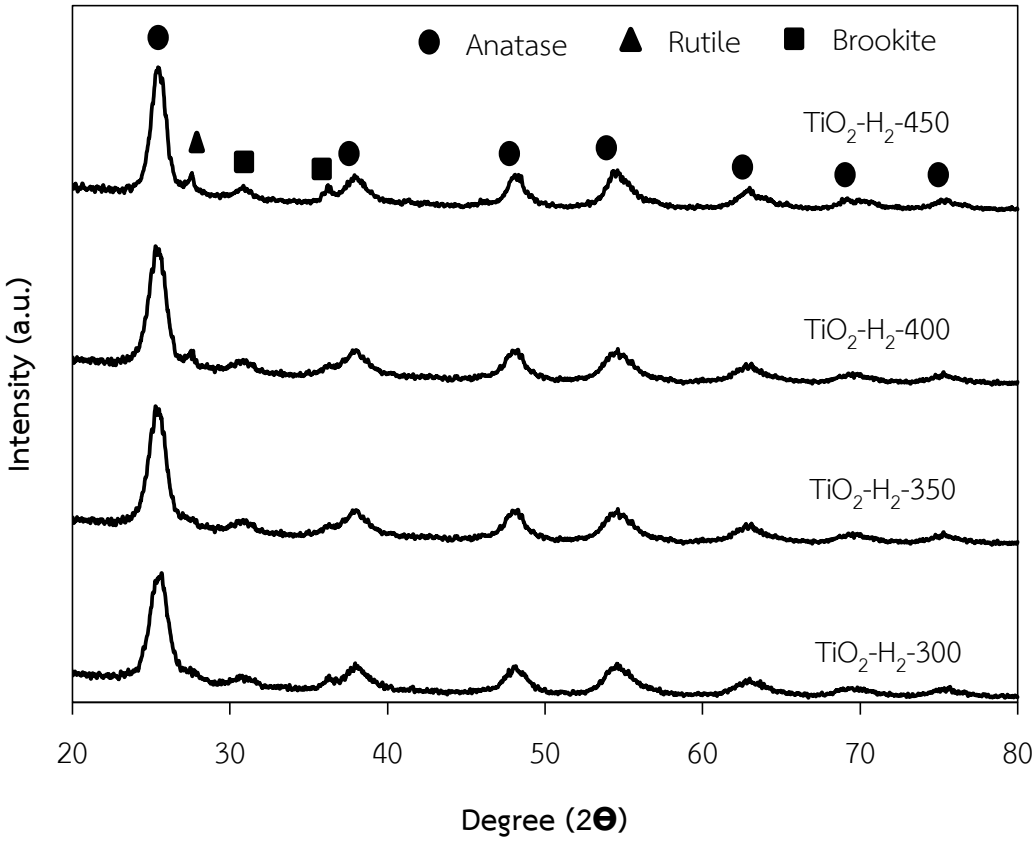

Figure 5.21 The XRD patterns of TiO_2 calcined at 300-450°C under H_2 atmosphere.

5.7.2 Electron Spin Resonance (ESR)

The ESR spectra of TiO_2 via sol-gel method at different calcination temperatures shown in **Figure 5.22**. It is reported that TiO_2 prepared by sol–gel method exhibited one major signal at g value of 1.975 which can be attributed to Ti^{3+} at the surface. The Titanium species (Ti^{3+}) are produced by trapping of electrons at defective sites in TiO_2 and the accumulated electrons may reflect the number of defective sites. The intensity of the Ti^{3+} signal was highest for TiO_2 calcined at 350°C suggesting that this preparation method produces the highest amount of defects on the TiO_2. Ti^{3+} surface defect can produce by reduction of Ti^{4+} to Ti^{3+} with H_2 treatment temperature. There are three types process for reduction of Ti^{4+} to Ti^{3+}. Firstly, H_2 interacted physically with adsorbed oxygen on the TiO_2 surface. Secondly, electrons were transfer from H atom to O atom in the lactic of TiO_2 when the O atom left with the H atom and form of H_2O. Then, the oxygen vacancies were formed. Thirdly, interaction between H_2 and TiO_2 lead to the electron transferred from oxygen vacancies to Ti^{4+} ions, and then Ti^{3+} ions were formed [70]. It is suggested that Ti^{3+} increases with the increase temperature and decrease after TiO_2 appeared rutile phase due to rutile titania is more thermodynamically and structurally stable than anatase.

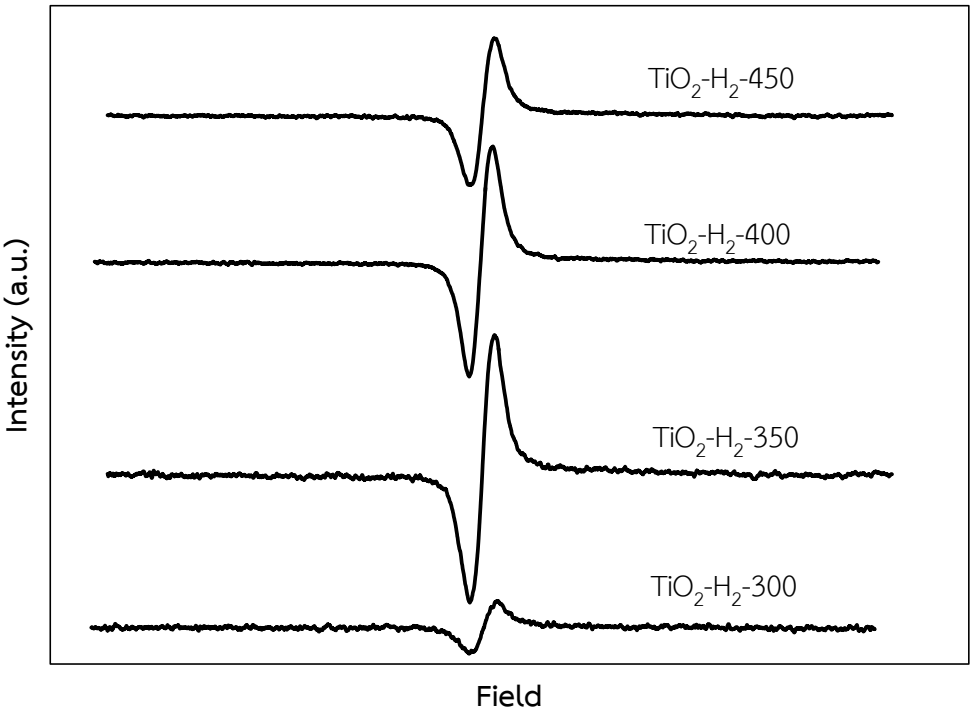

Figure 5.22 The ESR results of TiO_2 calcined at 300-450°C.

5.7.3 N_2-physisorption

The BET surface areas and average pore diameter for TiO_2 are shown in **Table 5.13** as a function of the calcianation temperature from 300 to 450°C. The values of BET surface area are 206-121 m^2/g, pore volume 0.15-0.31 cm^3/g, and average pore diameter 4-5 nm. The BET surface areas were decreased in the order: TiO_2-H_2-300> TiO_2-H_2-350> TiO_2-H_2-400> TiO_2-H_2-450 while the average particle size was increase with increasing temperature. At the low temperatures exhibited high surface area and smaller particle size than high calcination temperature lead to prevent the increase in the rate growth and sintering of the particles. [71].

Table 5.13 Physicochemical properties of TiO_2

Catalysts	Crystallite size[a] of TiO_2 (nm)	BET surface area (m^2/g)	Pore volume[b] (cm^3/g)	Avg. pore[b] diameter (nm)
TiO_2-H_2-300	3.9	206	0.31	4.7
TiO_2-H_2-350	4.4	198	0.30	4.8
TiO_2-H_2-400	5.3	135	0.22	5.0
TiO_2-H_2-450	6.0	121	0.15	5.1

[a] Based on the XRD results.

[b] Based on BJH method

5.7.4 X-ray photoelectron spectroscopy (XPS)

The XPS is used to determine the surface compositions of the TiO_2 supports. The survey XPS spectra convince the external surface element concentrations influence on the catalytic activity. The XPS spectra for anatase TiO_2 samples was recorded with photon energy of 1256 eV ($MgK\alpha$), the kinetic energies of the emitted electrons being in the range of 0-1000 eV. The binding energies of the Ti $2p_{3/2}$ are 458.8 to 459.0 eV and and Ti $2p_{1/2}$ peaks 464.5 to 464.8 eV, indicating of only Ti^{4+} in the TiO_2 [63]. The binding energy of the O1s peak is 530.0 to 530.5 eV. The binding energy and atomic concentration of Ti 2p and O 1s and the relative concentration of Ti and O on TiO_2 calcined in H_2 gas under different calcination temperature are summarized in **Table 5.14**. The ratios of Ti/O were found in the range of 0.24-0.25.

Table 5.14 The atomic concentration of Ti and O on TiO_2 surface from XPS results.

Catalysts	Ti 2p		O 1s		Atomic concentration		Ti/O
	B.E. (eV)	FWHM	B.E. (eV)	FWHM	Ti	O	
TiO_2-H_2-300	458.9	1.758	530.3	2.004	13.08	52.67	0.25
TiO_2-H_2-350	459.0	1.453	530.4	1.715	12.17	49.83	0.24
TiO_2-H_2-400	459.0	1.448	530.3	1.693	12.02	48.67	0.25
TiO_2-H_2-450	458.8	1.365	530.1	1.566	11.16	44.52	0.25

5.8. Properties of Pd/TiO_2 prepared by incipient wetness impregnation method.

In this section, the preparation of 1%Pd/TiO_2 catalysts by incipient wetness impregnation method via sol-gel derived TiO_2, which different calcination temperature for selective hydrogenation of acetylene at 40-100°C. The catalyst properties of the Pd/TiO_2 catalysts according to the characterization results from X-ray diffraction (XRD), transmission electron microscopy (TEM), N_2 physisorption, electron spin resonance (ESR), CO pulse chemisorption, X-ray photoelectron spectroscopy (XPS), pulse CO chemisorption and H_2 temperature programmed reduction (H_2TPR).

5.8.1 X-ray diffraction (XRD)

The XRD petterns of 1%Pd/TiO_2-H_2-300, 1%Pd/TiO_2-H_2-350, 1%Pd/TiO_2-H_2-400, and 1%Pd/TiO_2-H_2-450, which prepared by incipient wetness impregnation methods (I) are shown in **Figure 5.23**. There were no changes in the crystalline phase of the TiO_2 after palladium loading for all the catalyst samples. The crystallite size of 1%Pd/TiO_2-H_2-300, 1%Pd/TiO_2-H_2-350, 1%Pd/TiO_2-H_2-400, and 1%Pd/TiO_2-H_2-450 were 4.8-7.4 nm can be deduced from XRD line broadening using the Scherrer's equation.

The crystal sizes of anatase increased with increasing of calcination temperature, indicating aggregation of TiO_2 nanoparticles upon annealing. The fraction of rutile becomes greater with increasing reaction temperature, consistent with increasing the temperature of heat treatment accelerates phase transformation from metastable anatase to stable and more condense rutile phase.

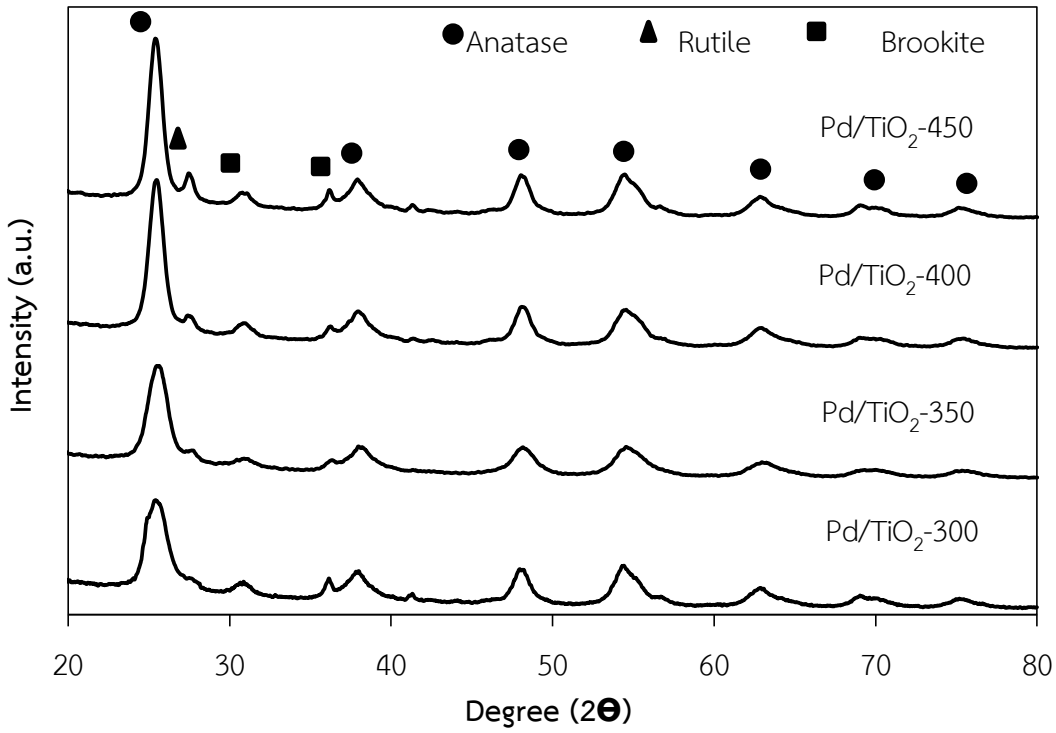

Figure 5.23 The XRD patterns of 1%Pd/TiO_2-H_2-300, 1%Pd/TiO_2-H_2-350, 1%Pd/TiO_2-H_2-400, and 1%Pd/TiO_2-H_2-450

5.8.2 N_2-physisorption

The average TiO_2 crystallite size, BET surface area, pore volume, and pore diameter are given in **Table 5.15**. The BET surface area of the Pd/TiO_2, which TiO_2 calcined under different calcination temperature from 300-450^{o}C were 156-80 m^2/g with pore volume 0.20-0.26cm^3/g and average pore diameter 4.1-4.6 nm. However, the BET surface area and pore volume of the Pd/TiO_2 decreased for all the catalysts after Pd loading with no significant change in the average pore diameter. The

decrease in surface area with metal loading may be due to the pore blockage of the support.

Table 5.15 Physicochemical properties of 1% Pd/TiO_2 prepared by impregnation method.

Catalysts	BET surface area (m^2/g)	Pore volume[a] (cm^3/g)	Avg. pore[a] diameter (nm)
$1\%Pd/TiO_2$-H_2-300	156	0.27	4.1
$1\%Pd/TiO_2$-H_2-350	144	0.23	4.4
$1\%Pd/TiO_2$-H_2-400	112	0.26	4.6
$1\%Pd/TiO_2$-H_2-450	80	0.20	4.6

[a] Based on BJH method

5.8.3 X-ray photoelectron spectroscopy (XPS)

The surface composition and electronic state surface of Pd/TiO_2 catalysts. The XPS spectra for Pd/TiO_2 samples was recorded with photon energy of 1256 eV ($MgK\alpha$), the kinetic energies of the emitted electrons being in the range of 0-1000 eV. The surface compositions of the catalysts as well as the interaction between Pd and the TiO_2 supports were confirmed by XPS analysis. The Pd 3d core level could be fitted with three main doublets of Pd^0, PdO (Pd^{2+}) and PdO_2 (Pd^{4+}) at the Pd $3d_{5/2}$ at 335.3, 337.1 and 338.4 eV [72]. The binding energies of Ti $2p_{3/2}$ were around 458.8 to 459.0 eV. The binding energies and atomic concentrations of Ti 2p, O1s and Pd 3d on various Pd/TiO_2 catalysts prepared by impregnation method are given in **Table 5.16**. The binding energy of Ti 2p around 459.8 eV and O 1s around 530.3 eV for all catalysts can be attributed to Ti^{4+} and oxygen lattice of TiO_2. The ratio of Pd/Ti surface concentration of $1\%Pd/TiO_2$-H_2-350, $1\%Pd/TiO_2$-H_2-400 and $1\%Pd/TiO_2$-H_2-450 were 0.02.

Table 5.16 The atomic concentration of Pd and Ti on TiO_2 surface from XPS results.

Catalysts	Ti 2p		O 1s		Pd 3d		Atomic concentration			Pd/Ti
	B.E. (eV)	FWHM	B.E. (eV)	FWHM	B.E. (eV)	FWHM	Pd	Ti	O	
1%Pd/TiO_2-H_2-300	458.8	1.602	530.3	2.214	338.2	1.585	0.33	9.58	53.70	0.03
1%Pd/TiO_2-H_2-350	490.0	2.054	530.4	2.412	336.5	1.752	0.20	10.53	47.22	0.02
1%Pd/TiO_2-H_2-400	459.2	1.529	530.6	2.412	338.6	1.433	0.20	9.53	47.22	0.02
1%Pd/TiO_2-H_2-450	459.0	1.449	530.3	1.816	337.4	1.869	0.22	11.63	54.37	0.02

5.8.4 Transmission electron microscopy (TEM)

The Transmission electron microscopy micrographs of Pd/TiO_2 prepared by incipient wetness impregnation method are shown in **Figure 5.24**. The particles of TiO_2 products by sol-gel synthesis showed spherical shape. Pd/TiO_2 particles are aggregated into clusters, it is difficult to measure the size of the primary spherical particles accurately. It was apparent that Pd particle is well dispersed on TiO_2 support. The particle size of Pd/TiO_2 increased with increasing calcination temperature of TiO_2 support. Pd/TiO_2 prepared by incipient wetness impregnation method indicates that aggregates and/ or agglomerates of crystals increasing the calcination temperature. However, some agglomeration of metal particles can be seen on the Pd/TiO_2-450.

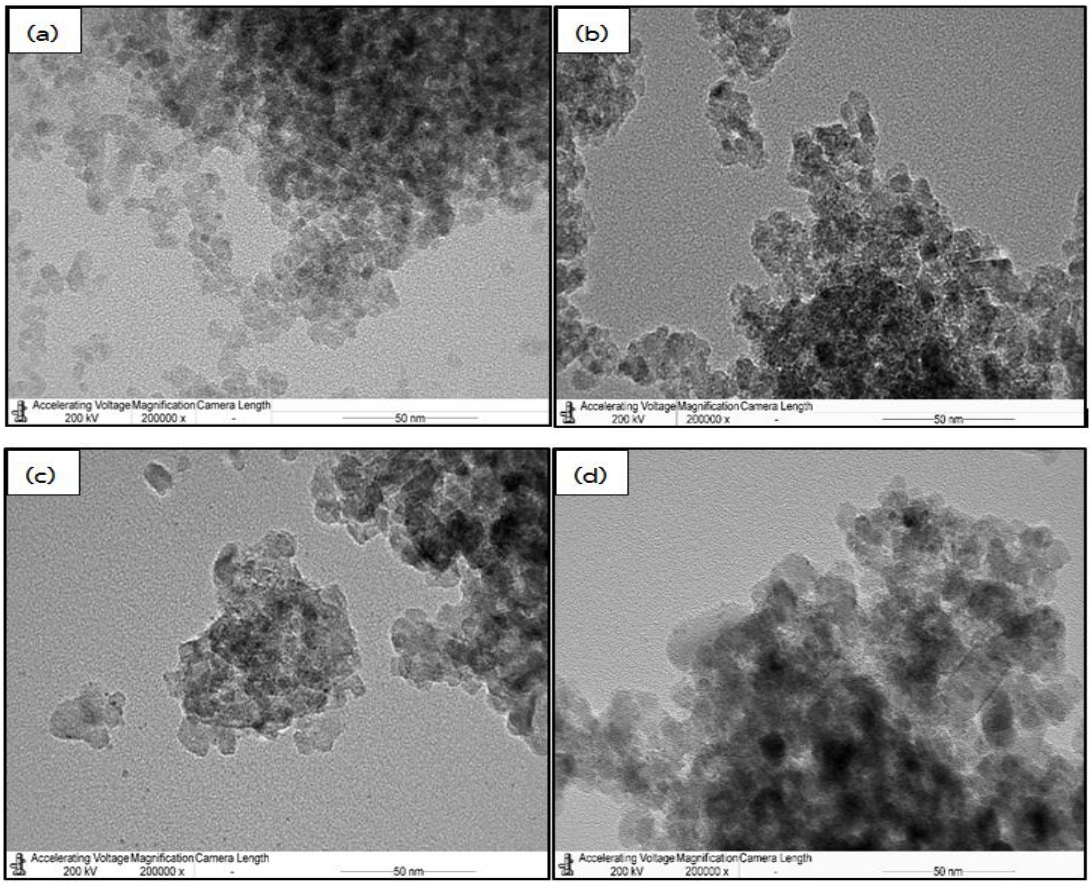

Figure 5.24 Transmission electron microscopy of Pd/TiO_2 catalysts prepared by impregnation method (a) 1%Pd/TiO_2-H_2-300, (b) 1%Pd/TiO_2-H_2-350, (c) 1%Pd/TiO_2-H_2-400 (d) and 1%Pd/TiO_2-H_2-450.

5.8.5 Hydrogen Temperature program reduction (H_2-TPR)

The reducibility of Pd/TiO_2 catalysts were studied by temperature-programmed reduction. The H_2-TPR profiles of Pd catalysts prepared by incipient wetness impregnation method 1%Pd/TiO_2-H_2-300, 1%Pd/TiO_2-H_2-350, 1%Pd/TiO_2-H_2-400, and 1%Pd/TiO_2-H_2-450 are shown in **Figure 5.25.** The TPR measurements were executed to study the reduction behaviors of palladium catalysts. The negative peak at about 80°C indicating the Pd-based catalysts on titania can adsorb hydrogen in the surface at lower temperatures and release hydrogen from the decomposition of palladium hydride species [65]. The Peak at about 300°C shows that Ti^{4+} reduced to Ti^{3+} in the presence of Pd at lower reduction temperature, which is chemsorbed hydrogen on palladium during from Pd to TiO_2 and reducing Ti^{4+} to Ti^{3+}. The peak at 450°C appeared at the TPR profiles shows that Ti^{4+} can be reduced to Ti^{3+}.

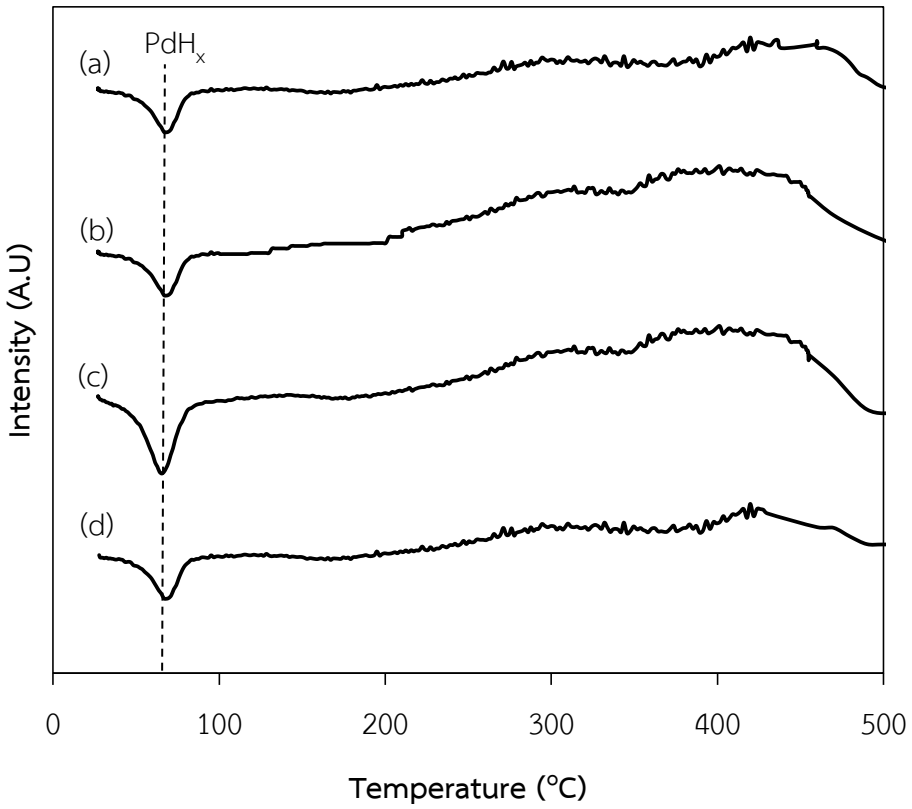

Figure 5.25 The H_2-TPR profiles of Pd catalysts.

5.8.6 CO-pulses chemisorption

The metal active sites measurement is based on chemisorption technique on the assumption that only CO molecule adsorbs on one palladium site. The amounts of CO chemisorption on the various Pd/TiO_2 catalysts reduced at 150°C and the percentages of palladium dispersion are also given **Table 5.17**. It was found that the $1\%Pd/TiO_2$-H_2-350 exhibited the highest amount of CO chemisorption and Pd dispersion. The Pd dispersion was increased in the order: Pd/TiO_2-350> Pd/TiO_2-400 > Pd/TiO_2-450 > Pd/TiO_2-300.

Table 5.17 CO chemisorption results of $1\%Pd/TiO_2$ catalysts prepared by impregnation method.

Catalysts	CO Chemisorption (x 10^{19} molecule CO/ g.)	Pd dispersion (%)	$d_P Pd^0$ (nm)
$1\%Pd/TiO_2$-H_2-300	2.4	47	2.4
$1\%Pd/TiO_2$-H_2-350	3.7	65	1.7
$1\%Pd/TiO_2$-H_2-400	3.3	54	2.1
$1\%Pd/TiO_2$-H_2-450	2.6	49	2.3

5.9. Reaction study in selective hydrogenation of acetylene.

The catalytic performances of Pd/TiO_2 catalysts containing $1\%Pd/TiO_2$-H_2-300, $1\%Pd/TiO_2$-H_2-350, $1\%Pd/TiO_2$-H_2-400 and $1\%Pd/TiO_2$-H_2-450 prepared by incipient wetness impregnation method were evaluated in the selective hydrogenation of acetylene with a vary temperature from 40°C to 100°C. The plots of acetylene conversion and ethylene selectivity versus temperature and catalytic performance of Pd/TiO_2 are shown in **Figure 5.26**, **Figure 5.27** and **Figure 5.28,** respectively. In general, acetylene conversion increased with increasing temperature while ethylene selectivity decreased. Since ethylene is produced as an intermediate in acetylene hydrogenation, which is a typical consecutive reaction, the ethylene selectivity decreases with acetylene conversion. The performance of Pd/TiO_2 catalysts was improved in the order of $1\%Pd/TiO_2$-H_2-350>$1\%Pd/TiO_2$-H_2-400>$1\%Pd/TiO_2$-H_2-450>$1\%Pd/TiO_2$-H_2-300. Pd catalyst supported TiO_2 calcined in H_2 atmosphere at 300°C is strongly adsorbed multi-**σ**-bond on Pd surface site than **π**-bond lead to C_2H_6 formation. It is clearly shown that the Pd catalyst supported TiO_2 calcined in H_2 atmosphere at 350°C exhibited the best catalytic performance the conversion rate of acetylene to 100% and selectivity of ethylene was up to 89% due to acetylene like to adsorbed **π**-bond species on single Pd atom and easily desorbed ethylene due to the adsorption is relatively weak . Based on the characterization results, the TiO_2 calcined in H_2 atmosphere at 350°C was attributed to the larger amount of surface Ti^{3+} enhance the dispersion and stability of supported metal, which promoted acetylene conversion.

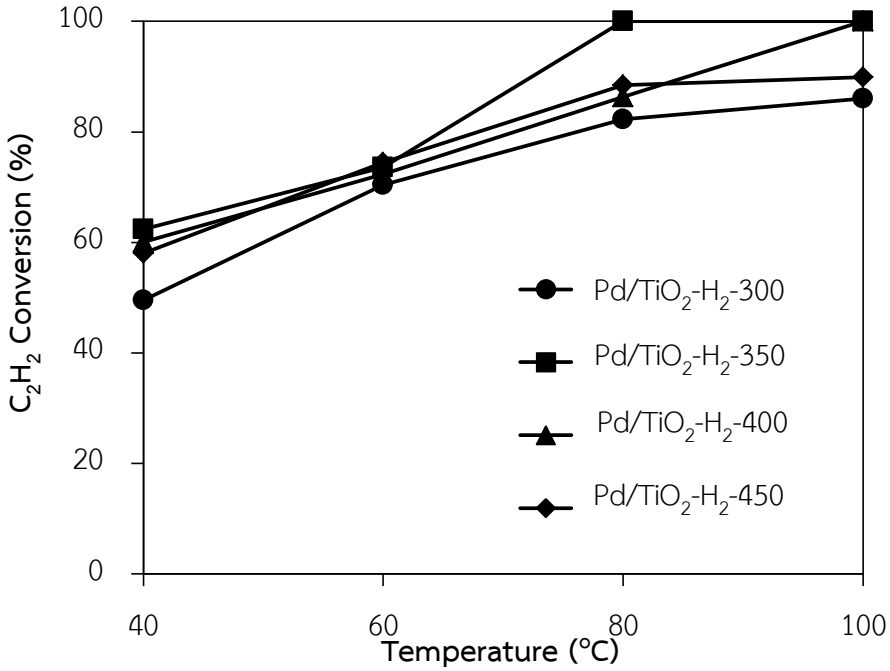

Figure 5.26 Acetylene conversion as a function of reaction temperature for 1% Pd/TiO_2 catalysts prepared by impregnation method.

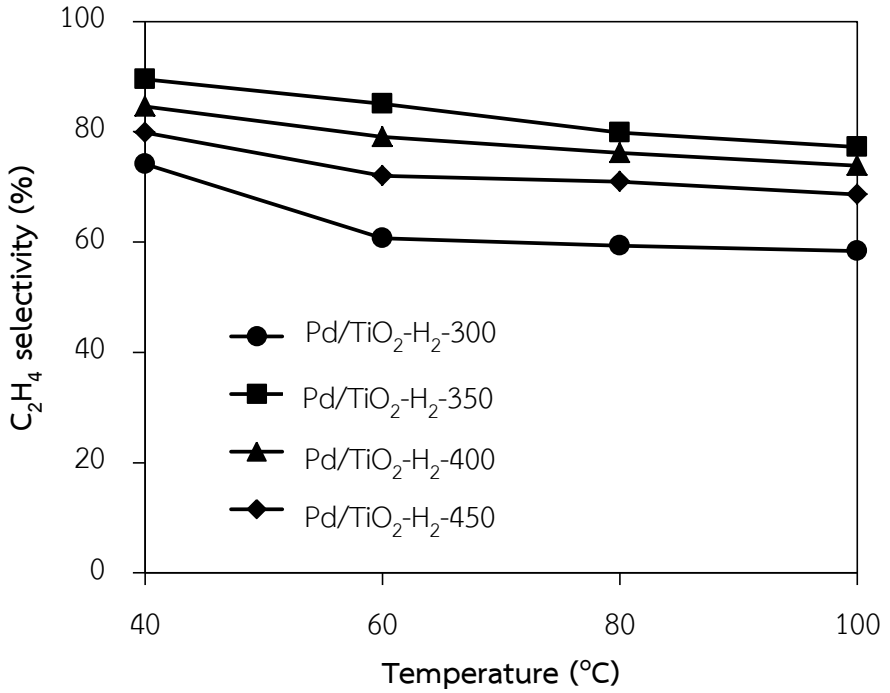

Figure 5.27 Ethylene selectivity as a function of reaction temperature for 1% Pd/TiO_2 catalysts prepared by impregnation method.

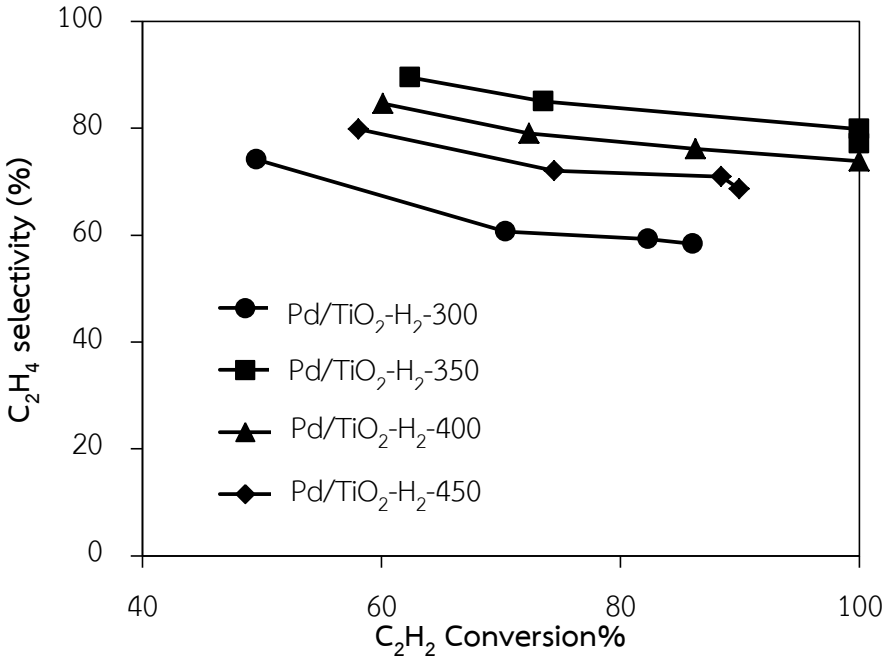

Figure 5.28 The catalytic performance of 1%Pd/TiO_2 catalyst in the selective hydrogenation of acetylene.

PART III

The characteristics and catalytic properties of TiO_2 supported bimetallic Pd-Ag catalysts prepared by electroless deposition method in the selective acetylene hydrogenation.

In the present communication, the scope of work to the bimetallic Ag-Pd/TiO_2 catalysts prepared by the strong electrostatic adsorption of Pd followed by the electroless deposition of Ag. In this case, the average particle size of Pd particles on the monometallic Pd/TiO_2 was very small and uniformly distributed on the TiO_2 support. The Ag–Pd/TiO_2 bimetallic catalysts having incremental surface coverage of Ag on the Pd surface were subsequently prepared by the electroless deposition. The catalysts were characterized by X-ray diffraction (XRD), atomic absorption spectroscopy (AAS), inductively coupled plasma optical emission spectroscopy (ICP), chemisorption using hydrogen pulse titration, and Scanning Transmission Electron Microscopy (STEM). Kinetics study of these catalysts in the selective hydrogenation of acetylene were also reported.

5.10 Characteristic and catalytic properties of Pd/TiO_2 prepared by strong electrostatic adsorption.

5.10.1 Inductively Coupled Plasma optical emission spectroscopy (ICP)

The point of zero chart of TiO_2 and the uptake survey for the SEA experiment using palladium tetraammine precursor with the TiO_2 support is shown in **Figure 5.29** and **Figure 5.30**. The Pd surface density, defined as the amount of Pd per m^2 of the support, is plotted against the final pH value of the slurries after 1 h on the rotary shaker. In order to determine the optimal pH condition leading to maximum metal loading. The maximum Pd uptake was observed at an equilibrium pH around 11.4.

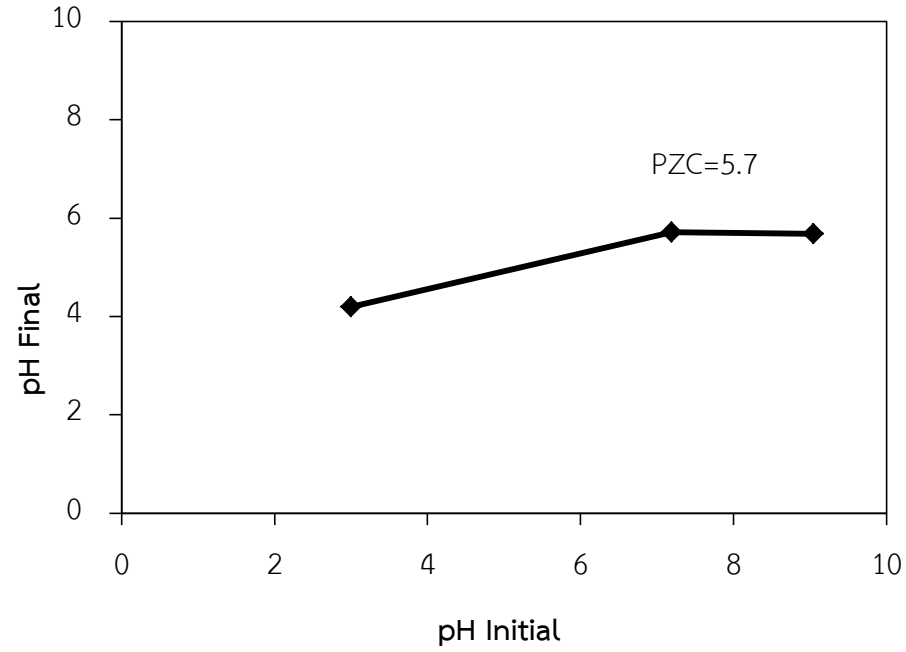

Figure 5.29 The point of zero chart of TiO_2

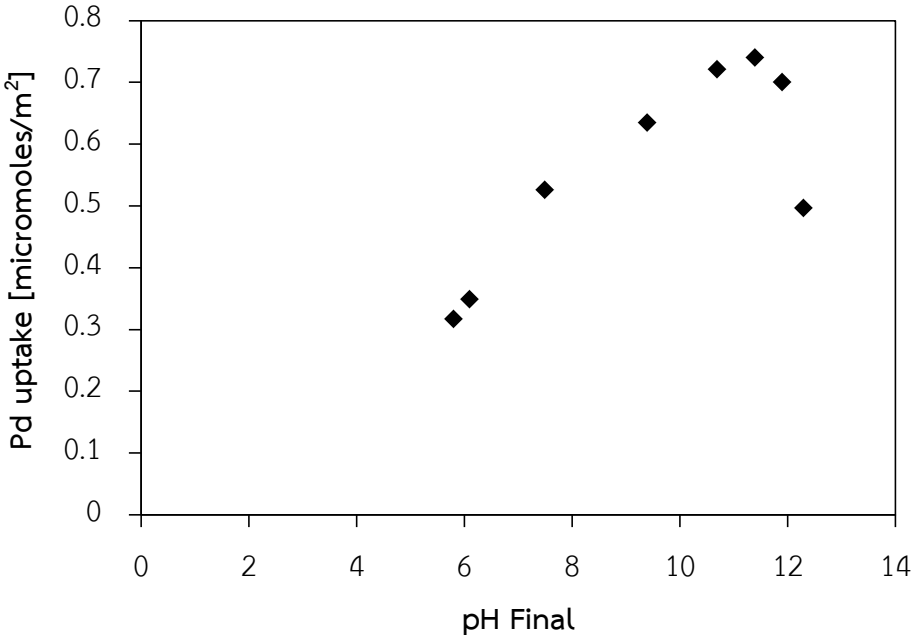

Figure 5.30 The uptake of Pd on TiO_2 support as a function of pH.

5.10.2 X-ray diffraction (XRD)

The XRD patterns of TiO_2 supports uncalcined and calcined in air at 250°C for 2 h and the 0.97%Pd/TiO_2 (SEA) reduced with 10%H_2 in He balance at 200°C for 2 h are shown in **Figure 5.31**. The measurements were carried out at the diffraction the angles (2**θ**) between 20° and 65°. The XRD characteristic peaks of anatase TiO_2 were presented at 2**θ** = 25° (major), 37°, 48°, 55°, 56°, and 62°. There were no changes in the crystalline phase of the TiO_2 after calcianation and loading of palladium. The XRD peaks corresponding to Pd species were no peak of Pd^0 at 2**θ** = 40.2° and 46.7° due to Pd crystallite size very small or low amount of Pd loading.

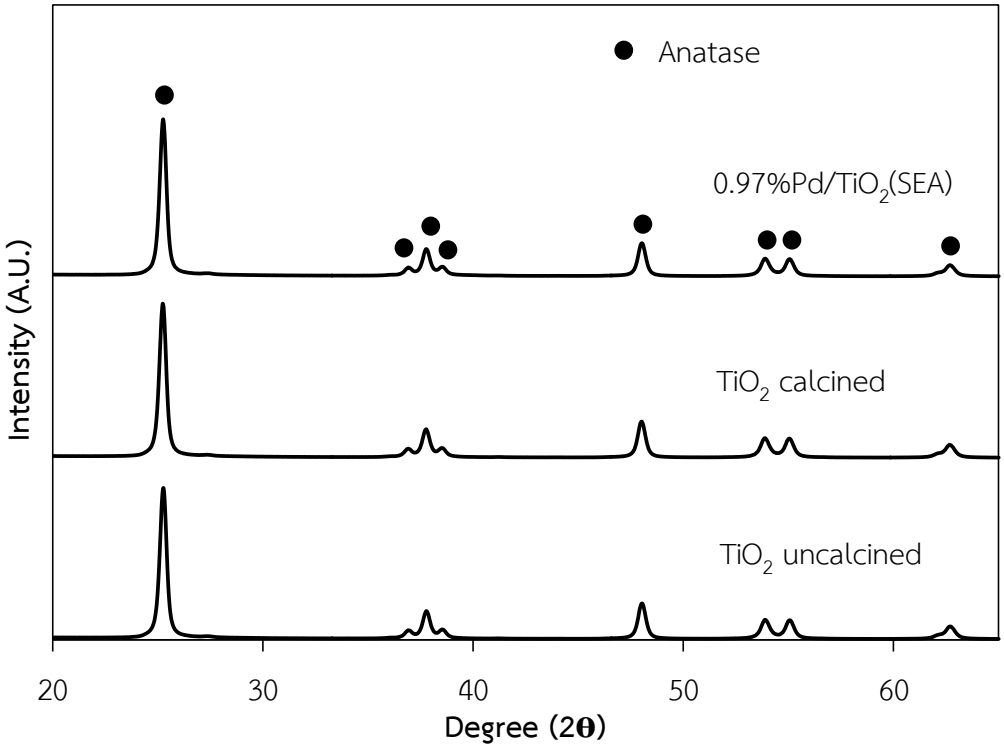

Figure 5.31 X-ray diffraction patterns of TiO_2 and Pd/TiO_2 (SEA).

5.10.3 Atomic Absorption Spectroscopy (AAS)

A series of Ag–Pd/TiO_2 bimetallic catalysts were prepared with increasing coverage of Ag metal on the Pd surface. The time dependent metal deposition profiles are summarized in **Figure 5.32**. The deposition curves indicate that TiO_2 alone does not result in deposition of Ag. Thus, the ionic interactions between the titania surface and the Ag metal salt did not occur. The concentrations of Ag in the bath solution of all samples were analyzed by AA analysis. The Ag in the bath was found to decrease with increasing deposition time. The aqueous solution in electroless baths are usually composed of a metal salt, a reducing agent, and stabilizing agent or a complexing agent. The complexing agent and stabilizing agent were added to improve bath stability, which also resulted in a corresponding decrease in the rate of deposition. The applicability of the electroless deposition bath depends on various concentrations of metal salt, reducing agent, pH in bath solution, monometallic catalyst, and temperature so that the rates and amounts of the metal deposited can be controlled.

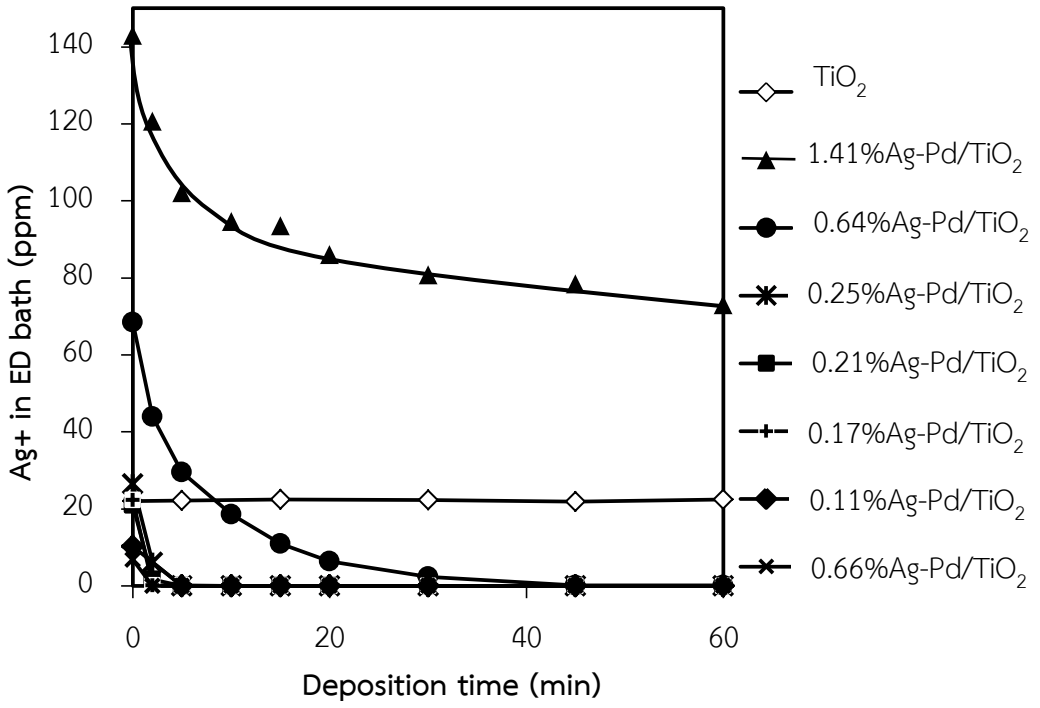

Figure 5.32 The time-dependent metal deposition profiles of Ag deposited.

5.10.4 Hydrogen–Oxygen Titration

The concentration of Pd surface sites for the Pd/TiO_2 and the bimetallic Ag-Pd/TiO_2 catalysts were determined by the chemisorption of hydrogen titration of oxygen-precovered Pd sites and the results are shown in **Table 5.18**. The average particle size of Pd on the monometallic Pd/TiO_2 was calculated from the chemisorption results to be ca. 5 nm. The active particle diameter increased and apparent metal dispersion decreased with increasing of Ag coverage. The lower hydrogen uptake with increased Ag wt. % was due to electroless deposition of Ag on surface Pd sites. In other words, the decrease in Pd surface site concentration suggests blockage of surface Pd sites by the deposition of a second metal.

The deviation of exposed Pd sites from the theoretical curves for monodisperse coverages of the Ag/Pd at 1:1 deposition stoichiometry is shown in **Figure 5.33**. It is suggested that an autocatalytic deposition occurred at approximately 0.68 coverage of Ag metal on Pd surface, in which the actual coverage of Ag started to deviate substantially from the theoretical coverage. The autocatalytic deposition increases as the higher concentration of the second metal and available surface Pd sites decreases, as expected for kinetically controlled deposition processes.

Table 5.18 Ag–Pd/TiO_2 bimetallic catalysts that were evaluated for acetylene hydrogenation. Theoretical coverage in monolayers (ML) represents monodisperse coverage of Ag on Pd surface, assuming 1:1 adsorption stoichiometry.

Sample	Active Particle Diameter(nm)	Apparent Metal Dispersion (%)	Theoretical coverage (ML)	Actual coverage
0.97%Pd/TiO_2 (SEA)	5.1	21.68	0	0
0.06%Ag-Pd/TiO_2 (ED)	8.1	13.79	0.32	0.36
0.11%Ag-Pd/TiO_2 (ED)	10.3	10.89	0.49	0.50
0.17%Ag-Pd/TiO_2 (ED)	16.8	6.66	0.81	0.68
0.21%Ag-Pd/TiO_2 (ED)	21.2	5.35	0.98	0.75
0.25%Ag-Pd/TiO_2 (ED)	26.1	4.29	1.27	0.80
0.64%Ag-Pd/TiO_2 (ED)	64.9	1.73	3.21	0.92
1.41%Ag-Pd/TiO_2 (ED)	89.4	1.20	6.50	0.95

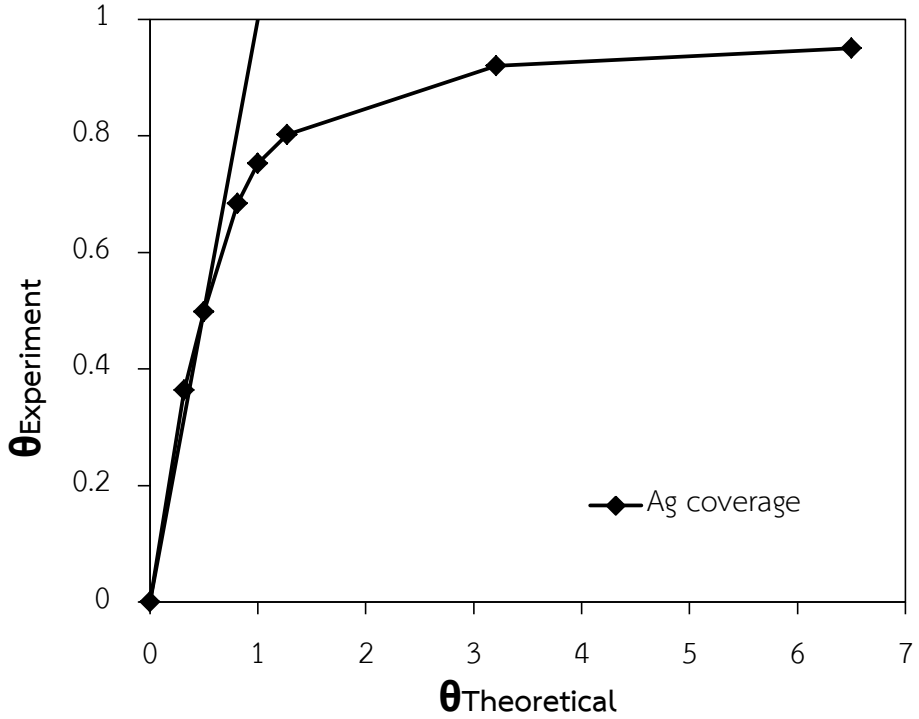

Figure 5.33 Actual coverage of Ag on Pd/TiO_2 as a function of Ag deposited.

5.10.5 Scanning Transmission Electron Microscopy (STEM)

The STEM images for Pd/TiO_2 and Ag coverage (θ_{Ag}) for 0.36 ML, 0.5 ML and 0.92 ML show in **Figure 5.34.** On the images it is seen that the metal particles size increase with increasing the Ag coverage due to Ag deposited on the Pd surface site. The ratio of Pd : Ag from EDX data show that the atomic ratio of Pd decrease with increasing of Ag at high coverage of Ag. The ratio of Pd : Ag from EDX data consistent with the AA analysis are shown in **Table 5.19**

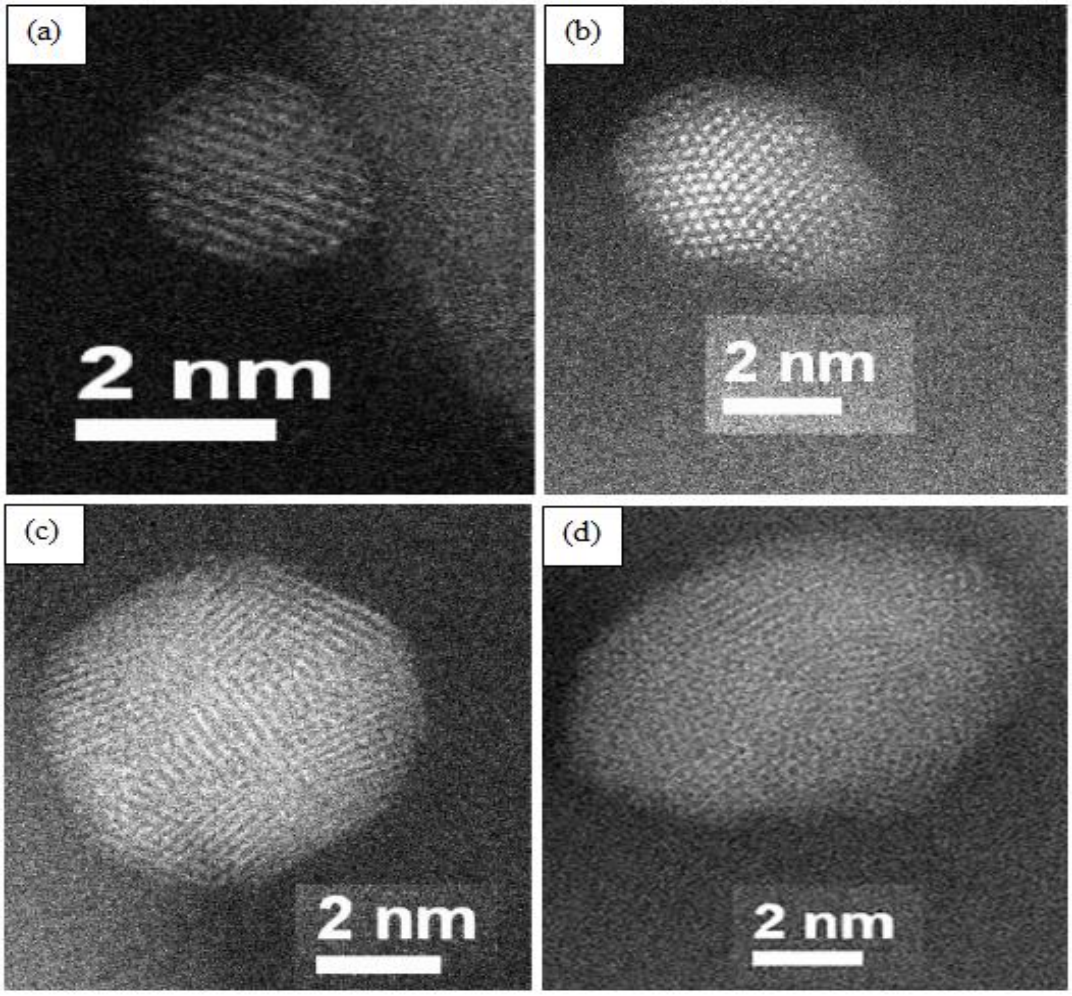

Figure 5.34 STEM images of (a) Pd/TiO_2, (b) Ag-Pd/TiO_2 (0.36 ML), (c) Ag-Pd/TiO_2 (0.5ML) and (d) Ag-Pd/TiO_2 (0.92 ML)

Table 5.19 Summary of Ag–Pd/TiO_2 composition.

Ag coverage (ML)	AA analysis		Pd/Ag	EDX		Pd/Ag
	%(wt)Pd	%(wt)Ag		Atomic% Pd	Atomic% Ag	
0ML	100	0	-	100	0	-
0.36 ML	0.97	0.06	16.2	94.2	5.8	16.2
0.5 ML	0.97	0.11	8.8	90.0	10.0	9.0
0.92 ML	0.97	0.64	1.5	60.5	39.5	1.5

5.11. Reaction study in selective hydrogenation of acetylene.

Prior to the start of each experimental run, the catalyst was reduced with in flowing 20% H_2/balance He at 200°C for 2 h. The reaction feed stream for catalyst screening consisted of 1% C_2H_2, 20% C_2H_4, 5% H_2, balance He at a total flow rate of 50 SCCM. The catalytic performances of the Pd/TiO_2 and $Ag\text{-}Pd/TiO_2$ were investigated in the selective hydrogenation of acetylene to ethylene. **Figure 5.35** shows the conversion of acetylene and ethylene selectivity of the catalysts as a function of Ag coverage (θ_{Ag}) ranging from 0 to 0.95. In this study, the calculation of acetylene conversion was based on moles of C_2H_2 converted with respect to C_2H_2 in feed and ethylene selectivity is defined as the percentage of C_2H_2 reacted over totally of C_2H_2 reacted, C_2H_6 formed and C_4s formed. It was found that the conversion of C_2H_2 decreased with increasing of Ag coverage on the Pd/TiO_2. The acetylene conversion of Pd/TiO_2 was 58% and C_2H_4 selectivity about 40%. The C_2H_4 selectivity increased monotonically to 84% with increasing θ_{Ag} to 0.92. At higher coverage of Ag, the C_2H_2 conversion decreased and the C_2H_4 selectivity increased. At low coverage of Ag is strongly adsorbed multi-**σ**-bond on Pd surface site than **π**-bond lead to C_2H_6 formation. The catalytic activity of C_2H_2 conversion decreased in parallel with the amounts of added Ag, which originated from the dilution of Pd active sites by added Ag. The **π**-bond ethylene species are adsorbed on single Pd atom and easily desorbed ethylene due to the adsorption is relatively weak. The di-**σ**-bonded ethylene species are strongly bound to Pd site and like to be fully hydrogenated to ethane [73].

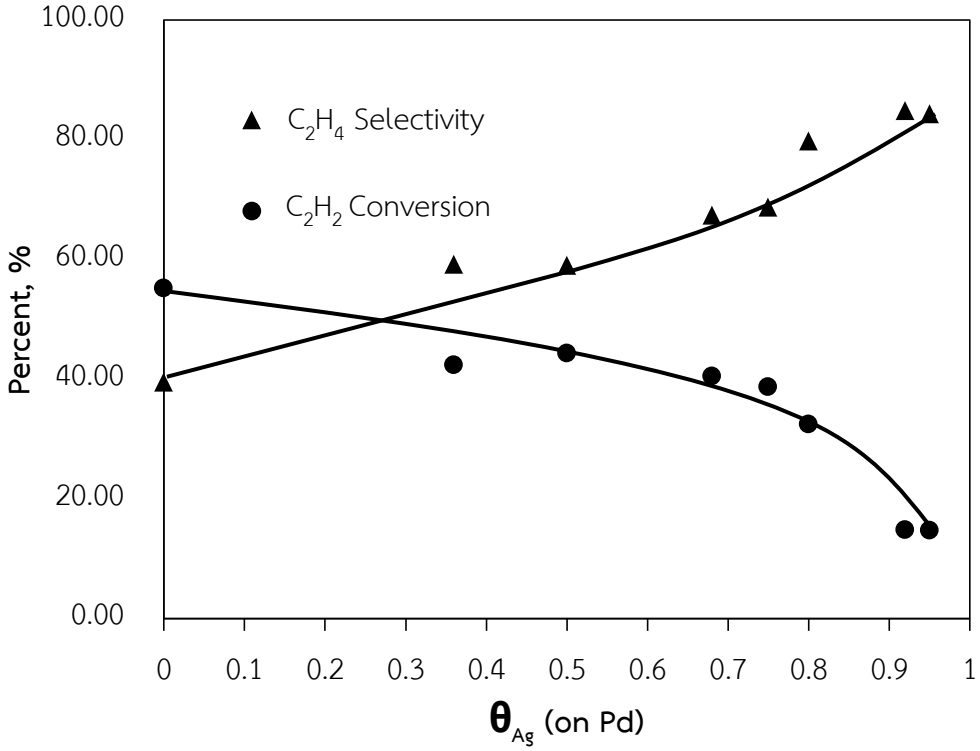

Figure 5.35 Conversion of acetylene and selectivity of acetylene to ethylene as a function of Ag coverage on Pd/TiO_2.

5.11.1 The Turnover Frequency (TOF)

The turnover frequency (TOF) values for C_2H_2 conversion and C_2H_6 formation for the Ag–Pd/TiO_2 catalysts are shown in **Figure 5.36.** The TOF values for C_2H_6 formation were relatively constant between 0 and 0.95 Ag coverage. The evolution of TOF for C_2H_2 conversion was increase at higher coverage of Ag on Pd. At higher coverage, most acetylene is strongly adsorbed as **π**-bonded species, on Pd surface sites than for di-**σ**-adsorbed species at low coverage. The lower TOF adsorbed strongly bound of ethylidyne species on the Pd site leads to the formation of C_2H_6 while high TOF adsorbed **π**-complex species favors the formation of ethylene. The high adsorption of C_2H_2 per Pd site increases the formation of C_2H_4 and decrease C_2H_6 formation. The presence of Ag on the Pd(1 1 1) surface also decreased the larger Pd

site lead to the C–C bond breaking ethylidyne formation. The acetylene conversion decreases with the slight increase of TOF.

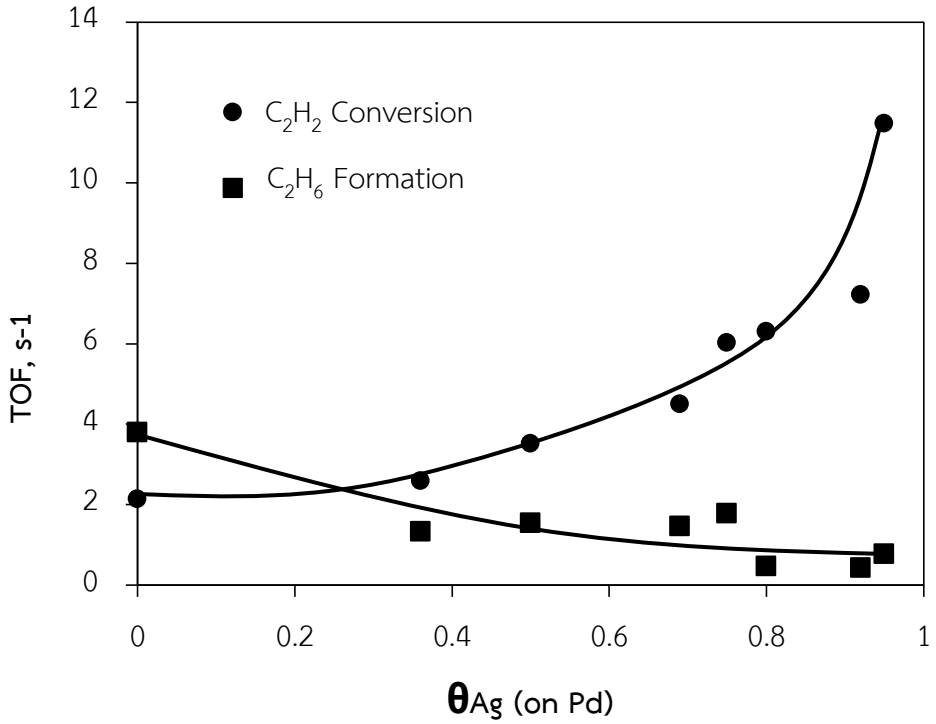

Figure 5.36 Effect of Ag coverage on Pd for TOF of acetylene hydrogenation.

5.11.2 Kinetic studies of acetylene hydrogenation

The kinetics studies of acetylene hydrogenation over the Pd/TiO_2 and $Ag–Pd/TiO_2$ catalysts. The kinetic measurements consisted of measuring the rate of acetylene consumption over a wide range of partial pressures of C_2H_2 over the catalyst at constant temperature. The catalyst was stabilized under the reaction conditions by passing the reaction mixture of, 20% C_2H_4 , 5% H_2, C_2H_2 pressure range from 0.005 (0.5%) to 0.012 atm (1.2%) and balance in He. The reaction temperature was 50°C and flow rate was 200 SCCM. The $Ag–Pd/TiO_2$ catalyst with 0.92 coverage of Ag on Pd was used for the kinetic study. The **Figure.5.37** shown C_2H_2 dependency for Pd/TiO_2 and $Ag\text{-}Pd/TiO_2$ (θ_{Ag} = 0.92) at constant x_{H_2}= 0.05. The corresponding acetylene pressure dependence measured using a H_2 pressure of 0.05 atm at 50°C,

also yields a good straight line corresponding to a reaction order of −0.87 ± 0.23 for Pd/TiO_2 and −0.57 ± 0.36 for $Ag–Pd/TiO_2$. The C_2H_2 pressure dependencies for both Pd/TiO_2 and $Ag–Pd/TiO_2$ catalysts confirm that at more negative reaction order for Pd/TiO_2 exhibited C_2H_2 is more strongly adsorbed ethylidyne on the Pd site than high coverage of Ag adsorbed as **π**-bonded species [74]

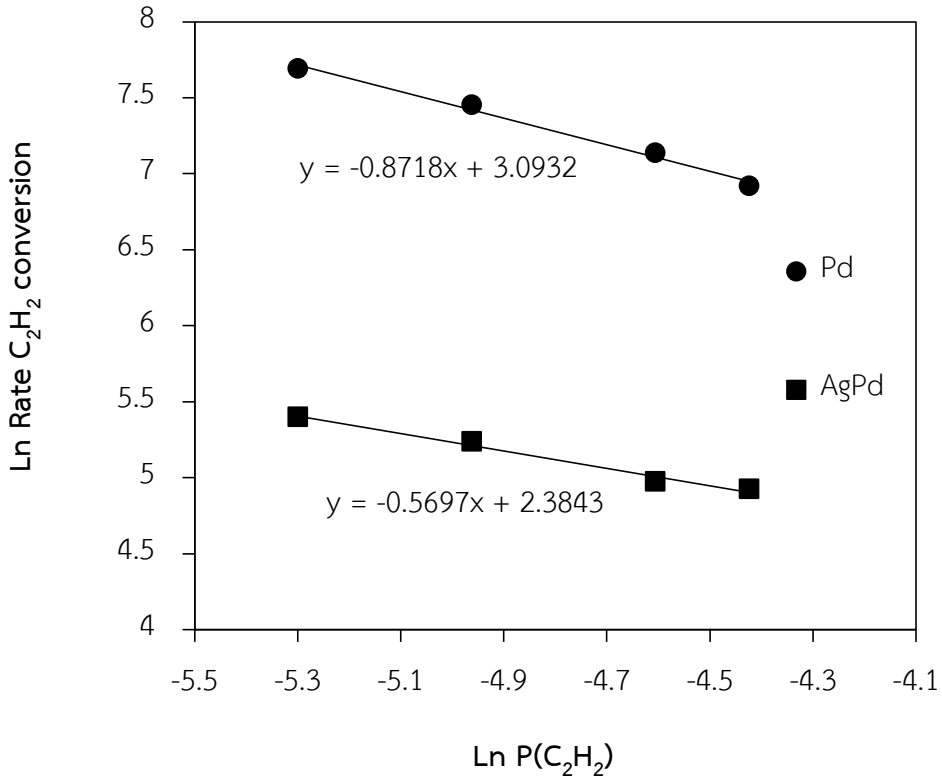

Figure 5.37 C_2H_2 dependency for Pd/TiO_2 and $Ag-Pd/TiO_2$ (θ_{Ag} = 0.92) at constant x_{H_2}= 0.05

The hydrogen pressure dependence is shown in **Figure.5.38** at a reaction temperature of 50°C using an acetylene pressure of 0.01 atm over H_2 pressure range from 0.02 (2.0%) to 0.10 (10%) atm. The straight line corresponding to a reaction orders of 1.53 ± 0.14 for Pd/TiO_2 and 0.88 ± 0.07 for $Ag–Pd/TiO_2$. The higher H_2 pressures increased the rate of acetylene hydrogenation and decrease the acetylene surface coverage. However, the increase of H_2 partial pressures also increased the

rate of ethylene and ethylidene hydrogenation that lead to the formation of ethane and the loss in the overall selectivity to ethylene [73].

The temperature dependence for acetylene hydrogenation for Pd/TiO_2 and $Ag\text{-}Pd/TiO_2$ (θ_{Ag} = 0.92) are shown in **Figure.5.39** at a reaction temperature of 40-70°C, C_2H_2 pressure of 0.01 atm and H_2 pressure of 0.05 atm. The reaction activation energy for Pd/TiO_2 is 12.08 ± 0.1 kcal/mol. The activation energy for $Ag–Pd/TiO_2$ is lower at 7.74 ± 0.2 kcal/mol due to consistent with weak adsorbed C_2H_2 at the surface reaction between adsorbed C_2H_2 and H. The acetylene conversion increased as the temperature increased. At higher temperatures increased the desorption of both ethylene and hydrogen. The reaction rates for C_2H_2 conversion over Pd/TiO_2 and $Ag–Pd/TiO_2$ can be stated as follows, where R is the gas constant (1.986 cal K^{-1} mol^{-1}). This allows a reaction rate to be given as:

For Pd/TiO_2,

$$\text{rate} = k_1 \, e^{\frac{-12080\pm100}{RT}} [p(C_2H_2)]^{-0.87\pm0.23} [p(H_2)]^{1.53\pm0.14}$$

For $Ag\text{-}Pd/TiO_2$ (θ_{Ag} = 0.92),

$$\text{rate} = k_2 \, e^{\frac{-7740\pm200}{RT}} [p(C_2H_2)]^{-0.57\pm0.36} [p(H_2)]^{0.88\pm0.07}$$

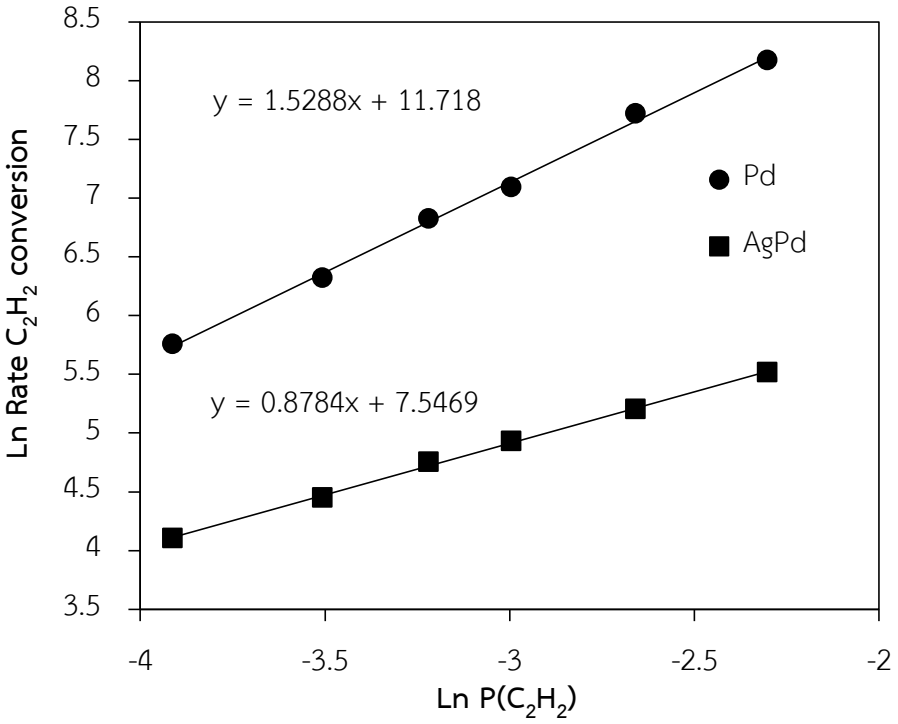

Figure 5.38 C_2H_2 dependency for Pd/TiO_2 and $Ag\text{-}Pd/TiO_2$ (θ_{Ag} = 0.92) at constant $x_{C_2H_2}$ = 0.01

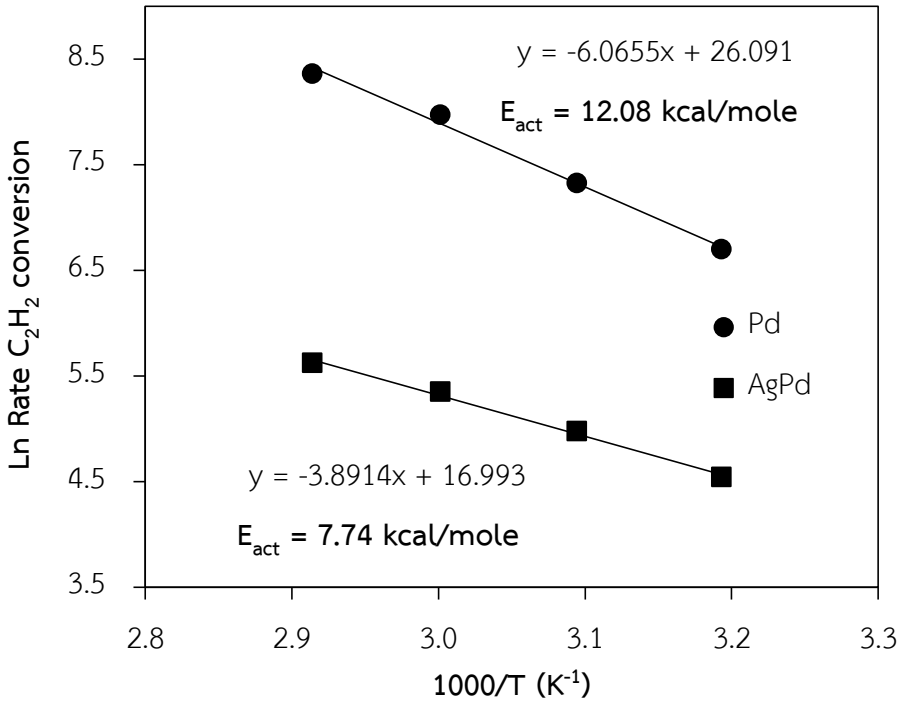

Figure 5.39 E_{act} for C_2H_2 conversion for Pd/TiO_2 and $Ag\text{-}Pd/TiO_2$ (θ_{Ag} = 0.92)

CHAPTER VI
CONCLUSIONS AND RECOMMENDATIONS

6.1 Conclusions

1) The TiO_2 supports were prepared by sol-gel and calcined under N_2, H_2, O_2, and air at 350°C. The samples were similar in terms of phase, average crystalline size and BET surface area. The calcination atmosphere affected the amounts of Ti^{3+} on the surface. The intensity of ESR signals of the TiO_2-N_2 and TiO_2-H_2 were found to be stronger than the TiO_2-Air and TiO_2-O_2, indicating a larger amount of Ti^{3+} defects on the TiO_2 surface. The large amount of Ti^{3+} surface defects on the TiO_2 resulted in a stronger interaction between Pd and TiO_2 and also higher Pd dispersion.

2) The catalytic performances of Pd/TiO_2 catalysts prepared by electroless deposition method in selective hydrogenation of acetylene were significantly improved when the TiO_2 support were calcined in H_2 atmosphere. The Pd/TiO_2-H_2 catalyst exhibited the highest conversion of acetylene and the selectivity of ethylene (~94%). The performances of Pd/TiO_2 catalysts were in order 1%Pd/TiO_2-H_2-ED > 1%Pd/TiO_2-N_2-ED > 1%Pd/TiO_2-Air-ED> 1%Pd/TiO_2-O_2-ED. The catalyst activities of Pd/TiO_2 were correlated with Pd dispersion, linearly CO bond with Pd sites, and the metal-support interaction, which were influenced by the presence of Ti^{3+} on Pd surface under reduction atmosphere.

3) The catalytic performances of Pd/TiO_2-H_2 catalysts prepared by incipient wetness impregnation method exhibited the highest catalytic performance in the selective hydrogenation of acetylene. The ethylene selectivity was improved in the order: 1%Pd/TiO_2-H_2-I > 1%Pd/TiO_2-N_2-I > 1%Pd/TiO_2-O_2-I> 1%Pd/TiO_2-Air-I. The results suggest that the H_2 and N_2-treated TiO_2 supports are likely to produce more active sites for selective hydrogenation of acetylene to ethylene. The dispersion of metal and the metal-support interaction were influenced by the presence of Ti^{3+} on

Pd surface under reduction atmosphere, leading to a significant increase of the catalytic activity in the selective hydrogenation of acetylene.

4) Comparing the Pd/TiO_2 catalysts prepared by two different methods, electroless deposition (ED) and incipient wetness impregnation methods. Using the TiO_2 calcined in H_2 gave higher conversion and selectivity of ethylene than those calcined in N_2, Air, and O_2 atmosphere regardless of the preparation method used. The preparation of Pd/TiO_2 by electroless deposition method exhibited higher catalytic activity compared to the incipient wetness impregnation method under similar reaction conditions. The higher Pd dispersion of Pd/TiO_2 prepared by electroless deposition method was correlated with the increase in the catalyst activities for acetylene hydrogenation.

5) The effect of calcination temperature on the TiO_2 supports prepared by sol-gel was investigated under H_2 at 300 - 450^{o}C. The crystallite sizes of the TiO_2 obtained at higher calcination temperature were slightly increased from 3.9 to 6 nm while the BET surface area decreased. The amounts of the Ti^{3+} was increased in the order: TiO_2-350 >TiO_2-400 >TiO_2-450 >TiO_2-300. It is suggested that Ti^{3+} were increased with increasing temperature and decreased after the TiO_2 anatase phase transformed into rutile phase. The large amount of Ti^{3+} surface defects on the TiO_2 promoted the stronger interaction between Pd and TiO_2 and Pd dispersion.

6) The catalytic performances of 1%Pd/TiO_2-H_2-300, 1%Pd/TiO_2-H_2-350, 1%Pd/TiO_2-H_2-400 and 1%Pd/TiO_2-H_2-450 prepared by incipient wetness impregnation method were evaluated in the selective hydrogenation of acetylene. The performance of Pd/TiO_2 catalysts were in order: 1%Pd/TiO_2-350 >1%Pd/TiO_2-400 >1%Pd/TiO_2-450 >1%Pd/TiO_2-300. It was found that dispersion of Pd and reducibility increased with the amount of surface defect present. The calcination temperature at 350^{o}C exhibited the highest dispersion of Pd and the highest the catalytic activity of acetylene hydrogenation.

7) The coverage of Ag on Pd/TiO_2 by electroless deposition method for acetylene hydrogenation resulted in higher selectivity of ethylene and TOFs in

acetylene conversion. The adsorption of acetylene on Pd sites was strongly adsorbed ethylidyne on large Pd ensembles, leading to the formation of ethane and adsorbed **π**-bonded species on small Pd ensembles favored ethylene formation.

8) The kinetics studies of acetylene hydrogenation over the Pd/TiO_2 and Ag–Pd/TiO_2 catalysts shows the reaction orders in C_2H_2 conversion of -0.87 and -0.57 for Pd/TiO_2 and Ag-Pd/TiO_2, respectively. The increases in the hydrogen partial pressure increased the activity but decreased ethylene selectivity over both Pd/TiO_2 and Ag-Pd/TiO_2. The apparent activation energy for the selective hydrogenation of acetylene over the high coverage of Ag decreased from 12.08 ± 0.1 kcal/mol to 7.74±0.2 kcal/mol due to consistent with weak adsorbed C_2H_2 at the surface reaction between adsorbed C_2H_2 and H. The presence of Ag on Pd surface also decreased the larger Pd ensembles, which can lead to the C–C bond breaking ethylidyne formation.

6.2 Recommendation

1. The effect of Ti^{3+} defect may be studied for other reactions such as liquid-phase hydrogenation reaction.

2. Other bimetallic modified on Pd/TiO_2 catalysts prepared by electroless deposition method should be studied in the future work.

REFERENCES

[1] Schbib, N.S., Garcia, M.A., Gigola, C.E., and Errazu, A.F. Kinetics of Front-End Acetylene Hydrogenation in Ethylene Production. Industrial &Engineering Chemistry Research 35(5) (1996): 1496-1505.

[2] Kang, J.H., Shin, E.W., Kim, W.J., Park, J.D., and Moon, S.H. Selective hydrogenation of acetylene on Pd/SiO2 catalysts promoted with Ti, Nb and Ce oxides. Catalysis Today 63(2-4) (2000): 183-188.

[3] Van Bekkum, H., Flanigen, E.M., Jacobs, P.A., and Jansen, J.C. Introduction to zeolite science and practice. Elsevier Science B.V. (2001): 682.

[4] Lambert, S., Cellier, C., Grange, P., Pirard, J.P., and Heinrichs, B. Synthesis of Pd/SiO2, Ag/SiO2, and Cu/SiO2 cogelled xerogel catalysts:study of metal dispersion and catalytic activity. Journal of Catalysis 221(2) (2004): 335-346.

[5] Thanh, N., Sarrazin, P., Cameron, C., and Didillon, B. Selective hydrogenation catalyst and a process using that catalyst US Patent (2000): 6,054,409.

[6] Yang, H. and Whitten, J.L. Dissociative adsorption of H[sub 2] on Ni(111). Chemical Physics 98(6) (1993): 5039-5049.

[7] Sarkany, A., Weiss, A.H., Szilagyi, T., Sandor, P., and Guczi, L. Green oil poisoning of a Pd/a1203 acetylene hydrogenation catalyst. Applied Catalysis 12(4) (1984): 373-379.

[8] Borodzinki, A. and Bond, G.C. Selective Hydrogenation of Ethyne in Ethene-Rich Streams on Palladium Catalysts. Part 1. Effect of Changes to the Catalyst During Reaction. Catalysis Reviews-Science and Engineering 48(2) (2006): 91-144.

[9] Bond, G.C. The Addition of Hydrogen to Carbon-Carbon Triple Bonds. Catalysis, New York, N.Y. 3 (1955): 109-148.

[10] Bond, G.C., Webb, G., Wells, P.B., and Winterbottom, J.M. Patterns of behavior in catalysis by metals. Journal of Catalysis 1(1) (1962): 74-84.

[11] Chen, M.H., Chu, W., Dai, X.Y., and Zhang, X.W. New palladium catalysts prepared by glow discharge plasma for the selective hydrogenation of acetylene. Catalysis Today 89(1-2) (2004): 201-204.

[12] Hong, J., Chu, W., Chen, M., Wang, X., and Zhang, T. Preparation of novel titania supported palladium catalysts for selective hydrogenation of acetylene to ethylene. Catalysis Communication 8(3) (2007): 593-597.

[13] Altinisik, O., Dogan, M., and Dogu, G. Preparation and characterization of palladium-plated porous glass for hydrogen enrichment. Catalysis Today 105(3–4) (2005): 641-646

[14] Cheng, Y.S. and Yeung, K.L. Effects of electroless plating chemistry on the synthesis of palladium membranes. Journal of Membrane Science 182 (1-2) (2001): 195–203.

[15] Rhoda, R.N. Electroless palladium plating. Trans. Inst. Met.Finish 36 (1959): 82.

[16] Shu, J., Grandjean, B.P.A., Ghali, E., and Kaliaguine, S. Simultaneous deposition of Pd and Ag on porous stainless steel by electroless plating. Membr. Sci. 96(1) (1993): 104.

[17] Chen, H.-I., Chu, C.-Y., and Huang, T.-C. Characterization of PdAgyAl2O3 composite membrane by electroless codeposition. Thin Solid Films 460(1-2) (2004): 62–71.

[18] Rebelli, J., Rodriguez., A.A., Ma, S., Williams, C.T., and Monnier, J.R. Preparation and characterization of silica-supported, group IB–Pd bimetallic catalysts prepared by electroless deposition methods. Catalysis Today 160(1) (2011): 170–178.

[19] Sinfelt, J.H. Bimetallic Catalysts: Discoveries, Concepts, and Applications. Wiley, New York (1983): 130-157.

[20] Li, W.S., Tian, L.P., Huang, Q.M., Li, H., Chen, H.Y., and Lian, X.P. Journal of Power Sources 104 (2002): 291-288

[21] Hindle, P.H., Yi, Q., Wu, G., Koczkur, K., and Chen, A. Electrocatalytic Activity of Nanoporous Pt – Ir Materials toward Methanol Oxidation and Oxygen Reduction. Journal of The Electrochemical Society 155(1) (2008): K5-K9.

[22] Rebelli, J., Detwiler, M., Ma, S., Williams, C.T., and Monnier, J.R. Synthesis and characterization of Au–Pd/SiO2 bimetallic catalysts prepared by electroless deposition. Journal of Catalysis 270 (2) (2010): 224–233.

[23] Ohashi, M., et al. Electrochemical and structural characterization of carbon-supported Pt–Pd bimetallic electrocatalysts prepared by electroless deposition. Electrochimica Acta 55(24) (2010): 7376–7384.

[24] Beard, K.D., Van Zee, J.W., and Monnier, J.R. Preparation of carbon-supported Pt–Pd electrocatalysts with improved physical properties using electroless deposition methods. Applied Catalysis B: Environmental 88(1-2) (2009): 185–193.

[25] Bai, L., Zhou , Y., Zhang, Y., Liu, H., Sheng, X., and Duan, Y. Effect of calcination atmosphere on the catalytic properties of PtSnNaMg/ZSM-5 for propane dehydrogenation. Catalysis Communications 10 (15) (2009): 2013–2017.

[26] Ku´s, S., Otremba, M., Tórz, A., and Taniewski, M. The effect of gas atmosphere used in the calcination of MgO on its basicity and catalytic performance in oxidative coupling of methane. Applied Catalysis A: General 230(1-2) (2002): 263–270.

[27] Choudhary, V.R., Rane, V.H., Rane, R., and Gadre, R.V. Influence of Precursors Used in Preparation of MgO on Its Surface Properties and Catalytic Activity in Oxidative Coupling of Methane. Journal of Catalysis 145(2) (1994): 300-311.

[28] Suriye, K., Praserthdam, P., and Jongsomjit, B. Impact of Ti3+ Present in Titania on Characteristics and Catalytic Properties of the Co/TiO2 Catalyst. Ind. Eng. Chem. Res. 44(17) (2005): 6599-6604.

[29] Samsonov, G.V. The Oxide Handbook, IFI/Plenum Press, New York. (1982).

[30] Grant, F.A. Properties of Rutile (Titanium Dioxide). Reviews of Modern Physics 31(3) (1959): 646.

[31] Satterfield, C.N. Heterogeneous Catalysis in Industrial Practice. McGraw-Hill, New York 2nd ed (1991).

[32] Kim, C.-S., Moon, B.K., Park, J.-H., Chung, S.T., and Son, S.-M. Synthesis of nanocrystalline TiO2 in toluene by a solvothermal route. Journal of Crystal Growth 254(3–4) (2003): 405–410.

[33] Kominami , H., Kohno, M., Takada, Y., Inoue, M., Inui, T., and Kera, Y. Hydrolysis of Titanium Alkoxide in Organic Solvent at High Temperatures: A New Synthetic Method for Nanosized, Thermally Stable Titanium(IV) Oxide. Industrial and Engineering Chemistry Research 38(10) (1999): 3925-3931.

[34] Kang, J.H., et al. Decomposition of toluene using an atmospheric pressure plasma/TiO2 catalytic system. Journal of Molecular Catalysis A:Chemical 180(1-2) (2002): 125-132.

[35] Wang, C., Deng, Z.X., Zhang, G., Fan, S., and Li, Y. Synthesis of nanocrystalline TiO 2 in alcohols. Powder Technology 125(1) (2002): 39-44.

[36] Nam, H.D., Lee, B.H., Kim, S.J., Jung, C.H., Lee, J.H., and Park, S. Preparation of Ultrafine Crystalline TiO2 Powders from Aqueous TiCl4 Solution by Precipitation. Japanese Journal of Applied Physics 37(8) (1998): 4603-4608.

[37] Su, C., Hong, B.Y., and Tseng, C.M. Sol–gel preparation and photocatalysis of titanium dioxide. Catalysis Today 96(3) (2004): 119-126.

[38] Nakaso, K., Okuyama, K., Shimada, M., and Pratinis, S.E. Effect of reaction temperature on CVD-made TiO2 primary particle diameter. Chemical Engineering Science 58(15) (2003): 3327-3335.

[39] Kominami, H., et al. Novel synthesis of microcrystalline titanium (IV) oxide having high thermal stability and ultra-high photocatalytic activity: thermal decomposition of titanium (IV) alkoxide in organic solvents. Catalysis Letters 46(3-4) (1997): 235-240.

[40] Shin, E.W., Kang, J.H., Kim, W.J., Park, J.D., and Moon, S.H. Performance of Si-modified Pd catalyst in acetylene hydrogenation: the origin of the ethylene selectivity improvement. Applied Catalysis A: General 223 (1-2) (2002): 161-172.

[41] Kim, W.J., Shin, E.W., Kang, J.H., and Moon, S.H. Performance of Si-modified Pd catalyst in acetylene hydrogenation: catalyst deactivation behavior. Applied Catalysis A: General 251(2) (2003): 305-313.

[42] Kang, J.H., Shin, E.W., Kim, W.J., Park, J.D., and Moon, S.H. Selective Hydrogenation of Acetylene on TiO2-Added Pd Catalysts. Journal of Catalysis 208(2) (2002): 310-320.

[43] Zhang, Q., Li, J., Liu, X., and Zhu, Q. Synergetic effect of Pd and Ag dispersed on Al2O3 in the selective hydrogenation of acetylene. Applied Catalysis A: General 197(2) (2000): 221-228.

[44] Shin, E.W., Kang, J.H., Kim, W.J., Park, J.D., and Moon, S.H. Performance of Si-modified Pd catalyst in acetylene hydrogenation: the origin of the ethylene selectivity improvement. Applied Catalysis A: General 223(1-2) (2002): 161-172.

[45] Derrien, M.L. Selective Hydrogenation Applied to the Refining of Petrochemical Raw Materials Produced by Steam Cracker. Studies in Surface Science and Catalysis 27(18) (1986): 613-666.

[46] Park, Y.H. and Price, G.L. Restrictive liquid-phase diffusion and reaction in bidisperse catalysts. Industrial & Engineering Chemistry Research 30(8) (1991): 1683-1693.

[47] Margitfalvi, J., Guczi, L., and Weiss, A.H. Reactions of acetylene during hydrogenation on Pd black catalyst. Journal of Catalysis 72(2) (1981): 185-198.

[48] Larsson, M., Jansson, J., and Asplund, S. The Role of Coke in Acetylene Hydrogenation on Pd/α-Al2O3. Journal of Catalysis 178(1) (1998): 49-57.

[49] Beard, K.D., Shaal, M.T., Van Zee, J.W., and Monnier, J.R. Preparation of highly dispersed PEM fuel cell catalysts using electroless deposition methods. Applied Catalysis B: Environmental 72(3-4) (2007): 262-271.

[50] Beard, K.D., Borrelli, D., Cramer, A.M., Blom, D.A., Van Zee, J.W., and Monnier, J.R. Preparation and Structural Analysis of Carbon-Supported Co Core/Pt Shell Electrocatalysts Using Electroless Deposition Methods. ACS Nano 3(9) (2009): 2841-2853

[51] Djokic, S.S. Electroless Deposition of Metals and Alloys. Modern Aspects of Electrochemistry 35 (2002): 51-133.

[52] Ohno, I., Wakabayashi, O., and Haruyama, S. Anodic Oxidation of Reductants in Electroless Plating. Journal of The Electrochemical Society 132(10) (1985): 2323-2330.

[53] Leviness, S., Nair, V., Weiss, A.H., Schay, Z., and Guczi, L. Acetylene hydrogenation selectivity control on PdCu/Al2O3 catalysts. Molecular Catalysis 25(1-3) (1984): 131-140.

[54] Kerr, C. and Walsh, F.C. Electroless Deposition of Metals. Transactions of the Institute of Metal Finishing 79(3) (2001): 41.

[55] Paunovic, M. Electroless Deposition of Metals and Alloys. Electrochemistry (1992): 479-497

[56] Steinmetz, P. Electroless deposition of pure nickel, palladium and platinum. Surface and Coatings Technology 43-44(1) (1990): 500–510.

[57] Diebold, U. The surface science of titanium dioxide. Surface Science Reports 48(5–8) (2003): 53–229.

[58] Ohno, I. Electrochemrstry of Electroless Plating. Materials Science and Engineering A146 (1991): 33-49.

[59] Barker, B.D. Electroless Deposition of Metals. Surf. Technol. 12 (1981): 77–88.

[60] Li, B., Wang, X., Yan, M., and Li, L. Preparation and characterization of nano-TiO2 powder. Materials Chemistry and Physics 78(1) (2002): 184–188.

[61] Nakaoka, Y. and Nosaka, Y. ESR Investigation into the Effects of Heat Treatment and Crystal Structure on Radicals Produced over Irradiated TiO2 Powder. Journal of Photochemistry and Photobiology A: Chemistry 110(3) (1997): 299-305

[62] Salama, T.M., Hattori, H., Kita, H., Ebitani, K., and Tanaka, T. X-ray absorption spectroscopic and electron paramagnetic resonance studies on the strong metal–support interaction of platinum supported on titania dispersed on silica. J. Chem. Soc., Faraday Trans. 89(12) (1993): 2067-2073.

[63] Xiong, L.-B., Li, J.-L., Yang, B., and Yu, Y. Ti3+ in the Surface of Titanium Dioxide: Generation, Properties and Photocatalytic Application. Journal of Nanomaterials 2012 (2013): 13

[64] Liu, X., et al. Green synthetic approach for Ti3+ self-doped TiO2−x nanoparticles with efficient visible light photocatalytic activity. Nanoscale 5(5) (2013): 1870-1875.

[65] Chen, G., Chou, W.-T., and Yeh, C.-T. The sorption of hydrogen on palladium in a flow system. Applied Catalysis 8(3) (1983): 389–397.

[66] Xu, J., Sun, K., Zhang, L., Ren, Y., and Xu, X. A highly efficient and selective catalyst for liquid phase hydrogenation of maleic anhydride to butyric acid. Catalysis Communications 6(7) (2005): 462–465.

[67] Monnier, J.R., Medlin, J.W., and Kuo, Y.-J. Selective isomerization of 2,5-dihydrofuran to 2,3-dihydrofuran using CO-modified, supported Pd catalysts. Applied Catalysis A: General 194 –195 (2000): 463–474.

[68] Kim, S.K., Lee, J.H., Ahn, I.Y., Kim, W.-J., and Moon, S.H. Performance of Cu-promoted Pd catalysts prepared by adding Cu using a surface redox method in acetylene hydrogenation. Applied Catalysis A: General 401 (2011): 12– 19.

[69] Soa, W.W., Parkb, S.B., Kima, K.J., and Moon, S.J. Phase Transformation Behavior at Low Temperature in Hydrothermal Treatment of Stable and Unstable Titania Sol. Journal of Colloid and Interface Science 191(2) (1997): 398–406.

[70] Liu, H., Ma, H.T., Li , X.Z., Li , W.Z., Wu, M., and Bao, X.H. The enhancement of TiO2 photocatalytic activity by hydrogen thermal treatment. Chemosphere 50 (1) (2003): 39–46.

[71] Gaber, A., Abdel- Rahim, M.A., Abdel-Latief, A.Y., and Abdel-Salam, M.N. Influence of Calcination Temperature on the Structure and Porosity of Nanocrystalline SnO2 Synthesized by a Conventional Precipitation method. Int. J. Electrochem. Sci. 9 (2014): 81-95.

[72] Sohn, Y. Interfacial electroic structure and ion beam induced effect of anatase TiO2 surface modified by Pd nanoparticles. Applied Surface Science 257(5) (2010): 1692-1697.

[73] Lee, J.H., Kim, S.K., Ahn, I.Y., Kim, W.-J., and Moon, S.H. Performance of Ni-added Pd-Ag/Al2O3 catalysts in the selective hydrogenation of acetylene. Korean Journal of Chemical Engineering 29(2) (2012): 169-172.

[74] Zhang, Y., Diao, W., Williams, C.T., and Monnier, J.R. Selective hydrogenation of acetylene in excess ethylene using Ag- and Au–Pd/SiO2 bimetallic catalysts

prepared by electroless deposition. Applied Catalysis A: General 469 (2014): 419–426

APPENDIX

APPENDIX A

CALCULATION FOR CATALYST PREPARATION

The calculation shown below is for 1%Pd/TiO_2 prepared by incipient wetness impregnation method. The titanium dioxide support weight used for all preparation is 4 g. Based on 100 g of catalyst used; the composition of the catalyst will be as follows:

Reagent: - Palladium (II) chloride ($PdCl_2$)

Molecular weight = 179.33g

- Titanium dioxide (TiO_2)

Palladium = 1 g

Titanium dioxide = 100 -1 = 99 g

For 4 g of titanium dioxide

Palladium required = (4 x 1)/99 = 0.0404 g

Palladium chloride dissolved in de-ionized water

$$\text{Then Pd content in stock solution} = \frac{\text{Weigth of Pd required} \times \text{M.W. of } PdCl_2}{\text{M.W. of Pd}}$$

$$= (0.0404 \times 179.33)/106.42$$

$$= 0.0681 \text{ g}$$

Since the pore volume of the titanium dioxide support is 0.3 ml/g and the total volume of impregnation solution which must be is 0.7 ml by the requirement of incipient wetness impregnation method, the de-ionized water is added until the total volume of solution is 0.7 ml.

APPENDIX B

CALCULATION OF THE CRYSTALLITE SIZE

Calculation of the crystallite size by Debye-Scherrer equation

The crystallite size was calculation from the half-height width of the diffraction peak of XRD pattern using the Debye-Scherrer equation.

From Scherrer equation

$$D = \frac{K\lambda}{\beta \cos\theta}$$

Where D = Crystallite size, Å

K = crystallite-shape fator = 0.9

λ = X-ray wavelength, 1.5418 Å for CuK_{α}

θ = Observed peak angle, degree

β = X-ray diffraction broadening, radian

X-ray diffraction broadening (β) is the corrected width of a powder diffraction free from all broadening due to the instrument. The α-alumina was used as standard sample to provide instrumental broadening data (see Figure B.1). The most common correction for the X-ray diffraction broadening (β) can be obtained by using the Warren's formula

Warren's formula:

$$\beta = \sqrt{B_M^2 - B_S^2}$$

Where B_M = The measured peak width in radians at half peak height

B_S = The corresponding width of the standard material

Example: Calculation of the crystallite size of **α**-alumina

The half-height width of peak = 2.0° (from the **Figure B.1**)

= (2**π** x 1.73)/360

= 0.0302 radian (B_M)

The corresponding half-height width of **α**-alumina peak (from the B_S value at the 2**θ** of 25.42° in **Figure B.2**= 0.0038 radian

The pure width, **β** $= \sqrt{0.0302^{2}-0.0038^{2}}$

= 0.0299 radian

β = 0.0299 radian

2**θ** = 25.42°

θ = 12.71°

λ = 1.5418

The crystallite size $= \dfrac{0.9\times 1.5418\text{Å}}{0.0299 \text{ radian}\times\cos 12.7}$

= 47.41 Å

= 4.7 nm

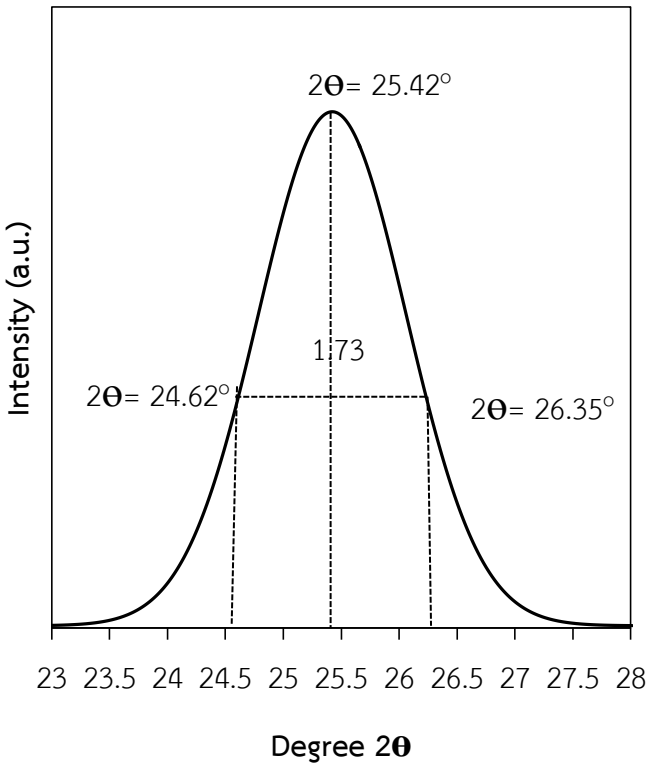

Figure B.1 The observation peak of **α**-alumina for calculating the crystallite size

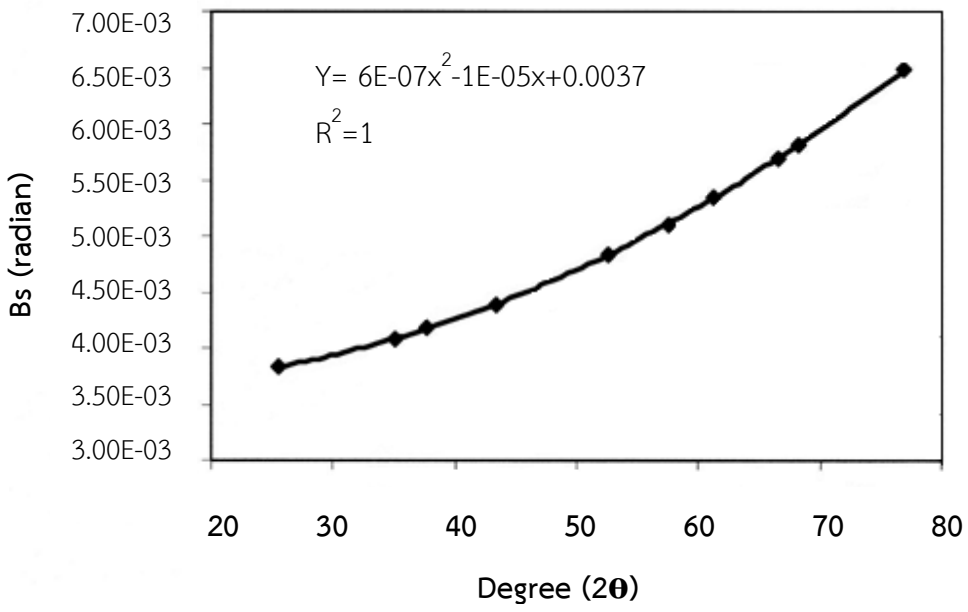

Figure B.2 The graph indicating that value of the line broadening attribute to the experimental equipment from the **α**-alumina standard.

APPENDIX C

CALCULATION FOR METAL ACTIVE SITES AND DISPERSION

Calculation of Pd active sites and Pd dispersion measured by CO adsorption is as follows:

$$\text{Metal dispersion} = 100 \times \frac{\text{Molecules of Pd from CO adsorption}}{\text{molecules of Pd load}}$$

$$V_{inj} = V_{loop} \times \frac{T_{std}}{T_{amb}} \times \frac{P_{amb}}{P_{std}} \times \frac{\%A}{100\%}$$

V_{inj} = loop volume injected 80 µL

T_{amb} = ambient temperature 295 K

T_{std} = standard temperature 273 K

P_{atm} = ambient pressure 743 mmHg

P_{std} = standard pressure 760 mmHg

%A = %Active gas 100%

$$V_{inj} = 80\ \mu L \times \frac{273\ K}{295\ K} \times \frac{743\ mmHg}{760\ mmHg} \times \frac{100\%}{100\%} = 72.38\ \mu L$$

Volume chemisorbed (V_{ads})

$$V_{ads} = \frac{V_{inj}}{m} \times \sum_{i=1}^{n} \left[1 - \frac{A_i}{A_f}\right]$$

V_{inj} = volume injected 72.38 µL

m = mass of sample 0.1 g

A_f = area of peak last peak

$$V_{ads} = \frac{72.38\mu L}{0.1014g} \times 1.152 = 822.26\ \mu L/g = 0.822\ cm^3/g$$

% Metal dispersion

$$\%D = S_f \times \frac{V_{ads}}{V_g} \times \frac{m.w.}{\%M} \times 100\% \times 100\%$$

S_f = stoichiometer factor, CO on Pd 1

V_{ads} = volume adsorbed 0.822 cm^3/g

V_s = molar volume of gas at STP 22414 cm^3/mol

m.w. = molecular weight of the metal 106.4 g/mol

%M = weight percent of the active metal 1%

$$\%D = 1 \times \frac{0.822\ cm^3/g}{22414\ cm^3/mol} \times \frac{106.4\ g/mol}{1\%} \times 100\% \times 100\% = 39.02\ \%$$

Pd active sites

$$\text{Pd active sites} = S_f \times \frac{V_{ads}}{V_g} \times N_A$$

S_f = stoichiometer factor, CO on Pd 1

V_{ads} = volume adsorbed 0.822 cm^3/g

V_s = molar volume of gas at STP 22414 cm^3/mol

N_A = Avogadro's number 6.023×10^{23} molecules/g

$$\text{Pd active sites} = 1 \times \frac{0.822\ cm^3/g}{22414\ cm^3/mol} \times 6.023 \times 10^{23} \frac{\text{molecules}}{\text{mol}}$$

$$= 2.21 \times 10^{19} \text{ CO molecules/g}$$

$$= 2.35 \times 10^{23} \text{ CO molecules/ mol Pd}$$

Active metal surface area

$$MAS_s = S_f x \frac{V_{ads}}{V_g} X \frac{100\%}{\%M} X N_A X \sigma_m X \frac{m^2}{10^{18} nm^2}$$

S_f = stoichiometry factor, CO on Pd 1

Vads = volume adsorbed 0.822 cm^3/g

Vg = molar volume of gas at STP 22414 cm3/mol

%M = weight percent of the active metal 1%

$$MAS_s = 1 x \frac{0.822 cm^3/mol}{22414 cm^3/mol} x \frac{100\%}{1\%} x\ 6.02x10^{23}\ molecules/g \times 0.0787 nm^2 X \frac{m^2}{10^{18} nm^2}$$

$= 173.74\ m^2/g_{metal}$

Average crystallite size

$$d = \frac{F_g}{\rho x MSA_m} X \frac{m^3}{10^6 cm^3} X \frac{10^9 nm}{m}$$

Fg = crystallite geometry factor 6

ρ = specific gravity of the active metal 12.0 g/cm

MSA_m = active metal surface area per gram of metal 173.74 m^2/g_{metal}

$$d = \frac{6}{12\ g/cm\ x 173.74 m^2/g} X \frac{m^3}{10^6 cm^3} X \frac{10^9 nm}{m}$$

$= 2.87$ nm

APPENDIX D

CALCULATION OF GAS HOURLY SPACE VELOCITY (GHSV)

Calculation of Gas Hourly Space Velocity (GHSV)

$$GHSV\ (h^{-1}) = \frac{\text{Flow rate}}{\text{Volume of catalyst}}$$

Volume of catalyst

Diameter of reactor (d) = 10 mm

High of catalyst (h) = 1.5 mm

$$\text{Volume} = \frac{\pi d^2 h}{4}$$

$$= \frac{3.14 \times 10^2 \times 1.5}{4}$$

$$= 120.12\ mm^3$$

Flow rate

$10\ cm^3/60\ s = (10x10x10x10x3600)/60$

$= 600{,}000\ mm^3/h$

Gas Hourly Space Velocity (GHSV)

$$GHSV\ (h^{-1}) = \frac{600{,}000}{120.12}\ h^{-1}$$

$$= 4995\ h^{-1}$$

APPENDIX E

CALCULATION CURVES

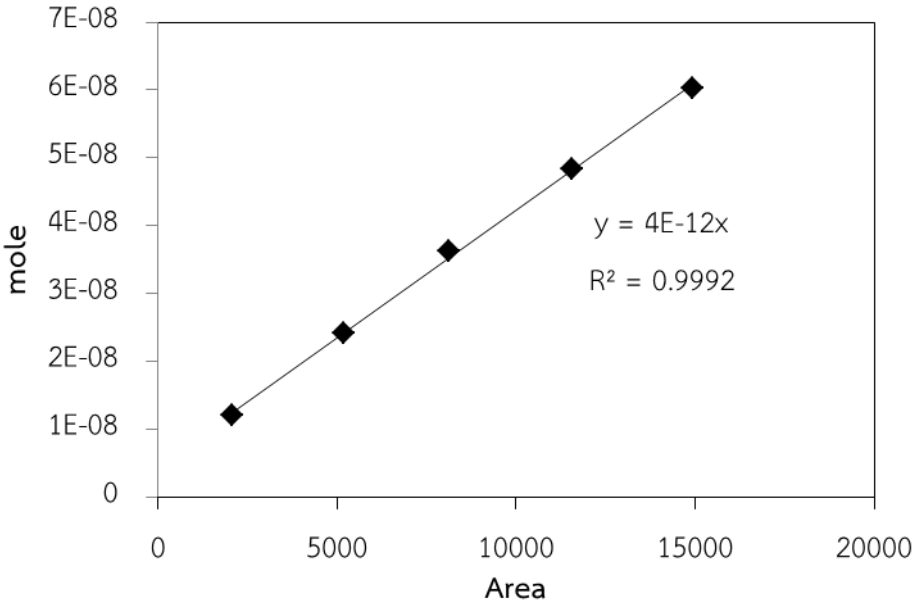

Figure E.1 The calibration curve of acetylene from GC-8APF (FID)

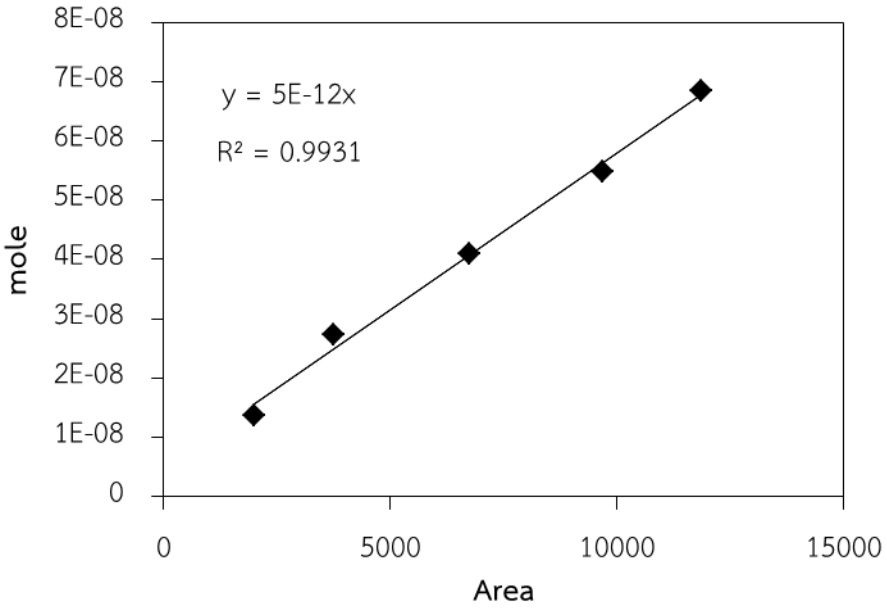

Figure E.2 The calibration curve of hydrogen from GC-8APT (TCD)

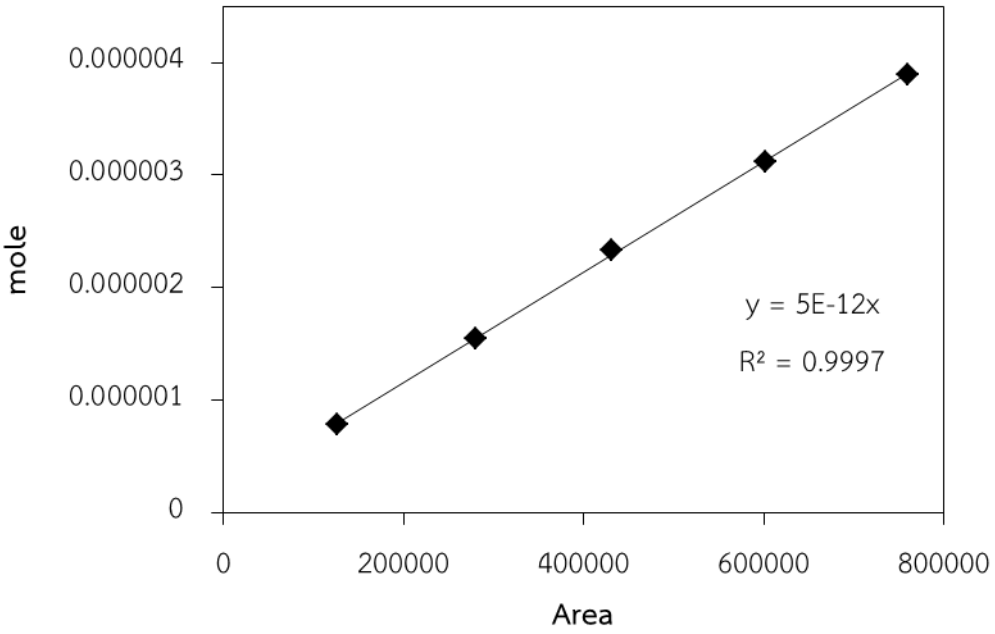

Figure E.3 The calibration curve of ethylene from GC-8APF (FID)

APPENDIX F

CALCULATION OF C_2H_2 CONVERSION AND C_2H_4 SELECTIVITY

The conversion of acetylene and ethylene selectivity was evaluated based on the following equation:

$$C_2H_2 + H_2 \longrightarrow C_2H_4$$
$$C_2H_4 + H_2 \longrightarrow C_2H_6$$

C_2H_2 conversion was calculated from moles of acetylene converted with respect to acetylene in the feed :

$$C_2H_2 \text{ conversion (\%)} = \frac{100\times[\text{mole of } C_2H_2 \text{ in feed-mole of } C_2H_2 \text{ in product}]}{\text{mole of } C_2H_2 \text{ in feed}}$$

Where mole of acetylene can be measured from the calibration curve of C_2H_2 in **Figure E.1** APPENDIX E.

C_2H_4 selectivity was calculated from moles of H_2 and C_2H_2 :

$$C_2H_4 \text{ selectivity (\%)} = \frac{100\times[dC_2H_2 - (dH_2 - dC_2H_2)]}{dC_2H_2}$$

Where dC_2H_2 = mole of C_2H_2 in feed - mole of C_2H_2 in product

dH_2 = mole of H_2 in feed - mole of H_2 in product

mole of H_2 can be measured employing the calibration curve of H_2 in **Figure E.2** APPENDIX E.

Mole of H_2 = (area of H_2 peak from integrator plot on GC-8APT)x5x10^{-12}

LIST OF PUBLICATIONS

1. Sumonrat Riyapan, Yuttanant Boonyongmaneerat, Okorn Mekasuwandumrong, Hiroshi Yoshida, Shin-Ichiro Fujita, Masahiko Arai, Joongjai Panpranot, "Improved catalytic performance of Pd/TiO_2 in the selective hydrogenation of acetylene by using H_2-treated sol–gel TiO_2", *Journal of Molecular Catalysis A: Chemical*, 383–384 (2014) 182– 187.

2. Sumonrat Riyapan, Yuttanant Boonyongmaneerat, Okorn Mekasuwandumrong , Piyasan Praserthdam, Joongjai Panpranot, "Effect of surface Ti^{3+} on the sol–gel derived TiO_2 in the selective acetylene hydrogenation on Pd/TiO_2 catalysts", *Catalysis Today,* 245 (2015) 134–138.

3. Sumonrat Riyapan, Yuttanant Boonyongmaneerat, Piyasan Praserthdam, and Joongjai Panpranot, "Effect of surface Ti^{3+} on the sol-gel derived TiO_2 in the selective acetylene hydrogenation on Pd/TiO_2 catalysts", Oral presentation in the framework of Catalyst Preparation & Characterization, 6th Asia-Pacific Congress on Catalysis, Taiwan, October 13-17, 2013.

4. Sumonrat Riyapan, Yuttanant Boonyongmaneerat, Piyasan Praserthdam, and Joongjai Panpranot, "Selective hydrogenation of acetylene using sol-gel TiO_2 supported Pd-based catalysts" Poster presentation in RGJ-Ph.d. Congress XIV at Pattaya, Chonburi, April 5-7, 2013.

VITA

Miss Sumonrat Riyapan was born on September 27th, 1986 in Phatthalung, Thailand. She received the Bachelor's Degree in Chemical and Biology Engineering from Ubon Ratchthani University. She entered the doctor of Engineering program in Chemical engineering at Chulalongkorn University.